Robust control strategies based on fractional calculus for robotic platforms

by

Jorge Muñoz Yáñez-Barnuevo

A dissertation submitted by in partial fulfillment of the requirements
for the degree of Doctor of Philosophy in
Electrical Engineering, Electronics and Automation

Universidad Carlos III de Madrid

Advisors:
Concepción Alicia Monje Micharet
Carlos Balaguer Bernaldo de Quirós

Tutor:
Concepción Alicia Monje Micharet

December, 2020

A Juan, Luna y Aurora.

Acknowledgments

First of all, I want to thank my children (Juan, Luna and Aurora) for all the support and encouragement they have given to me. This thesis would not have been possible without them for several reasons. Firstly, because they are my main motivation for embarking on any venture. And secondly because they have done the most important work of all. Any child requires constant attention, but they, with the help of their mother (María Laura) of course, have been able to give me the necessary peace of mind and time to develop this thesis. This shows me how great people they already are, and makes me feel very proud to be their father.

Secondly, the invaluable help received from my thesis director, Concha Monje, an excellent person in all aspects, and of course, an academic of international standing, whose advice and guidance have made it possible to bring all the work of these years to a successful conclusion. Her help, both to encourage me in the most challenging moments and to put my feet on the ground, has been key throughout the development. Without her, I would probably now have nothing but a mountain of messy papers containing pencil calculations. I would also like to thank my other tutors, Carlos at the Robotics Lab, and Egidio at the Sant'anna Biorobotics Institute. Their support has been essential in certain key moments.

The support of my colleagues has also been essential. Starting with the long and brilliant talks with Álvaro, which always resulted in more questions than answers, and which helped us grow as researchers and as persons. A good part of my research, and I suppose his too, advanced thanks to those good moments. The same could be said of many other former colleagues, such as Tamara, Nicolás, Quijano, Silvia, Alejandro, David, and a very long list. Although they all took different paths that ended up distancing our professional lives, the friendship that was formed then will remain strong for many years to come.

The colleagues Lisbeth, Luis, Juan Miguel, Carlos, Fernando and Santiago deserve a very special recognition. Their help during the long laboratory hours invested has been essential to achieve the extraordinary results obtained in the projects that we have developed together. Apart from the work in the laboratory, the collaboration with Vicente and Carlos, whose remarkable work gave and will give excellent results in the future, is also to be thanked.

Finally, we must not forget that all this would not have been possible if it weren't for the support of all the people who are part of the Robotics Lab and Carlos III University. Both for trusting me, through scholarships or simply a place to work, and for providing me with the necessary facilities to carry out the research.

And speaking of trusting and providing the necessary means, my parents, Andrés and María, cannot be missed. They have always known how to support and motivate me (and often bear with me) in any of my endeavors, from my first steps, literally.

Thank you all from the heart.

Agradecimientos

En primer lugar, quiero agradecer a mis hijos (Juan, Luna y Aurora) todo el apoyo y ánimo que me han dado. Esta tesis no habría sido posible sin ellos por varias razones. En primer lugar por ser mi motivación principal para abordar cualquier aventura. Y en segundo lugar porque ellos han hecho el trabajo más importante de todos. Cualquier niño requiere atención constante, pero ellos, con la ayuda de su madre (María Laura) por supuesto, han sabido darme la tranquilidad y el tiempo necesarios para poder desarrollar esta tesis. Eso me demuestra lo grandes personas que ya son, y me hace sentir muy orgulloso de ser su padre.

En segundo lugar, la inestimable ayuda recibida de mi directora de tesis, Concha Monje, una excelente persona en todos los aspectos, y como no, una académica de categoría internacional, cuyo consejo y guía han hecho posible que todo el trabajo de estos años haya llegado a buen puerto. Su ayuda, tanto para animarme en los momentos más complicados, como para ponerme los pies en la tierra, ha sido clave durante todo el desarrollo. Sin ella, probablemente ahora no tendría más que una montaña de papeles desordenados con cálculos a lápiz. También querría agradecer a mis otros tutores, a Carlos en el Robotics Lab, y a Egidio en el Instituto de biorobótica de Sant'anna. Su apoyo ha sido indispensable en varios momentos clave.

También ha sido imprescindible el apoyo de mis compañeros. Empezando por las largas y geniales charlas con Álvaro, que siempre terminaban con más preguntas que respuestas, y que nos vieron crecer como investigadores y como personas. Buena parte de mi investigación, y supongo que la suya también, avanzó gracias a aquellos buenos momentos. Lo mismo podría decir de muchos otros antiguos compañeros, como Tamara, Nicolás, Quijano, Silvia, Alejandro, David, Dorin y una larguísima lista. Aunque cada uno eligió caminos distintos que terminaron por separar nuestras vidas profesionales, la amistad que surgió entonces se mantendrá intacta por muchos años que pasen.

Merecen un reconocimiento muy especial los compañeros Lisbeth, Luis, Juan Miguel, Carlos, Fernando y Santiago. Su ayuda durante las largas horas de laboratorio invertidas ha sido imprescindible para conseguir los extraordinarios resultados obtenidos en los proyectos que hemos desarrollado juntos. Aparte de los trabajos en el laboratorio, las colaboraciones mantenidas con Vicente y Carlos, cuyo admirable

trabajo, dio y dará excelentes resultados en el futuro, son también de agradecer.

Por último no hay que olvidar que todo esto no habría sido posible sin el apoyo de todas las personas que forman parte del Robotics Lab y la universidad Carlos III. Tanto por depositar su confianza en mí, a través de becas o simplemente un sitio en el que trabajar, como por proporcionarme los medios necesarios para realizar la investigación.

Y hablando de depositar su confianza y de proporcionarme los medios necesarios, no podrían faltar mis padres, Andrés y María, que han sabido siempre apoyarme y motivarme (y muchas veces aguantarme) en cualquiera de mis peripecias, desde mis primeros pasos, en sentido literal.

Gracias a todos, de corazón.

Published and submitted content

During the development of this thesis the following research works were published:
A. Journals:

1. Muñoz, J.; Monje, C. A.; Nagua, L. F. & Balaguer, C. (2020), 'A graphical tuning method for fractional order controllers based on iso-slope phase curves', ISA Transactions. (Q1, Impact Factor: 4.305).

2. Flores, C.; Muñoz, J.; Monje, C. A.; Milanés, V. & Lu, X.-Y. (2020), 'Iso-damping fractional-order control for robust automated car-following', Journal of Advanced Research 25, 181 - 189. (Q1, Impact Factor: 6.992).

3. Mena, L.; Monje, C. A.; Nagua, L.; Muñoz, J. & Balaguer, C. (2020), 'Test Bench for Evaluation of a Soft Robotic Link', Frontiers in Robotics and AI 7, 27.

4. Muñoz, J.; Monje, C. A.; Casa, S. M. d. l. & Balaguer, C. (2019), 'Joint Position Control Based on Fractional-Order PD and PI Controllers for the Arm of the Humanoid Robot TEO', International Journal of Humanoid Robotics 16(06), 1950042. (Q4, Impact Factor: 1.394).

   - Pending publications (accepted):

5. Muñoz, J.; Copaci, D. S.; Monje, C. A.; Blanco D. & Balaguer, C. (2020), 'Iso-m based adaptive fractional order control with application to a soft robotic neck', IEEE Access. (Q1, Impact Factor: 4.098).

6. Copaci, D. S.; Muñoz, J.; González, I.; Monje, C. A.; & Moreno, L. (2020), 'SMA-driven soft robotic neck: design, control and validation', IEEE Access. (Q1, Impact Factor: 4.098).

B. Conferences:

1. Quevedo, F.; Munoz, J.; Castano, J.A.; Monje, C. A. & Balaguer, C. (2020), Model Identification of a Soft Robotic Neck, in '2020 IEEE/RSJ International Conference on Intelligent Robots and Systems (IROS)', IEEE, , pp. –.

2. Mena, L.; Monje, C. A.; Nagua, L.; Muñoz, J. & Balaguer, C. (2019), Sensorización de un sistema de eslabón blando actuando como cuello robótico, in 'Actas de las Jornadas Nacionales de Robótica', Universidad de Alicante, , pp. 98-102.

3. Munoz, J.; Monje, C. A.; Martin, F. & Balaguer, C. (2018), A Robust Control Method for the Elbow of the Humanoid Robot TEO Based on a Fractional Order Controller, in '2018 IEEE/RSJ International Conference on Intelligent Robots and Systems (IROS)', IEEE, , pp. 6378–6383.

4. Nagua, L.; Muñoz, J.; Monje, C. A. & Balaguer, C. (2018), A first approach to a proposal of a soft robotic link acting as a neck, in 'Actas de las XXXIX Jornadas de Automatica, Badajoz, 5-7 de Septiembre de 2018', Área de Ingeniería de Sistemas y Automática, Universidad de Extremadura, , pp. 522-529.

5. Nagua, L.; Monje, C.; Muñoz Yañez-Barnuevo, J. & Balaguer, C. (2018), Design and performance validation of a cable-driven soft robotic neck, in 'Actas de las Jornadas Nacionales de Robótica', Universidad de Valladolid, .

Chapter 2 describes in detail the mathematical development of the iso-m method. The research contributions of this chapter have been published in the high impact paper [A1].

A complete theoretical description of an adaptive scheme application to the aforementioned iso-m method can be found in chapter 3. The research contributions of this chapter will soon be published in the high impact paper [A5].

One of the systems improved using the proposed robust controller is shown in chapter 4. The results presented in this chapter have also been published in the high impact paper [A2].

Chapter 5, describes a system developed for the robust control of the TEO humanoid robot right arm joint. The results presented in this chapter have been also published in the high impact papers [A4], [B3].

During chapter 6, the system developed for soft neck inclination control and its results are described. The different results presented in this chapter have been also published in the high impact papers [B1], [B2], [B4], [B5], [A1] , and [A5].

Other research merits

- Award: Best paper in "Special Issue on Modelling and Control of Humanoid Robots (IROS 2018)" For the paper: 'Joint Position Control Based on Fractional-Order PD and PI Controllers for the Arm of the Humanoid Robot TEO', International Journal of Humanoid Robotics.

Abstract

The proportional integral derivative feedback control is currently the most widely used system at industrial level, not just for simple systems, but also for highly complex ones, or even for new research developments. The main reason behind their widespread use is their simple implementation and the large number of available design tools. Only when it is strictly required, more advanced techniques such as robust, adaptive, predictive, or intelligent control are applied. In one way or another, all these advanced control systems have a common task: to achieve satisfactory results in the control of a system where classical techniques fail.

One difficult problem to solve from a classical control point of view is uncertainty. The classic methods approach is based on some specifications and a model of the system to be controlled. This model, although it is considered to have some modeling error, is assumed to be invariable and correct. In other words, it is assumed to be certain. However, the reality is very different. At best, we can say that the system is invariant to some degree, and that the error is small enough. This lack of information about the system is known in the literature as uncertainty.

One of the existing solutions to this problem comes from robust control, whose strategy is to design systems that are unaffected by plant variations, meaning that even with an inaccurate model, or with changing parameters, usually gain, the system response remains almost constant. Some examples of robust control are H-infinity control, sliding mode control or quantitative feedback theory. All these methods are complicated in both implementation and design, and therefore, are usually applied only when classical control fails.

Halfway between the complexity of these methods and the simplicity of classical control is the fractional order control, based on the application of non-integer calculus to classical control methods. The great advantage of fractional order control compared to the previous methods consists in its close similarity to the classic control techniques, allowing many tools to be adapted from the classic control. Another great advantage compared to classic control is their great versatility, providing robust designs for a wide range of different plants.

Naturally, fractional control also has its drawbacks. Firstly, the implementation of fractional order operators is more difficult than the integer ones, leading to a

significant research effort, still growing, to find straightforward and reliable implementations. Secondly, the tuning of fractional order controllers involves the solution of non-linear equations, which normally requires high computational effort and added complexity.

The problem of fractional controller tuning is addressed in this thesis in a novel way, seeking always simplicity in the calculations. The approach derives from a basic concept, followed by a mathematical analysis that provides simple but meaningful operations to calculate the parameters of the controller. Thanks to this approach, the solution can be found avoiding the use of numerical methods, while providing extensive information on the tuning process. The result is the formulation of a new tuning method that is swift and straightforward and avoids the limitations of the currently available methods.

The excellent results obtained are coincident with other more complex solutions, but avoiding the use of numerical methods at all times. The precision and simplicity of the tuning method also allows an adaptive approach when a system identification algorithm is provided. Available alternatives in the field of fractional adaptive control are currently based on implicit adaptive techniques. The low computational cost of the new tuning method also makes explicit adaptive control possible, resulting in a robust control with an optimal operating point at all times.

This solution, novel in the field of adaptive fractional control, allows a more complete solution to the uncertainty problems, since it combines the robustness of fractional order control with the flexibility of adaptive control. On the one hand, the robust controller prevents fast plant parameter changes to affect the system's performance, as long as they are close to the operating point. On the other hand, the adaptive algorithm changes the operating point in case of a major variation in plant parameters. The key to this combination is that the fractional controller provides the time needed for adaptation, which is usually on the order of seconds, while maintaining the robustness of the system's behavior.

In addition, since the computational cost of the proposed methods is very low, their implementation on low-cost embedded platforms offers an amazing opportunity for the development and standardization of advanced control techniques. This in turn would allow the improvement of many current systems without the need of large equipment investment and the application of robust adaptive control to a much larger number of systems than those covered in the current landscape.

The excellent results offered by both robust and adaptive fractional control methods are widely evidenced in the experimental part of this thesis through their application to several plants, including robotic joints, soft robotic links and autonomous vehicles.

Resumen

El control proporcional integral derivativo con realimentación es en la actualidad el sistema más usado a nivel industrial, no solo en sistemas sencillos, sino también en sistemas de gran complejidad, incluso en nuevos desarrollos de investigación. Este tipo de control es muy usado debido sobre todo a su sencilla implementación y al gran número de herramientas de diseño disponibles. Solo en caso de ser estrictamente necesario, se aplican técnicas mas avanzadas como el control robusto, adaptativo, predictivo, o inteligente. De una u otra forma, todos estos sistemas de control avanzado tienen una tarea en común: conseguir resultados satisfactorios en el control de un sistema cuando fallan las técnicas clásicas.

Uno de los problemas con difícil solución desde un punto de vista clásico de control es el de la incertidumbre. El enfoque de los métodos clásicos es el del diseño en base a una serie de especificaciones y un modelo del sistema a controlar. Este modelo, aunque se considera que puede tener cierto error de modelado, se supone invariable y perfecto. Dicho de otro modo, se supone como cierto. Sin embargo, la realidad es muy distinta. En el mejor de los casos, podemos afirmar que el sistema es invariable hasta cierto punto, y que el error es suficientemente pequeño. Toda esta falta de información sobre el sistema se conoce en la literatura como incertidumbre.

Una de las soluciones existentes a dicho problema es el control robusto, cuya solución pasa por diseñar sistemas imperturbables por las variaciones de la planta, de forma que, a pesar de que el modelo sea impreciso, o que los parámetros, normalmente la ganancia, cambien, la respuesta del sistema permanezca lo más invariable posible. Algunos ejemplos de control robusto son H-infinity control, sliding mode control o quantitative feedback theory. Todos estos métodos son más complicados tanto en la implementación como en el diseño, y por lo tanto, se aplican por lo general exclusivamente cuando el control clásico falla.

A medio camino entre la complejidad de estos métodos y la simplicidad del control clásico se encuentra el control de orden fraccionario, basado en la aplicación del cálculo no entero a las técnicas de control clásico. La gran ventaja del control de orden fraccionario frente a las técnicas anteriores radica en su gran parecido con las técnicas clásicas de control, lo que permite que muchas de las herramientas disponibles se puedan adaptar desde el control clásico. La otra gran ventaja en comparación con

el control clásico es su gran versatilidad, lo que permite realizar diseños robustos para muy diversos tipos de planta.

Por supuesto, el control fraccionario también tiene sus desventajas. En primer lugar, la implementación de los operadores de orden fraccionario es más complicada que los de orden entero, lo que ha originado un gran esfuerzo de investigación, aún en auge, para encontrar implementaciones sencillas y fiables. Por otro lado, el ajuste de los controladores de orden fraccionario implica la solución de ecuaciones no lineales, lo que requiere normalmente de técnicas con un esfuerzo computacional elevado y una complejidad añadida.

En esta tesis se trata el problema del ajuste del controlador fraccionario desde una forma novedosa, buscando en todo momento la simplicidad en los cálculos. La propuesta parte de un concepto sencillo, seguido de un desarrollo matemático que resuelve el cálculo de los parámetros del controlador mediante operaciones simples pero significativas. Gracias a este enfoque, la solución se plantea evitando el uso de métodos numéricos, a la vez que se ofrece abundante información sobre el proceso de ajuste. Esto permite el desarrollo de un nuevo método de ajuste rápido y sencillo que evita las desventajas de los métodos actualmente disponibles.

Los resultados obtenidos son excelentes, coincidiendo en su solución con otros más complejos, pero evitando en todo momento el uso de métodos numéricos. La precisión y sencillez del método de ajuste permite además su aplicación en sistemas adaptativos en caso de disponer de un algoritmo de identificación de sistemas. Actualmente, las propuestas disponibles en el campo del control adaptativo fraccionario se basan en técnicas adaptativas implícitas. Dado el coste computacional mínimo del nuevo método de ajuste, el control adaptativo explícito también es posible, permitiendo el control robusto en un punto óptimo de operación en todo momento.

Esta solución, de novedosa aplicación en el campo del control fraccionario adaptativo, permite una solución más completa a los problemas de incertidumbre, ya que une la robustez del control de orden fraccionario con la flexibilidad del control adaptativo. Por un lado, el controlador robusto permite que las variaciones rápidas en los parámetros de la planta no afecten al comportamiento del sistema, siempre que estén cerca del punto de operación. Por otra parte, el algoritmo de adaptación cambia el punto de operación en caso de una variación mayor en los parámetros de la planta. La clave de esta combinación está en que el controlador fraccionario proporciona el tiempo necesario para la adaptación, que suele ser del orden de segundos, mientras que mantiene la robustez en el comportamiento del sistema.

Además, dado que el coste computacional de los métodos propuestos es muy reducido, su implementación en plataformas embebidas y de bajo coste ofrece una increíble oportunidad de desarrollo y estandarización de las técnicas avanzadas de control. Esto permitiría la mejora de muchos sistemas actuales sin la necesidad de una gran inversión en equipos y la aplicación del control adaptativo robusto a un

número de sistemas mucho más amplio de los que se abordan en el panorama actual.

Los excelentes resultados que ofrecen ambos métodos de control fraccionario robusto y adaptativo están ampliamente demostrados en la parte experimental de esta tesis mediante su aplicación en varias plantas, entre las que se encuentran articulaciones robóticas, eslabones robóticos blandos y vehículos autónomos.

Contents

List of Tables

List of Figures

Chapter 1

Introduction

Control engineering has dealt with uncertainty since its inception. In fact, something so fundamental such as the concept of negative feedback, emerged as a solution to an uncertainty problem.

During the development of the first telephone lines, electronic amplification devices had a strong non-linear behavior. That was not a problem for the telegraph lines, that use constant signals, because it can be solved with a simple gain adjustment. But voice signals traveling through the newly developed phone lines, were fluctuating and uncertain, resulting in wave distortion due to non-linear amplification. Harold Stephen Black then proposed applying negative feedback to electronic amplifiers to improve the tracking of the input reference. As a result, the amplifier output is linear to the input, and therefore it is possible to boost the signal with much less distortion.

Previous works had already discussed the feedback topic, but Harold Black was the first to propose negative feedback as a control method in [11], and therefore is considered a pioneer in the field. To some point, the foundations of control engineering were built by Black, and later by Harry Nyquist and Hendrik Wade Bode, during those years in the Bell Telephone Laboratories.

In this case, the use of negative feedback made possible to address the problem of uncertainty in the input and disturbance signals. This method is still today the main solution to input uncertainty, but this is only one of the uncertainties existing in a control system. The other two uncertainty problems found in control engineering are modeling uncertainties and noise. The scope of this thesis falls into the second problem: model uncertainty.

Most control strategies are based on the analysis of a system model, but the concepts of uncertainty and modeling are closely linked, like those of measurement and error. Absolutely all models are subject to uncertainty, showing a different degree depending on the system, from small uncertainties, such as an almost ideal simple pendulum model, to large uncertainties, as is the case of weather evolution. This

modeling uncertainty can also be divided into two other groups. Systems that have a known structure but unknown parameters are usually classified under parametric uncertainty, to differentiate from the systems with unmodeled dynamics, usually due to non-linear behaviors.

Problem severity due to uncertainty is also different depending on the system considered, for example, weather forecasts work with large uncertainties, but the consequences of a prediction error are slight. However, a small modeling uncertainty in one of the systems in a nuclear power plant can have catastrophic results. Most control systems are halfway between these ends, therefore, some uncertainties may be neglected depending on the application, although they are always problematic.

For example, common uncertainty problems found in robotics and automation range from accuracy errors to system instability. All of them are undesirable, but the second group is much more dangerous than the first. Although stability errors are not catastrophic, they can lead to a good deal of damage, to the system itself and to the environment, including people in the area.

Therefore, many control approaches evolved to cope with uncertainty. As an example, without the aim of providing a complete list, the following control strategies pursue the solution of these problems:

- Feedback: Input uncertainties and disturbances.
- Stochastic: Signal uncertainties or noise.
- Robust: Model uncertainties and non-linearity.
- Adaptive: Time varying and non-linear systems.

Robust and adaptive techniques address the uncertainty of system parameters from different perspectives. Robust control consists of making the system insensitive to parameter variations using a constant controller while adaptive control addresses the variability of system parameter by changing the controller parameters in order to achieve a uniform final performance.

This thesis contribution is based on these two strategies, robust and adaptive control, from a fractional calculus perspective, which deals with the generalization of classical calculus by using non-integer (fractional) orders.

While in integer calculus the operators are integral or derivative, using the exponent to specify how many times the operator is applied, in fractional calculus the same exponents and operators are used, but the exponent is allowed to have any real number value. Therefore, concepts such as second order derivative (d^2/dx^2) are allowed, but one and a half order derivative ($d^{1.5}/dx^{1.5}$) is also possible.

This exponent generalization do not have still a known definite physical meaning, such as, for instance, the integer derivative, but this is not a problem as long as the

mathematics remains coherent. In fact, the integer derivative is also no more than a concept, commonly used for real world modeling because it is consistent with reality, but still a concept.

Although this idea may look strange at first, there are many operators that have been generalized in mathematics, producing valuable results. For instance, consider the ubiquitous power function.

Multiplication leads to power function as the notation of a repeated product:

$$b \cdot b \cdot \overset{n}{\ldots} \cdot b = b^n = x; \quad b, x \in \mathbb{R}, n \in \mathbb{Z}.$$

Letting the exponent to be a fraction, we find the concept of root, where b can be found as $b = x^{\frac{1}{n}}$, because:

$$b^n = b \cdot b \cdot \overset{n}{\ldots} \cdot b = x^{\frac{1}{n}} \cdot x^{\frac{1}{n}} \cdot \overset{n}{\ldots} \cdot x^{\frac{1}{n}} = x; \quad x \in \mathbb{R}, n \in \mathbb{Z}.$$

Similarly, repeated use of a fractional derivative operator ($D^{\frac{1}{n}}$) results in:

$$D^{\frac{1}{n}} D^{\frac{1}{n}} \overset{n}{\ldots} D^{\frac{1}{n}} f(t) = Df(t) = \frac{d}{dt} f(t); \quad n \in \mathbb{Z}, \tag{1.1}$$

showing the concept of fractional operator. Note that these operators can be grouped, therefore, Eq. (1.1) can be written as:

$$D^{\alpha_1} D^{\alpha_2} ... D^{\alpha_m} f(t) = \frac{d}{dt} f(t); \quad \alpha_i \in \mathbb{Q}, \alpha_1 + \alpha_2 + ... + \alpha_m = 1 \tag{1.2}$$

Since D^{α_m} is a separate operator, it is also possible to apply just this fractional operator to $f(t)$:

$$D^{\alpha_m} f(t) = g(t); \quad \alpha_m < 1, \quad g(t) = \frac{d^{\alpha_m}}{dt} f(t) \tag{1.3}$$

and since $\alpha_m < 1$, and the composition of all the operators is $df(t)/dt$, the outcome $g(t)$ must fall somewhere between $f(t)$ and $df(t)/dt$. Do not take the above example as a demonstration, for a complete fractional order derivative definition see [12].

This particular class of operators are useful in control engineering, both in the modeling of physical systems, as they improve the models based on ordinary differential equations (ODEs), and also in the design of robust controllers, improving their performance compared to their integer counterparts.

Modeling using fractional differential equations (FDEs) has been successfully used in the mathematical description of many processes such as heat transmission, flow diffusion, abnormal relaxation, and other physical phenomena, including engineering systems modeling. Detailed reference on general FDEs can be found at [13] or [14], some modeling examples are shown in [12] or [15], and common plants used in control engineering like DC motors are modeled using fractional derivatives in [16] or [17].

Robust controller design using fractional operators is known in the literature as fractional order control. The advantage of fractional controllers over integer controllers lies in their superior versatility. Just as fractional modeling with FDEs can describe behaviors that are impossible to model using ODEs, fractional controllers are able to implement filters that can shape plant characteristics in a way that integers cannot. Note that a controller can be seen as a filter applied to the error signal.

Hendrick Bode was the first describing a fractional order calculus application to robust control, which later described in [18]. According to this paper, the fractional transfer function model $G_{bi} = (\omega_{gc}/s)^{\mu}$ would be able to maintain overshoot characteristics despite changes in the system gain. This feature is known today as iso-damping, and the transfer function G_{bi} is generally called Bode's ideal because of that.

The advantage of fractional order controllers applied to robust control will be evidenced by their frequency response analysis in chapter 2. The tightness of integer controllers, hampers robustness specifications in many cases, while their fractional counterparts can meet any robustness specification as their frequency response is much more varied and flexible.

Given their advantages, robust fractional controllers have been the subject of intensive research over the past three decades, addressing the essential issues, although there are still a lot of issues that need to be solved. There are many tools available for integer controller tuning, but unfortunately they are not directly applicable to fractional order control.

The problem of fractional controller tuning has been addressed many times from the early works in [19] to the latest proposals like [20]. Due to the nonlinear nature of the equations to be solved, a common problem in these proposals is the high computational complexity and the lack of information on the tuning process.

Although recent works such as [21] and [22], or the follow-up [23] use a graphical solution to avoid the computational complexity, the proposed plots do not offer information about the process and the graph is tailored for the combination of a controller and a plant, therefore, a new plot is needed for different plants. Moreover, an observer must visually spot the curve intersection, which impairs the computerization of the algorithm.

This thesis addresses that problem by using a graphical solution for the nonlinear equations, but the graphs are designed to be meaningful about the controller parameters, providing a great understanding of the tuning process. This provides a quick and easy solution for the class of controllers defined with a fractional operator known as fractional proportional derivative (FPD) and fractional proportional integral (FPI), which can be used in robust control of any given system.

Also, the algorithm is straightforward and the graph can be tabulated, meaning that the entire process can be easily computerized. This provides a direct and unique tuning solution using very low complexity software capable of running on low

cost/power boards and embedded hardware systems. This is a very interesting feature, useful in areas like robotics and automation, automotive industry, aerospace and many others.

Furthermore, this leads to the second proposal of this thesis, which is an indirect fractional order adaptive controller (FOAC). Many works address this issue through a direct approach, generally with a fractional reference model, but an indirect approach is not available to date. Although both strategies show good results, there are important differences in terms of implementation and applicability.

While direct strategies can sometimes result in simple equations that reduce computational complexity, they are limited to systems that meet certain conditions, and often adapt to them. For example, given that one of the implementation conditions is stability of both the plant and its inverse (minimum phase systems), the range of controllable plants that use this strategy is reduced, especially for discrete time systems. Also, performance must be specified using a reference model, therefore, even if the model is feasible, the controller required to achieve these specifications may not be.

Although different solutions have been proposed to overcome some of these limitations, as discussed in [24] or [25], direct adaptive control cannot always be used. Find a detailed description of direct adaptive methods in [26].

Unlike the direct approach, indirect (or explicit) adaptive methods use current plant parameter estimates to determine controller parameters using a tuning method. This allows for a wide variety of control laws and plant estimation combinations. However, a previous system identification is always required.

Regarding parameter estimation, the general idea is based on an adjustable plant model to compare predicted and actual output. That difference is used by a model adaptation algorithm to minimize this error, so that a correct description of the plant is achieved asymptotically for the current sequence of inputs and outputs. See [27] for a summary of current parameter estimation methodologies.

Once the plant parameter estimation convergence is solved, which is indeed a critical issue for indirect adaptation schemes, literally any tuning method based on a plant model can be used. That leads to the second main contribution of this thesis, a novel fractional adaptive control scheme based on the previously described tuning method.

Given the high computational requirements of currently existing tuning methods, all fractional adaptive strategies are direct, using fractional reference models, but keeping integer order in adaptation algorithms and controllers. This thesis describes and demonstrates how an indirect adaptive strategy can also be used in a fractional order controller. The key is that all tuning operations can be carried out within a sampling period thanks to the efficiency of the new proposed method. This is considered one of the major contributions of this thesis.

1.1 Background

The existing solutions to the problem of parametric uncertainty raised above are very diverse, from the simplest proportional integral derivative (PID) controller, to the latest control techniques, each with its pros and cons.

PID controllers are very simple and inexpensive, which is a great advantage when it comes to implementation, but the results are not so impressive. Advanced controllers can be very effective, but also difficult to implement, and often require special equipment or advanced skills.

Midway between these two ends, other techniques are available, which are also very efficient in solving the problems described. For example, the solution proposed from the field of robust control is to make the final system resistant to changes in the parameters through a controller designed to minimize the impact of those changes.

The two problems addressed here are uncertainty and variability of system parameters, generally known as parametric uncertainty. In classic control theory, these parameters refer to coefficients of the transfer function, as in:

$$\frac{Y(s)}{U(s)} = G(s) = \frac{b_{nb}s^{nb} + .. + b_1 s^1 + b_0}{a_{na}s^{na} + .. + a_1 s^1 + a_0}, \tag{1.4}$$

or the place of system poles and zeros in the s plane as follows:

$$\frac{Y(s)}{U(s)} = G(s) = k\frac{(s - o_1)(s - o_2)..(s - o_{no})}{(s - p_1)(s - p_2)..(s - p_{np})}. \tag{1.5}$$

Note that differences in plant and model coefficients may be due to an incorrect modeling or also to plant time variability.

On the contrary, non-parametric uncertainty refers to those behaviors that are not considered in the model, but that exist in the actual system. This can happen due to unmodeled dynamics, truncation of high frequency modes, or non-linearity.

Although robust controllers are known to cope with both types of uncertainties, the objective of the robust controllers considered here is to provide robustness to parameter variations due to modeling uncertainties or plant changes during system operation. Non-parametric uncertainty will be addressed later in this work through the use of adaptive strategies.

1.1.1 Parametric robustness

The robust control concept is based on achieving desired design performance despite potential plant changes. Although the idea is very simple, a wide range of solutions are possible, from a basic robust PID control as in [28] or [29] to more advanced

works such as the sliding mode control shown in [30], or the methods described in [31], based on applying non-integer calculus to PID controllers.

A commonly accepted consensus on robust control origins, place it in the feedback stability analysis works by Harry Nyquist [32] and Hendrik Bode [18], where the ideas of stability or gain and phase margins were introduced.

Based on these concepts, the most widely used robust control approach was devised. Since feedback behavior depends on open loop system parameters such as phase margin and crossover frequency (see [33] for details), a system that maintains these values static should display a closed loop constant behavior despite parameter variations. For example, the closed loop metrics that are directly dependent on it, such as overshoot, will remain constant. This is generally known as iso-damping, and is a generally desired feature of robust systems. For example, consider the following Bode's ideal transfer function:

$$G_1 = \frac{1}{s^{1.5}}, \tag{1.6}$$

which has a constant phase margin at all frequencies. As shown on the left side of Fig. 1.1, any variation in system gain will result in the same phase margin, resulting in the constant overshoot on the right side of the figure.

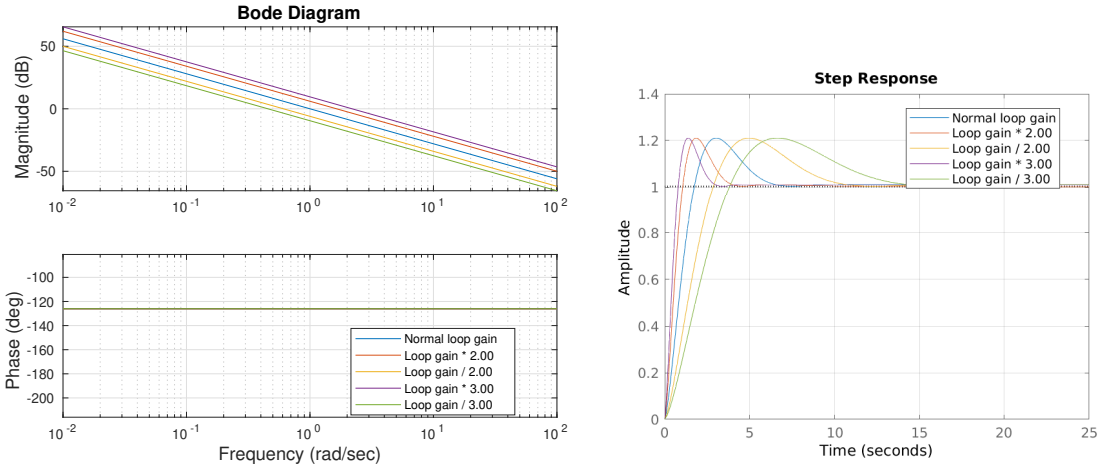

Figure 1.1: Open loop Bode diagram and feedback time response for Eq. (1.6) example system showing constant overshoot despite gain variability (iso-damping).

Note that, due to different crossover frequencies, other metrics such as peak or settling times actually change.

A fractional exponent in the Bode's ideal transfer function is needed to allow the phase margins to be different from 0 deg and 90 deg, which is why many authors consider the works in [18] as the beginning of the development of the fractional order

control field. Likewise, chapter 2 will show how fractional controllers bring significant benefits to robust system design using this approach.

Although the usual physical systems considered in control engineering are far from being robust in the sense described, a controller that keeps these values constant is possible, which means that we can improve the robustness of the system by using a convenient controller. This is the approach commonly followed in fractional order control.

Many works like [34], [31], [35], or [36], to name a few, use flat phase specification in open loop as a robustness constraint in robust controller design. Its formulation is shown in the following equation:

$$\left(\frac{d(\arg\left(C(j\omega_{gc})G(j\omega_{gc})\right))}{d\omega}\right)_{\omega=\omega_{gc}} = 0. \tag{1.7}$$

The flat phase specification in Eq. (1.7) will ensure that changes in plant gain will not change the open loop phase around a frequency of interest. As described before, thanks to the similar phases for different gains, the system response will show a constant overshoot despite the gain variations.

1.1.2 Performance specifications

Apart from robustness, other specifications should be considered for controller tuning. Since the robustness constraints are best described in the frequency domain, it is common for the rest to be specified in the same way, and the same approach will be used in this thesis.

As discussed above, the frequency domain design specifications are based on the phase margin and crossover frequency features of the open loop frequency response. These are related to closed loop features such as bandwidth frequency and resonant peak height, which in turn are related to transient time response properties such as overshoot and peak time. Table 1.1 shows a summary of the most common constraints used in the frequency domain performance specification.

Physical meaning	Effect defined	Closed loop specification	Open loop specification
Damping ratio	Overshoot	Resonant peak dB	Phase margin
Response speed	Peak time	Bandwidth	Crossover frequency

Table 1.1: Equivalence between frequency specifications and time response.

These correspondences are often complex formulas (see [37]), therefore, a common practice is to specify performance directly in terms of open loop variables which is

easier, knowing the expected time response results. For example, the curves shown in 1.2, obtained from [37], allow to find the phase margin from any desired damping ratio, and approximate the bandwidth frequency (i.e., the time response speed) from the open loop gain crossover frequency.

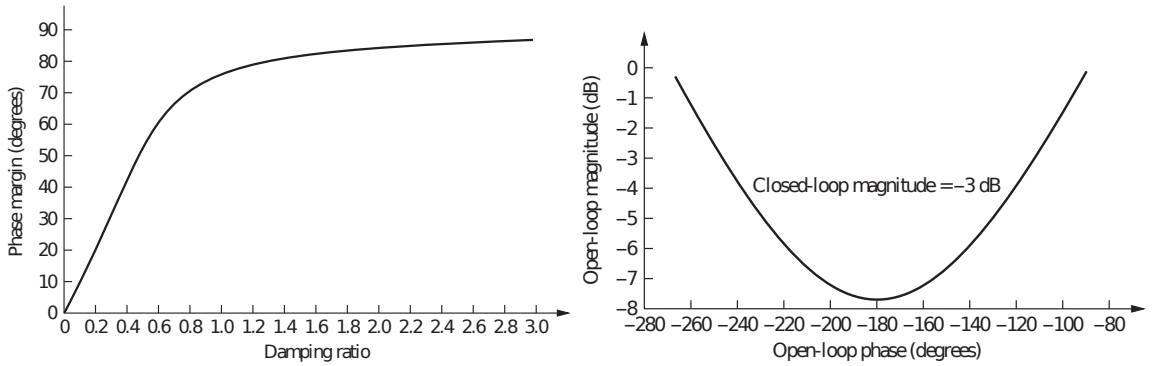

Figure 1.2: Curves showing relationships between phase margin and damping ratio (left) and between bandwidth frequency and crossover frequency (right). Source: Norman S. Nise, Control Systems Engineering.

Therefore, in related works such as [29] and [38], the usual control specifications are crossover frequency (ω_{gc}) and phase margin (ϕ_m). As stated, the first is related to the system responsiveness (peak time) and the second to stability (overshoot). Equations (1.8) and (1.9) formulate these specifications, respectively:

$$|C(j\omega_{gc})G(j\omega_{gc})|_{dB} = 0\,\text{dB}, \tag{1.8}$$

$$\arg\left(C(j\omega_{gc})G(j\omega_{gc})\right) = -\pi + \phi_m, \tag{1.9}$$

where $C(j\omega_{gc})$ is the controller frequency response at ω_{gc}, $G(j\omega_{gc})$ is the plant frequency response at ω_{gc}, and ϕ_m is the desired open loop phase margin for the controlled system.

Once the gain crossover frequency ω_{gc} and the phase margin ϕ_m are selected, a set of three nonlinear equations with three unknowns must be solved to find the controller parameters.

Since the standard design is based on the general second order model shown in Eqs. (1.10) as follows:

$$G(s) = \frac{\omega_n^2}{s(s + 2\xi\omega_n)} \tag{1.10a}$$

$$F(s) = \frac{\omega_n^2}{s^2 + 2\xi\omega_n s + \omega_n^2}, \tag{1.10b}$$

only two parameters (ξ and ω_n) can be defined.

Therefore, the usual performance specifications are based on the last two constrains defined in Eqs. 1.8 and 1.9. Considering more constraints would require more adjusting parameters, and, since plant conditions are normally fixed, a controller with sufficient setting parameters is required.

Considering three constraints, a robust design using reduced PID variants such as PI or PD is not possible due to the reduced number of parameters, unless one specification is dropped, or another parameter is introduced as in fractional control. A controller having at least three adjusting parameters will be needed in order to meet the three requirements discussed.

1.1.3 Robust control

The simplest first type of controller that we can use to meet robust constraints along with performance specifications is the standard PID controller. Although their control parameters are sufficient to achieve specifications defined in Eqs. (1.8), (1.9) and (1.7), their integer nature with fixed asymptotes and slope, makes it difficult to meet these three requirements at the same time.

It will be shown in chapter 2, that controller and plant slopes must be opposites at the crossover frequency to fulfill Eqs. (1.9) and (1.7) at the same time, therefore, the results are restricted to a series of conditions for the plant and specifications. For example, chapter 2 shows how small plant slopes will force the controllers to have phases close to -90, 0 or 90 deg. The possible specifications are then reduced to the cases where the equation solution is possible, which is a reduced set of the possibilities described in the previous section 1.1.2. Therefore, using a PID controller leaves some performances out of scope due to controller limitations.

Despite these limitations, the simplicity of PID controllers implementation makes them very attractive, and therefore several works attempt to get a robust performance using them, but the result is always restricted to certain plant types, and often require specific conditions or limited specifications.

For example, in [28] a Bode's ideal transfer function is used as the performance specification model, and then a minimization method is used to obtain the parameters that best approximate the step response of the model. Works like [39] and [40] deal with the robustness problem also by optimizing a PID controller, with similar results in different plant types.

In [29], the relay method is used to obtain the plant parameters, and then a set of rules derived from Eqs. 1.9, 1.7, and a particular constraint, are used to find

the PID parameters that make the system robust. The drawback of this method is that crossover frequency can not be specified, which restricts the number of useful specifications.

Among the tuned controllers in [1], a PID is considered for comparison, and is tuned by the numerical solution of Eqs. 1.8, 1.9 and 1.7. The result, in addition to losing a parameter by producing a zero solution for the derivative gain, is only possible by relaxing the constraint in Eq. (1.7), resulting in a system whose phase is not completely flat.

All the aforementioned works must restrict the controlled plants or the specifications reached to cope with the limited PID robustness possibilities. A solution to these limitations while keeping the PID controller structure, and almost all simplicity, is discussed below.

1.1.4 Fractional order controllers

A better approach to satisfy Eq. (1.7) is fractional order control. When the derivative and integral exponents are allowed to be non-integers, additional degrees of freedom can be used, making it possible to meet more specifications. So, a fractional order PD (FOPD), shown in Eq. (1.11), or a fractional order PI (FOPI), shown in Eq. (1.12), can be used to grant all three control specifications:

$$C(s) = k_p + k_d s^{\mu}, \tag{1.11}$$

$$C(s) = k_p + \frac{k_i}{s^{\lambda}}. \tag{1.12}$$

As chapter 2 will show, the key advantage of fractional calculus in robust control applications is the astonishing variety of frequency responses that a fractional order system can provide. For example, the final phase (at the asymptotic curve) of a fractional derivative can range from 0 deg to 90 deg while the exponent ranges from 0 to 1, while the phase of integer first order derivative has a fixed value of 90 deg. This feature allows fractional controllers to shape any open loop system with a flat phase around a specified frequency, as discussed above, achieving robustness around that specified design frequency.

The large number of contributions using fractional controllers to solve the robustness problem in control reveals the convenience of this approach when it comes to finding controllers capable of meeting the above robustness requirements. Some works use root locus analysis for the fractional controller tuning (see [41], [15]), but most current methods are based on frequency analysis, probably due to its straightforward generalization from integer calculus and its convenience in robust controller

design. According to [42], the existing frequency-based tuning methods for fractional controllers can be classified into three groups:

- Analytical: Solving the constraint equations for controller parameters. This group needs the solution of equation sets for controller tuning. Since these equations are often nonlinear, a numerical solution is generally needed, but the problem formulation remains analytical. A good example of this approach is found in [31].

- Numerical: Finding controller parameters by optimizing selected fitness functions. The numerical approaches used in fractional order controller tuning are based on different optimization methods. Some of them are:

  Particle swarm optimization (PSO) described in [43],

  Artificial bee colony (ABC) as in [44],

  Cuckoo search (CS) from [45], or

  Differential evolution (DE) stated in [46],

  but literally any method can be used to find the controller parameters. Some examples using optimization algorithms for fractional controller tuning can be found in [47].

- Tuning rules: Formulas that define controller parameters based on fixed conditions. Through these methods, only a certain set of specifications is possible, the same set that is used to calculate the formulas, so their application is very restricted, and can often only provide approximate results. Find an example of fractional controller tuning rules in [39].

Recent developments that explore the use of iterative methods for parameter tuning, are found in [22], but only some parameters are solved in this way, and the flat phase specification is still solved by optimization. Therefore, we could still place this approach within the category of numerical methods.

See [42] for a more detailed description of current fractional tuning methods.

Some recent works have proposed an alternative apart from this classification. Graphical equation solving methods (linear and nonlinear) have gained a lot of attention in the field of fractional order control. It avoids the problems of numerical solvers, but current proposals that follow this approach are based on highly complex graphical representations, and require a complete restart of the algorithm if the control requirements or problem conditions change.

This thesis addresses these problems mentioned above through a fractional-order control design methodology presented in chapter 2. It provides full tuning of any FPI or FPD controller based on the specifications defined by Eqs. 1.8, 1.9, and 1.7. Once

the desired loop phase margin and crossover frequency have been selected, a series of steps ensures the resulting controller robustness through an intuitive graphical representation of the iso-slope curves showing all possible controller tuning possibilities.

Although the robust fractional controllers discussed above are appropriate for linear time invariant (LTI) systems, they experience limitations when the controller is used in time variant (LTV) or nonlinear (NLTI). The problem is that the fractional controller is fixed and designed for a specific plant, and therefore, the robustness range is limited to that specification. When plant parameters change beyond some point, the robust control steps out of the range, and the robust performance is weakened.

A useful method to address this plant parameter variation problem is adaptive control. The different controller designs using this approach are described below.

1.1.5 Adaptive controllers

Adaptive control addresses uncertainties and plant variability through the analysis of system inputs and outputs. Tracking the plant model changes, they can adapt the controller so that final system performance remains unchanged.

This field has attracted the interest of many researchers around the world, resulting in a large number of contributions and many adaptive schemes with different approaches. Modern adaptive control systems may be classified into the following groups:

- Open-Loop: This method uses the values of environment variables for the controller adjustment, based on previous plant knowledge and the desired performance. Therefore, it is called open-loop, because it is not dependent on current system performance but on the variables chosen. A good example of this approach is gain scheduling control, in which the controller parameters are found in a table (schedule) depending on the environment measured variables.

- Multiple Model Switching: The idea behind this approach is to update the plant model by choosing it from a previously identified model list. A separate block, usually called supervisor, is in charge of selecting the model that best matches the system's current response and set the controller accordingly. There are some similarities with open loop adaptive control in the sense that controller calculations can also be performed offline, resulting in a gain scheduling method based on system response rather than an environment variable.

- Direct: Also called implicit. This approach is based in the performance defined by a target model. The current system output is compared with this target model performance, then, the error is used to adjust the controller so that the resulting system performance is as close as possible to the target model. The

flagship example of this method is the model reference adaptive control (MRAC) method.

- Indirect: Also called explicit. The concept underlying this kind of control is not difficult. Given an on-line identification method providing a plant model, and a controller whose tuning is based on the previous model and performance specifications, applying the tuning method to an up to date plant model will bring the resulting system up to specification despite plant changes. This idea was originally introduced by Rudolf Emil Kálmán in [48].

The aim of this introduction is not to provide a detailed list, but to show that the ways in which this objective can be achieved are very diverse, although they still have common elements.

Since all of them depend on system identification, a common drawback of adaptive systems is that the time required for model parameter stabilization may be long, which makes adaptive systems unable to track rapid variations.

The speed of parameter change is not important in robust controllers, as long as these variations fall within the operation range.

Therefore, by combining these two systems, an adaptive robust controller can address both problems. The main problem of adaptive systems can be addressed with a robust controller and the drawbacks of time variability can be addressed by applying an adaptive scheme.

The application of an adaptive scheme in combination with robust controllers, is usually known in the literature as adaptive robust control. This topic will be described next.

1.1.6 Adaptive robust control

Combining a robust controller with an adaptive control method, the robustness properties can be improved by extending its operation to LTV or NLTI systems, resulting in a system with stable performance in the presence of rapid plant variations and able to cope with long-term plant variability.

When the robust controller used has a fractional order, it is known in the literature as adaptive fractional control. Although this approach has only recently been discovered, the large number of contributions suggests a broad interest from the control community in combining the robustness of a fractional order controller with the flexibility of adaptive control.

In the second part of this thesis, the fractional order controller tuning method detailed in the first part (iso-m) will be improved using continuous adaptive methods. This method is not based on a reference model, but rather on performance specifications, thus it is included in the classification of indirect adaptive methods, keeping

the benefits of a performance-based controller tuning while extending its capabilities to LTV and NLTI systems. There is no similar approach found in the literature.

In the next section, we will discuss a summary of current solutions to the uncertainty problems discussed above, and the control approaches proposed to deal with them. A discussion of early and current proposals in the fields of fractional, robust, adaptive, robust-adaptive, and adaptive-fractional control applications are shown.

1.2 State of the art

Most control systems deployed today in industrial applications are based on proportional integral derivative (PID) controllers (see [49]). The mathematical description of a PID is based on a differential equation that relates the input error signals to the control signal as shown at Eq. (1.13).

$$PID(t) = k_p e(t) + k_i \int_0^t e(t) + k_d \frac{d}{dt} e(t), \tag{1.13}$$

where $e(t)$ is the measured error obtained through negative feedback, and $PID(t)$ is the control signal produced by the PID controller.

That well-known integral and derivative operators used in Eq (1.13) are attributed to the renowned scientists Isaac Newton and Gottfried Leibniz.

During the early days of infinitesimal calculus, another field arose from Leibniz's idea of using non-integer exponents in a derivative operator. At this point, the basics of fractional order calculus were settled.

Despite this early start, it fell into oblivion for many years, as no direct application was found. Then, new breakthroughs in physics required a new advanced modeling tool, more accurate than classic calculus. The usual integer modeling was found to be not accurate enough to define some systems in physics and materials science, and a straightforward solution was found using non-integer calculus.

1.2.1 Fractional order systems

The fractional order calculus was then rediscovered to provide a better mathematical description of recently discovered physical phenomena, such as abnormal material relaxation of viscous-elastic materials, and to improve the accuracy of the old ones, such as heat diffusion. Since then, it has been successfully used in very different fields, from economics, for example in [50], where the fractional order model of an economic system is used, to physics, for example in [51] where the use of fractional order models for anomalous relaxation processes is proposed.

Fractional order system modeling has also found applications in control engineering, as shown in the works of [16], which proposes a fractional model of a DC motor,

and that of [17], which uses a fractional order model of a synchronous motor belonging to a servomechanism, reporting a significant improvement in accuracy versus the integer order model. A more theoretical approach is found in [52], where simulations of the dynamic properties of fractional order systems are shown using numerical and analytical methods.

However, the main engineering application of fractional calculus is undoubtedly the design of robust controllers.

1.2.2 Fractional order controllers

The reasons leading to the discussed PID controllers widespread are their simple implementation and the large number of easy tuning methods available. Nevertheless, this simplicity has its drawbacks.

Although PID controllers perform very well in many well-defined linear time invariant (LTI) systems, more advanced control techniques are needed when the plant exhibits different problems such as non-linear behavior or time variant properties.

Although every model has some degree of uncertainty, most common control engineering applications that show these problems are nonlinear and time variant systems. A perfect solution for the extension of the classic control functionalities while maintaining a good amount of its tools and simplicity is found in fractional order controllers (FOC).

One of the first proposals that uses fractional calculus and robust systems together is the "Commande Robuste d'Ordre Non Entier" (CRONE) system. It was first described in [19], followed by two revisions and currently in its third version (see [53]). The CRONE system not only solves the controller tuning problem, but it also addresses the implementation of fractional operators, which is still an open topic today. Subsequently, in [54], the fractional derivatives and integrals (FDI) control was proposed, where trial and error tuning showed superior performance compared to variable structure controllers (VSCs).

The Fractional Proportional Integral Derivative controller (FOPID or $PI^{\lambda}D^{\mu}$) was later introduced by Podlubny in [55], establishing a baseline that was supported initially by many contributions. Although this extension of the ubiquitous PID controller is by far the most widely used today, the possibilities for defining fractional controllers are broader, as showed in this survey by Xue [56] in 2002, where four different fractional order controllers, including CRONE, lead-lag, fractional order PID, and tilted-integral-derivative (TID) controllers are compared.

Nevertheless, most contributions address fractional controllers as a generalization of the PID controller. This is probably due to the simple control law and strong similarities to the ubiquitous PID controller, allowing classic design tools to adapt from integer to fractional exponents.

Based on this scheme, a flexible joint manipulator control was successfully addressed in [34], featuring a tuning using frequency specifications. Later, in [31], one of the most popular tuning and auto-tuning approaches of such controllers was proposed, which included a comprehensive experimental study, followed by the proposal of implementation of these controllers in commercially available hardware in [38].

Since then, after these initial steps, the field of fractional robust control has received a lot of attention, mainly from the fields of robotics and automation, and the automatic guided vehicle.

In the world of automatic guided vehicle (AGV), recent studies (see [57]) have shown how integer order controllers have performance limitations related to some control requirements. As discussed before, fractional order controllers provide a good balance between dealing with a more demanding control structure while maintaining simplicity and easy tuning capabilities, therefore, some proposals use them to avoid the limitations of this integer order controller.

For example, in [58] a FOPID controller is used for parking maneuver lateral control, and a fractional controller is explored in [59] where the relationship between vehicle speed and fractional order of the controller is considered.

Cruise control systems are also good candidates for robust controller implementation, as system parameters use to change, for instance, when different slopes are found in the road. For example, a fractional order proportional integral (FOPI) controller is used in [60] for speed control of a gas-propelled vehicle, and in [61] a hybrid fractional controller is used for adaptive cruise control (ACC) of low speeds.

In the field of automation, some important works are, for example, the DC motor feedback fractional controller proposed by [35], [62] and [63] to name a few. For further reference on fractional control applied to electric motors, find a survey in [47].

Regarding the application of fractional control in robotics, the work in [64] is devoted to the fractional control of a legged robot, later works such as [36] and [4] show the application of fractional controllers to service and humanoid robotics.

An emergent field showing non-linearity issues is soft robotics, where material properties show a high non-linear behavior due to the presence of plastics and rubbers. In recent years, an increasing number of robust soft robotics applications have been proposed. These systems show significant control complexity due to the non-linear properties of soft materials, but in works such as [65] or [1], a successful robust control of the nonlinear soft link of a robotic soft neck has been reported through the use of fractional order controllers.

But fractional control is not exclusively applied in Robotics and AGV. Some other contributions are, for example [66] in the aerospace engineering, or the wind turbine robust control in [30] and the power plant fractional fuzzy controllers of [67] in the field of energy.

There are still many open problems to solve in the fractional order control field, but

the principal current issues are the implementation of fractional order operators, and the controller tuning. Implementation is a more mathematical issue, and is outside the scope for this engineering thesis, but a very detailed description of the problem can be found in the books [12] and [42]. A good introduction to the controller tuning problem can also be found in these books.

However, this thesis approach is centered on the controller tuning problem. A summary of the current approaches available for fractional order controller tuning is provided below, followed by a discussion on recent and past contributions.

Although some works address fractional controller tuning using root locus like [41] and [15], most methods are based on frequency analysis, probably due to their straightforward generalization of integer calculus and their convenience in robust controller design. According to [42] the existing frequency-based tuning methods for fractional controllers can be divided into three groups:

- Analytical: Solving the constraint equations for controller parameters
- Numerical: Finding controller parameters through optimization of selected fitness functions
- Tuning rules: Formulas defining controller parameters that roughly meet control specifications

Examples of the analytical approach can be found in [31] and later works, such as [35], [36], or [68]. This option requires the solution of equation sets for controller tuning. Since these equations are often nonlinear, a numerical solution is often needed, but the formulation of the problem remains analytical, and these methods are still considered in the first group.

Numerical approaches used in fractional order controller tuning are based on different optimization methods. One example is, for instance the work in [63], using the PSO algorithm to find the controller parameters for a DC motor robust control scheme. Other works like [62], use an ABC algorithm for tuning a fractional controller in a speed control scheme. A similar approach with CS algorithm is used in [69] for controller tuning of an artificial muscle actuator, and in [70] to find the controller gains in a six-degrees of freedom under-actuated system. More examples are available at [67] or [71], and a comparative study of fractional order controllers tuned by optimization algorithms can be found in [47].

Finally, tuning rules can also be used on fractional controllers like in [39], but they can only provide approximate results and their application is restricted to a limited number of plant types.

Recent developments have explored the use of iterative methods for parameter tuning, as in [22], but only some parameters are solved in this way, and the flat phase specification is still solved by optimization.

An important drawback of classic tuning methods found in the literature is their computational complexity, which is addressed mainly through numerical or optimization methods as discussed above. Although they can be very accurate, numerical and optimization solvers are highly dependent on initial conditions and tend to get stuck at local minima, therefore, they often need some trial and error or additional information.

This problem has been solved in very different ways. For example in [31], an elegant solution was proposed, using an integer tuning method as a first approximation to the fractional order controller parameters. In this way, the initial conditions are close enough to the final solution, and the problem of convergence is solved. Also, narrowing down the possible solutions, as proposed in [72], can help, but even so, the numerical solution of nonlinear equations is tricky and computationally complex.

To avoid the numerical solver, some authors have proposed a graphical solution to the controller tuning problem, such as [73], [21] and [23]. In that works, the plots of selected controller parameters are drawn on the same graph, based on the constraint equations. Finding the curve intersections will show what parameter values satisfy all the equations at once. This approach avoids the complex numerical solution described before, but requires a new plot for each controller tuning. Therefore, start over is needed in the event of changes in control requirements or plant parameters, and the implementation in a computer algorithm is difficult, as the curve intersection must be found through visual inspection.

This reveals another drawback of the current approaches. During the application of these previous methods, no information about the result accuracy is provided, and there are no directions on how to reduce the error. A different approach, providing information on the contribution of each parameter to the final loop performance could contribute to the state of the art and solve this problem.

In this thesis, an approach having all these features is proposed. The tuning method for fractional order controllers described in chapter 2 provides a great insight about the tuning process while avoids the use of numerical solvers. The resulting nonlinear equations are arranged in a way that provide an important insight about the tuning process, and allow the solution through many methods. Among them, the graphical approach is highly recommended, because all possible controller tuning possibilities are shown at a glance in the graphs, offering a great understanding of the tuning process.

This method is based on the specifications defined by Eqs. 1.8 and 1.9. When the desired loop phase margin and crossover frequency are specified, a series of steps provides the required controller parameters in order to have a robust behavior according to Eq. 1.7.

Unlike other methods shown in the literature, equations and curves have been

arranged in such a way that the fractional controller tuning can be done in a very intuitive and simple way, since a designer can observe the effects of parameter variations graphically and change the controller accordingly to reduce the error.

This not only makes it easier to tune the controller parameters, but also avoids problems related to local minima. Therefore, the method adapts easily to any type of system dynamics, which is ideal for promoting the widespread adoption of fractional controllers.

Since the computational effort is drastically reduced compared to the aforementioned methods, this approach can be implemented in low power embedded hardware platforms, reducing weight, energy and cost, making it an optimal solution for robust control embedded applications.

Although fractional controllers are suitable for time variant (LTV) or non-linear (NLTI) systems, their application has some limitations. The problem is that they are designed for a static system, so the range is limited to that particular specification. When plant parameters exceed a certain value, the control design becomes unreliable, weakening robust performance. As discussed earlier, adaptive control is often proposed as a solution to this problem.

1.2.3 Adaptive control

Adaptive control is a popular method for addressing the parametric uncertainty. With this approach, plant uncertainties and variability are addressed through system input-output analysis and identification, with the goal of controller re-calibration to ensure consistent final performance.

Therefore, the essential component of an adaptive approach is system identification. The entire algorithm is based on the characteristics of that component, and especially on its convergence and stability properties. An excellent description of modern system identification algorithms is available at [27].

Although there are many options available for system identification with impressive parameter estimation results, convergence and stability problems are much more critical in adaptive systems, therefore, in many approaches a very simple system identification algorithms like the least squares algorithm is used.

This algorithm is usually attributed to Gauss for his "method of calculating the orbits of celestial bodies", but in Legendre's previous book [74], the basis was already established. Its excellent properties converted this method in a standard with numerous revisions and variations. One of the most used is the recursive least squares (RLS) identification algorithm, which is the choice for the adaptive system described in this thesis. For references on recursive least squares and similar algorithms see [75].

Having a reliable system identification, there are many ways in which adaptive

properties can be achieved in a system, leading to a variety of adaptive control strategies.

During adaptive control inception around the 1950s (see [76]), many adaptive schemes were described using different approaches, including works with the relevance of [48] by Rudolf Emil Kálmán. Since then, this field has attracted the interest of many researchers around the world, which has generated numerous contributions.

As discussed before, adaptive control systems can be classified in four groups: Open-Loop, Multiple Model Switching, Direct and Indirect.

- Open-Loop: The values of some environment variables are used for controller tuning, but the system performance is not considered. For example, gain scheduling control.

- Multiple Model Switching: A model is selected from a list by the supervisor block based on the current response and is used for controller tuning accordingly. Similar to the previous scheme, but based on the system response instead of the environment variable.

- Direct: Performance based on a target model. The controller tuning is carried out so that system performance is as close as possible to the target model. This method is also called implicit in other classifications.

- Indirect: Based on system identification and a general controller tuning method. Keeping control specifications constant, the resulting performance should be similar despite plant changes. This method is also called explicit in other classifications.

Apart from the above classification, some recent works have introduced artificial intelligence systems to solve different direct adaptive control problems, for example, in [77] a neural network is used to find the near-optimal control signal during a gravity compensation task of a two-link flexible-joint robot, and then the results are compared to different control schemes, showing the new approach advantage.

Some recent works using adaptive control strategies are provided below.

Open-Loop adaptive methods were developed during the beginning of high altitude plane flights in the past century. Gain scheduling control systems were used to solve the problem with changing flight conditions due to different airplane altitudes. Examples of current applications in robotics are the feed-forward control schemes in the works of [78], where an invariant performance is achieved for different inclinations in a humanoid robot with a gain scheduling method, or the proposal in [79], where a model predictive control and a gain scheduling control are used to obtain invariant push recovery behavior in a wheeled humanoid robot.

Multiple model switching was developed together with the open-loop adaptive method. Both methods have many similarities, but an important difference is the concept of supervisor block. Some examples of this approach applied in industrial systems are found in [80] and [81]. During the development of artificial intelligence around the 1980s, new supervisor options appeared, and proposals such as [82], using fuzzy logic, or [83], based on neural networks, were developed. Some recent works using this method are [84], [85], [86], and [87].

Direct adaptive control beginning could be placed in the past century fifties decade. Early works on direct adaptive control can be found in [88] where the popular model reference adaptive control approach (MRAC) was proposed .This was soon followed by [89], where a method based on least squares and pole placement design was described. Later, in [90], it was reported computational speed improvements compared to indirect schemes due to a double system identification algorithm. Find a detailed survey on initial direct adaptive works in [91].

Today's works following this methodology are, for example, [92], where a robot gripper grasps arbitrary solids using an adaptive algorithm based on slip and force sensor measurements, or [93], where a projection algorithm is used to enhance the MRAC turbulence isolation system precision and is compared to recursive least squares based RLS-MRAC and standard controllers.

Indirect adaptive control was also developed during the 1950s decade. Using a plant identification along with a general tuning method was originally introduced by Kálmán in [48].

The important work in [94] soon followed, changing to a more static approach, where the plant subject to adaptation has unknown parameters, but they are considered constant. Although the definition is not clearly stated, this static approach is generally known in the literature as self tuning regulators (STR). This work importance resides in the fact that also addresses the stability problem, a very important issue in adaptive control, through parameter convergence. Another important contribution in [95] soon followed on stability conditions for the RLS-based family of MRAC controllers.

Following closely, contributions such as [89] were proposed, using a pole placement technique together with RLS identification to propose three different direct and indirect adaptive control algorithms, including a discussion on the limitations of some direct methods and the similarities between both schemes. An important issue described in this paper is that direct methods using zero cancellation have a significant limitation on the minimum phase plant requirement. Therefore, the use of other controller tuning methods is recommended to avoid the problem. A good example of using this control scheme can be found in [96], along with a summary on stability conditions, a fundamental topic in adaptive control.

Thanks to its flexibility, contributions to indirect adaptive control are very diverse,

as literally any tuning method can be used since system identification provide with proper plant parameters. For example, in [97], the online adjusted neural network model of a system is used to train a neural controller for a specified target behavior. Both networks are models of a single hidden layer, and experiments report good tracking capabilities in linear and non-linear plants.

The controllers used can be quite advanced like the neural network proposal above, or very simple like in [98], where an RLS based piece-wise estimation algorithm is used to find the process parameters of a car engine catalyst, and then tune a PID controller in order to deal with parameter uncertainty as the catalyst ages. A similar example is the work presented in [99], where piece-wise linear models of an aircraft are estimated in case of damage, and a model reference controller is used to keep the impaired response as close as possible to normal conditions.

The above discussion is intended to provide an overview of past and current adaptive methods. See [100] for a more detailed description of the above classification. See also [101] for an overview of the adaptive control development from early works to current contributions and [102] for a detailed survey of different modern adaptive control applications.

Although adaptive systems can address any issue related with NLTI or LTV systems, there are some problems that affect this kind of controllers. The main drawback of adaptive systems is the long time required for model parameter stabilization, which means that adaptive systems cannot track rapid variations.

When the non-linearity of the system is small, or the plant changes are slower than the identification algorithm, this is not a problem. However, it is only applicable to very specific situations, such as parameter changes caused by system aging. A more general application for NLTI and LTV systems requires some additional considerations.

Fortunately, the robust control performance discussed in the previous sections is not affected by rapid system variations as long as they are within the operating range. Thus, on the one hand, the main problem of adaptive systems can be addressed with a robust controller, and on the other hand, the time variability drawbacks of robust systems can be addressed by applying an adaptive scheme. This leads to the combination of both methods to obtain a robust controller capable of coping with a wide range of time varying systems. The result is a system with stable performance in the presence of rapid plant variations and capable of dealing with long-term plant variability.

1.2.4 Robust adaptive control

This synergy was thoroughly studied some years ago by researchers such as Landau and Karimi, who used a multiple model adaptive scheme and a closed-loop output

error (CLOE) algorithm in [81] for the tuning of a set of robust control schemes, including CRONE and state feedback controllers.

Other more recent proposals are, for example, [103], which uses the sliding mode control (SMC) after a RLS based plant estimator to combine robustness with adaptability in one single system, or [104], where a recursive algorithm is introduced to identify an uncertain Wiener nonlinear plant and then used for a SMC controller adjustment.

If a certain type of controller is chosen to increase the system robustness of the adaptive scheme, a more specific field arises. For example fractional order control combined with an adaptive scheme leads to a field known in the literature as adaptive fractional control. In this case, the robustness properties of the fractional controller are improved by the adaptive system, allowing to extend the controller's operation to LTV or NLTI systems.

1.2.5 Adaptive fractional order control

This is a very recent field, but the large number of contributions suggests significant interest from the control community in a system that combines the robustness of fractional controllers with the flexibility of adaptive control.

Different authors have addressed the problem of fractional controller adaptation in very different ways. For example, in [105], a fractional pole is used in a Model Reference Adaptive Control (MRAC), improving the set of candidates to be used as a model, thus enhancing the set of specifications. In a similar approach, Ladaci [106] uses a different transfer function that also offers a new set of model candidates, naming the method as fractional order model reference adaptive control (FOMRAC) scheme.

In these approaches, the controller exponent is not part of the adaptation, resulting in a system that adapts the controller parameters to meet fractional specifications, but using an integer order controller.

A similar approach is used in [107], where an Internal Mode Control (IMC) scheme with a fractional parameter is applied. This approach features a non-integer exponent inside the loop, but it is still different from a fractional order controller adaptation, as no controller tuning is performed.

All the previous methods are based in a model reference approach, and despite using fractional order operators, they do not take full advantage of the adaptive fractional order controllers, since the control approaches they propose are either adaptive with an integer order controller, using a fractional order reference model, or FOC controllers with fixed parameters and an adapting filter.

The only approach found in the literature using an actual robust fractional order controller, tuned through an adaptive algorithm is the one proposed in [38]. In that

work, an initial identification based on the relay's algorithm is applied to obtain the current plant parameters, and then Monje's method [31] is used to tune the fractional controller. After tuning, the system enters the operational state, where no further identification or tuning is done.

Given that system identification is only available during the initial stage, any eventual plant changes deteriorate the controller performance, making the proposal useful for time invariant plants, but showing the same drawbacks discussed regarding robust controllers for LTV or NLTI plants.

In order to use the properties of robust fractional control in an adaptive scheme suitable for to LTV and NLTI systems, the controller should be re-tuned for any eventual plant changes. In this point is where all the previous approaches fail, as the current fractional tuning methods are too slow for that, several times slower than the real plant, making this approach impossible.

In [1] and Chapter 2, a tuning method with reduced computation efforts and very competitive performances results is described. Using this method, the controller tuning is possible inside a single loop during the plant operation.

This leads to the second proposal of this thesis; The improvement of the fractional tuning method from Chapter 2 through the use of adaptive methods, as described in Chapter 3. This method is not based on a reference model but on parameter specifications, therefore it falls within the classification of indirect adaptive methods, keeping the benefits of a performance based controller tuning.

1.3 Objectives

Given the drawbacks discussed in Section 1.1 regarding the existing methods, a workaround that addresses these issues may prove useful in the field of control engineering. The main objective of this thesis is to provide that approach and address the problems described.

1.3.1 Tuning approach for robust fractional order controllers

In the case of fractional order control, the state-of-the-art in section 1.2 describes how current approaches are often based on numerical methods and optimization, making the adjustment process difficult and unreliable.

The problems related to these solvers are well known. First, the initial conditions are critical to find a successful solution for the system, since the algorithm convergence depends on these initial conditions. And secondly, the local minima found during the execution of the algorithm can lead to incorrect solutions. Also, an expert knowledge of the solver is important to guarantee reliable results.

Although careful attention must be paid to the process to ensure a correct result, the solver does not provide any information on how the outcome can be improved, often resulting in a series of trial and error attempts. This requirement of a close process supervision limits its integration with other systems, such as adaptive control, and also makes it difficult to retune the controller in the event of a specification change. One valuable virtue of PID controllers is that parameter changes have a well-defined effect on the plant, allowing the controller to be retuned and fine adjusted to change the desired behavior. This is not possible using the current approaches available in fractional order controllers.

This thesis proposes a new fractional order control design methodology (iso-m) described in chapter 2 that combines the simplicity of a PID with the robustness of a fractional controller. The proposed tuning algorithm can be used to solve both problems described. The graphical solution of the proposed nonlinear equation avoids the problems of numerical methods of initial conditions and convergence. Additionally, it provides a single, straightforward solution for the fractional exponent value needed to meet the required performance specifications. Due to the particular layout of the graphics, a great deal of information is provided during the tuning process. The controller limits are directly observed thanks to the iso slope curves, allowing the designer to see all the control options for a given plant at a glance.

The graph also shows how the change direction of controller parameters to fit a single specification without affecting the others. This is particularly useful for mismatch correction and for controller fine-tuning, e.g., during equipment commissioning.

These features were evidenced in the experimental works shown in chapters 4, 5 and 6, and in the works published in the papers [4], [5], [1], and [3].

Specially in [1], a detailed description of the iso-m approach is given, and is completed by a step-by-step application example. Furthermore, the new method is compared with similar results from the implementation of different alternatives, including Monje's method [31] and with a PID designed by using the method described in [29].

In this research papers, the particular cases of FOPD and FOPI have been considered, since they are sufficient to meet all robustness specifications, while the complete FOPID controller can be considered in a future research if needed.

1.3.2 Tuning approach for adaptive fractional order controllers

Another advantage of the new proposed method for controller tuning is that all the parameters are bounded or computed using bounded functions, which is important for the application of adaptive techniques, as shown in Chapter 3. Nevertheless, the most relevant iso-m method property for its application in an adaptive scheme, is the minimal computing power required. This allows for an indirect (or explicit) adaptive approach using a fractional controller, which is unique at the moment, as no similar

approach could be found in the literature.

Current adaptive fractional methods show very limited use of fractional controllers, due to the significant computational effort required for tuning. This is why the new method is critical for the proposed fractional adaptive algorithm, since it allows the controller parameters to be recalculated in a tiny fraction of the time compared to current methods. Also, since the computations are extremely simple, they can be implemented on a standard computer without the need for specific hardware or software tools. The computer code written specifically for the experimental tests, available at `https://github.com/munozyanez/fcontrol` shows how the operations needed for the tuning are extremely simple. This code was programmed as a control library providing all functions that solve the necessary operations for both proposed control approaches.

The closest approach found in the literature using an actual fractional controller tuning method is described in [38].

Unlike the other adaptive fractional order methods, based in a model reference approach, this proposal is based on performance specifications and a specific tuning method. A system identification is run in the plant during initial calibration. Later, using that plant model, and a tuning method, the controller is adjusted in order to get the specified system performance. Therefore, this work fits within the category of self tuning regulators (STR).

STR approach is useful for time invariant plants, but, although it provides very good results applied to LTI systems, it has the same drawbacks stated regarding robust controllers for LTV or NLTI. In the event of plant changes during the system operation, the controller performance will be affected. For the adaptation to be valid for these systems, identification must be continuously done during system operation, usually known in the literature as online identification.

The scheme using online identification combined with some controller tuning method is known in the literature as continuous adaptation (CA). This approach is similar to STR, but with the difference of applying the adaptation during system operation. Therefore, when plant changes are detected, the adaptation scheme will update the controller parameters in order to keep the initial specifications.

The classic fractional tuning methods are very slow for this purpose, with computing times much longer than most plant's time constants, making a continuous adaptation approach impossible. The only way to use a fractional controller tuning inside a CA scheme is by means of a method fast enough to run in-line within the control loop. Having updated tuning parameters for every loop iteration, the STR can be turned into an adaptive CA system, extending its use to a broader range of plants, from totally invariant to time variant or non-linear.

Chapter 2 and the works in [1], show how it is possible to reduce the computational efforts while achieving very competitive controller performances, allowing application

of the tuning method in real time. Therefore, controller adaptation based on control specifications could be carried out during the plant operation, avoiding the constant plant parameters constraint of a self tuning regulator.

This proposed fractional adaptive control scheme is composed by:

- Identification algorithm
- Iso-m tuning method
- Fractional controller Implementation

Whether these three items can run in real time, a continuous adaptation is possible, resulting in the new adaptive method described in Chapter 3. The obvious benefit of this approach is the power to cope with time invariant plants, obtaining a robust and adaptable system, capable of dealing with plant changes and uncertainties at the same time.

Both new proposed methods can be useful in many applications, including the control of variant and non-linear systems, such as the three platforms proposed below for testing and validation. All of these plants share a common problem: uncertainty. However, their types are different depending on the system.

The first platform, an autonomous car, allows us to experience robustness in the presence of the uncertainty caused by load changes.

The second platform, the TEO humanoid robot, will allow to experiment with load changes in a system showing different kinds of non-linearity.

Finally, the soft neck, a challenge in robust control design, presents all kinds of uncertainties. On the one hand, the highly non-linear soft material presents a variety of elastic and plastic behaviors. On the other hand, the design and geometry of the neck cause plant parameter changes for the different tendon configurations. Because of that, it is particularly difficult to obtain a dynamic model and design a robust control for this system.

A summary of these platforms is shown next.

1.3.3 Experimental platforms

A short description of the three systems considered and their uncertainties is provided here, but a detailed description of each platform is provided along with the experiments and results at the end of the thesis, in Chapters 4, 5, and 6.

1.3.3.1 Autonomous car

The first system considered is the Hybrid Honda Accord 2014 autonomous car shown in Fig. 1.3.

Figure 1.3: Autonomous car proposed as a test platform.

This car is equipped with all the sensors and actuators needed for any task in advanced driving assistance systems (ADAS), and is available for researchers in the Lawrence Berkeley National Laboratory (US). One useful ADAS task currently under research is the ability to automatically control the accelerator and brake pedals simultaneously is known as adaptive cruise control (ACC).

ACC systems must maintain a desired speed similar to current cruise control systems, but if an object or vehicle is detected, the set speed must change to maintain a safe distance accordingly. Two control loops are usually needed in order to perform this task.

The high-level control is designed to adjust the distance to the vehicle in front, while the low level loop represents the system that manages the accelerator and brake actuators to follow a certain reference acceleration generated by the upper layer. The vehicle position and speed variables are fed back and used to define the desired distance.

However, it has been observed how the vehicle speed does not fully reach the reference, which is probably due to unmodeled dynamics. Other potential performance problems are changes in the mass of the vehicle or the slope of the road.

As a summary, parameter uncertainties in this system are:

- Changing payloads

These uncertainties will be solved using the robust fractional controller described in Chapter 2. All the tuning process, results and discussions are shown in Chapter 4 .

1.3.3.2 Humanoid robot TEO

Another controller testing platform considered is the Task Environment Operator (TEO) humanoid robot in Fig. 1.4, a robot built by the Robotics Lab team of the Carlos III University of Madrid.

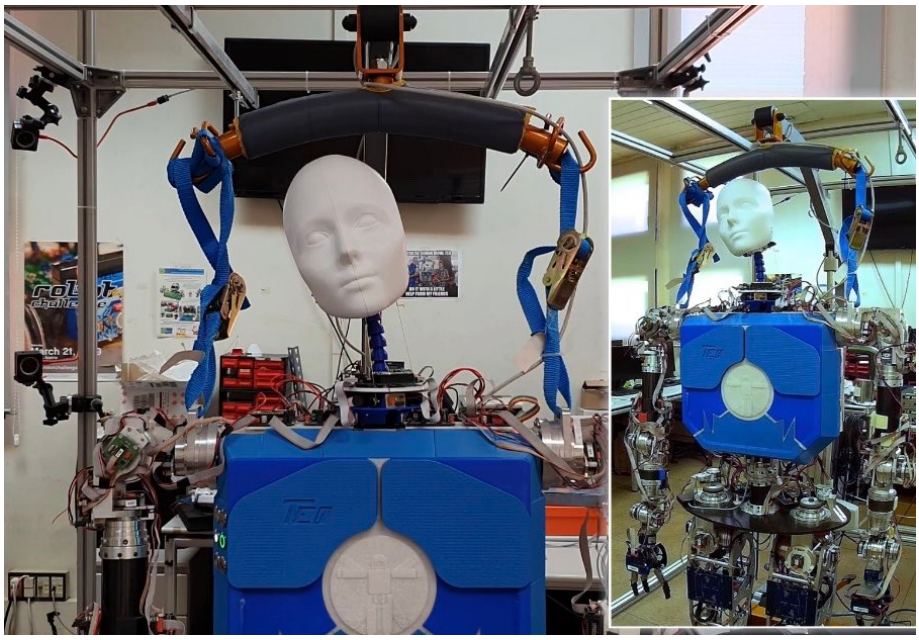

Figure 1.4: Humanoid robot TEO.

The parameters of the system are not unknown in this case, but there are two sources of uncertainty; Gravitational effects on robot forearm link and the changing payloads held by the robot gripper. The first issue causes plant model mismatches during operation, and the second affects the system gain.

Therefore, a fractional robust control on robot joints is proposed to avoid performance variability.

A complete description of the system, the tuning process, and a discussion of the results are provided in Chapter 5. Also, a comparison of the different robust control approaches and the system robustness to mass changes will be shown.

Two fractional order controllers (FPD and FPI), tuned with different methods are used in the robot forearm joint position control. The methods used for tuning are; The Monjes's method as described in [31], the ABC optimization algorithm from [44], and the proposed iso-m from Chapter 2.

As a summary, the uncertainties of the TEO elbow joint parameters are due to:

- Changing payloads

- Gravity effects

1.3.3.3 Soft robotic neck

The last platform considered is the soft neck described in [7] shown at Fig. 1.5.

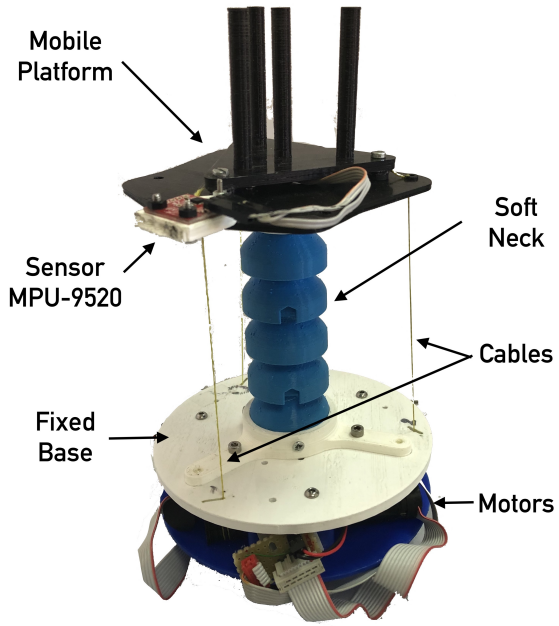

Figure 1.5: Soft robotic neck used for validation.

This robotic platform is an excellent test bed for robust and adaptive controllers, due to its inherent operational characteristics.

This robot system is designed to act as the neck of a humanoid. It is bio-inspired in the sense that it intends to replicate the same movement capabilities of a human neck. The central soft link acts as the cervical spine made of soft material, which is bent by three tendons, allowing any neck inclination and orientation to be reached.

Since we are talking about a neck, it must handle weights mounted on the humanoid head, such as cameras, electronics or whatever else is required. Therefore, a variable payload of up to 1000 g has been considered. It is expected to operate properly despite changes in load or tilt, with no change in performance, like a human neck.

The challenge is that even under constant payload, the force required to bend the central link increases with the bending angle due to the elastic properties of the material. Also, there are different effects of payload gravity based on mass and inclination. As a result, the different inclinations of the neck change the parameters of the plant.

Also, the models available in [6] and [7] provide only kinematics, and there is no transfer function available that describes the behavior of the soft link, making system identification a must.

As a summary, the uncertainties of the plant parameter present in the soft neck are due to:

- Unknown dynamic model
- Changing payloads
- Gravity effects
- Time variability

The proposed new adaptive fractional control system was used to address these uncertainty problems. Chapter 6 will show how robust and adaptive controllers outperform standard control in comparison.

1.3.4 Control problem

The problems found in these platforms are related to uncertainty as discussed above.

Since both the reference and perturbation signals are unknown, there is input uncertainty. The solution, both in classic and robust control, is provided through a feedback loop. All methods discussed in this thesis are based on this premise.

Furthermore, the described systems have changing loads or non-linearity, which makes the plant parameters variable or unknown, which is generally known as modeling uncertainty.

The problems of this type found in the previous plants are:

- Parameter variability
- Non linearity

The aim of this thesis is to describe two new easy-to-use methods for tackling these kinds of problems. In that direction, the theory of fractional order control is used to achieve system robustness to parameter changes, and the theory of adaptive controllers is used to provide the system with adaptability to time variability or

non-linearity problems. Two new methods, robust and adaptive, are proposed as a solution to this problem while addressing the drawbacks found in current alternative methods.

A wide range of systems can be improved by using the new robust and adaptive methods. For example, the applications of this thesis approaches in the control of the soft neck described in [7] had excellent results. Likewise, TEO humanoid robot, described in [108], and the autonomous car described in [3] show how effective and useful the proposed methods are.

The new methodologies are detailed in Chapters 2 and 3.

In order to assist in the description of the new methods, two example systems will be used throughout the document where appropriate.

1.3.5 Systems for theoretical validation

Two systems will be used as an example throughout the description of the algorithms proposed in this thesis. First and second order standard systems are very convenient for this, as they can be used to define a wide variety of systems to be controlled and present a wide range of possible tuning problems.

The standard models used in control engineering, described with Eqs. (1.10) have two defining parameters. To use the simplest possible example system with a full set of time response specifications, we will use the following values:

- $\omega_n = 1\,\text{rad/s}$,
- $\xi = 0.5$,

resulting in the following first order system:

$$G(s) = \frac{1}{s(s+1)}. \tag{1.14}$$

The frequency and time response of this system is shown below in Fig. 1.6

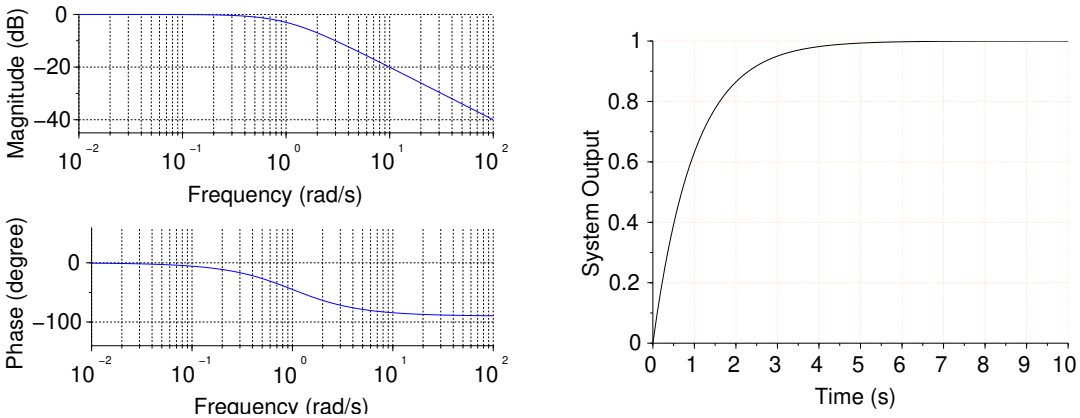

Figure 1.6: Frequency and time response of the first order example system.

Using an integrator and unitary feedback in the system described by the Eq. (1.14) results in the standard second order system definition described by Eq. (1.15).

$$F(s) = \frac{1}{s^2 + s + 1}. \tag{1.15}$$

The frequency and time response of this second order system is shown below in Fig. 1.7.

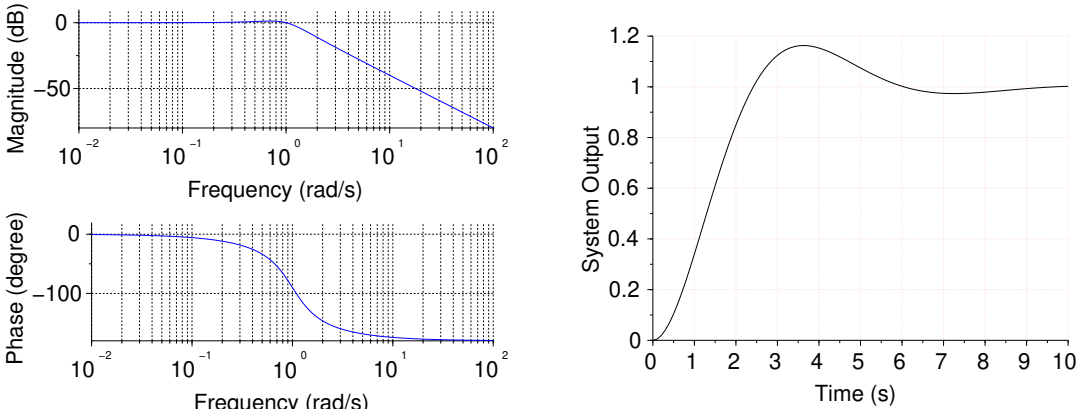

Figure 1.7: Frequency and time response of the second order example system.

These systems will be helpful in the description of the tuning methods proposed in Chapters 2 and 3.

1.4 Scientific contributions

During the development of this thesis the following research works were published:
A. Journals:

1. Muñoz, J.; Monje, C. A.; Nagua, L. F. & Balaguer, C. (2020), 'A graphical tuning method for fractional order controllers based on iso-slope phase curves', ISA Transactions. (Q1, Impact Factor: 4.305).

2. Flores, C.; Muñoz, J.; Monje, C. A.; Milanés, V. & Lu, X.-Y. (2020), 'Iso-damping fractional-order control for robust automated car-following', Journal of Advanced Research 25, 181 - 189. (Q1, Impact Factor: 6.992).

3. Mena, L.; Monje, C. A.; Nagua, L.; Muñoz, J. & Balaguer, C. (2020), 'Test Bench for Evaluation of a Soft Robotic Link', Frontiers in Robotics and AI 7, 27.

4. Muñoz, J.; Monje, C. A.; Casa, S. M. d. l. & Balaguer, C. (2019), 'Joint Position Control Based on Fractional-Order PD and PI Controllers for the Arm of the Humanoid Robot TEO', International Journal of Humanoid Robotics 16(06), 1950042. (Q4, Impact Factor: 1.394).

    - Awarded with: Best paper in "Special Issue on Modelling and Control of Humanoid Robots (IROS 2018)"

    - Pending publications (accepted):

5. Muñoz, J.; Copaci, D. S.; Monje, C. A.; Blanco D. & Balaguer, C. (2020), 'Iso-m based adaptive fractional order control with application to a soft robotic neck', IEEE Access. (Q1, Impact Factor: 4.098).

6. Copaci, D. S.; Muñoz, J.; González, I.; Monje, C. A.; & Moreno, L. (2020), 'SMA-driven soft robotic neck: design, control and validation', IEEE Access. (Q1, Impact Factor: 4.098).

B. Conferences:

1. Quevedo, F.; Munoz, J.; Castano, J.A.; Monje, C. A. & Balaguer, C. (2020), Model Identification of a Soft Robotic Neck, in '2020 IEEE/RSJ International Conference on Intelligent Robots and Systems (IROS)', IEEE, , pp. –.

2. Mena, L.; Monje, C. A.; Nagua, L.; Muñoz, J. & Balaguer, C. (2019), Sensorización de un sistema de eslabón blando actuando como cuello robótico, in 'Actas de las Jornadas Nacionales de Robótica', Universidad de Alicante, , pp. 98-102.

3. Munoz, J.; Monje, C. A.; Martin, F. & Balaguer, C. (2018), A Robust Control Method for the Elbow of the Humanoid Robot TEO Based on a Fractional Order Controller, in '2018 IEEE/RSJ International Conference on Intelligent Robots and Systems (IROS)', IEEE, , pp. 6378–6383.

4. Nagua, L.; Muñoz, J.; Monje, C. A. & Balaguer, C. (2018), A first approach to a proposal of a soft robotic link acting as a neck, in 'Actas de las XXXIX Jornadas de Automatica, Badajoz, 5-7 de Septiembre de 2018', Área de Ingeniería de Sistemas y Automática, Universidad de Extremadura, , pp. 522-529.

5. Nagua, L.; Monje, C.; Muñoz Yañez-Barnuevo, J. & Balaguer, C. (2018), Design and performance validation of a cable-driven soft robotic neck, in 'Actas de las Jornadas Nacionales de Robótica', Universidad de Valladolid, .

1.5 Document organization

The document is divided into seven chapters, of which the first four are introductory and theoretical developments, and the following, from Chapter 4 onwards, are devoted to experimental results and conclusions.

In the first chapter, an introduction to the problems addressed in the thesis is provided. Chapter 1 starts introducing the uncertainty problem, describing the different kinds of uncertainties found in control systems.

These problems are usually solved through robust and adaptive techniques, also introduced and described in this chapter. Section 1.1 provides a detailed definition of robustness and the different uncertainty problems that can be solved using these methods. The central scope of this thesis, the fractional order control, is also described in more detail during this section. Finally, a definition of adaptive systems is also provided, specially oriented to its application to robust control systems.

After this introduction, a deeper analysis of the current solutions to similar problems found in the literature is reviewed in the section 1.2 with the title of State of the art. During this section, the strengths and shortcomings of the different approaches are discussed, while giving possible solutions to the problems raised. This thesis address many of the discussed problems through the proposal of two novel methods, which are discussed in the subsequent chapter.

The discussion of section 1.3 gives a detailed idea of how the proposed methods solve the problems described in the previous sections. In addition, three test platforms and two example plants are introduced. These systems will be used during the thesis for description of the methods, and for testing and experimentation. The aim of this section is merely introductory. A much more detailed description of the real plants

and the experiments performed is provided in the second part of the thesis, during the last chapters.

Once the problems and solutions are described, the thesis theoretical development is presented. The chapters 2 and 3 provide a detailed description of the mathematical foundations of the thesis.

Chapter 2 describes in detail the mathematical development of the iso-m method. All operations and procedures are deeply explained in this section, providing theoretical proof of the proposed method validity. Also a detailed step-by-step description of the method application is found in this chapter. The example plants are used here in order to make a clearer explanation of the method application. The research contributions of this chapter have been published in the high impact paper [1].

In the same way, a complete theoretical description of an adaptive scheme application to the aforementioned iso-m method can be found in chapter 3, where the theory behind the adaptive iso-m method can also be found. The research contributions of this chapter will soon be published in the high impact paper [2].

Finally, last chapters are devoted to describe the experimentation which has been carried out in different real systems, including an autonomous car, a humanoid robot, and a soft neck.

One of the systems improved using the proposed robust controller is shown in chapter 4. In this case, a cruise control system for an autonomous vehicle is involved. These systems have a high uncertainty due to changes in the road, which can be addressed, as explained in this chapter, by robust fractional control. The results presented in this chapter have also been published in the high impact paper [3].

Chapter 5, describes a system developed for the robust control of the TEO humanoid robot right arm joint. These systems are variant and non-linear because of the variable load applied to the motor due to the different configurations of the robot. Also, the masses of the grasped objects are different, adding more system uncertainty. The results presented in this chapter have been also published in the high impact papers [4], [5].

During chapter 6, the system developed for soft neck inclination control and its results are described. In this case, the high non-linearity of the plant required full system application, robust and adaptive. As shown in this chapter, the system high variability makes the robust control fail in the most extreme inclinations. Although the results of only robust control are quite good, it is observed how the adaptive control improves system response in cases where plant parameters are out of the robust control range. The different results presented in this chapter have been also published in the high impact papers [6], [7], [8], [9], [1] [10] , and [2].

As a summary, the proposed methods, that solve many of the robust control drawbacks described in the first part of the thesis, can be used in literally any system to provide a robust control. The method simplicity makes it a great option in order

to promote the use of robust and fractional systems in a wide variety of plants.

Finally, chapter 7 outlines the main conclusions extracted from this thesis and its results, pointing out the most promising ideas in this area and the future works that will follow.

Chapter 2

Tuning approach for robust fractional order controllers

2.1 Introduction

Current fractional order tuning methods discussed in chapter 1.2 have one common drawback, a complete lack of awareness during the tuning process. Solving a set of non-linear equations can be done accurately with a numerical solver, but no information about the tuning process is obtained. Usually, a priori knowledge about the controller tuning, or even trial and error may be required. A common problem is the use of wrong initial conditions that lead to local minima, offering unsuitable solutions, or no solution at all.

Therefore, it is important to find new tuning methods that show a better insight and help to avoid such situations by offering tuning directions trough the entire process.

The new method discussed here address the tuning problem through a graphical approach. To meet the design specification described by Eq. (1.7), an opposite slope is sought in the controller, resulting in slope cancellation in the open loop frequency response.

As a numerical solver is avoided in the non-linear equation set solution, the computing effort is drastically reduced, resulting in simple algorithms that are well suited for applications with limited computation resources, such as embedded hardware or PLCs, while showing very competitive results compared to the current methods.

2.2 Slope cancellation tuning methods

According to the phase additive property, cascading systems such as controller and plant result in a new combined diagram with curves equivalent to the sum of their individual plots. Since the slope is the curve derivative, the slopes are also added, due to derivation linearity property.

Based on that, a controller needs an opposite plant slope at the specified frequency (ω_{gc}) to cancel the slopes to zero. For example, first order plants show negative phase slopes in the range of 0 rad/dec to -1.1513 rad/dec (-65.96 deg/dec). If the slope at some specific frequency is, say, -1 rad/dec, using a controller with an equivalent positive slope (1 rad/dec) will result in a flat slope at this frequency.

The first attempt to find such a controller can be made using a standard PID approach. Although it is possible in some cases, these controllers have severe limitations as will be shown below.

2.2.1 Slope cancellation for PID controllers

The integer PID controller defined by Eq. (2.1) has a pole at origin, therefore, the minimum phase (Φ_{pid}) it can achieve is -90 deg, as $\lim_{\omega\to 0}\Phi(C(s)) = -j$, and having two zeros, the phase will increase to a maximum of 90 deg, as $\lim_{\omega\to\infty}\Phi(C(s)) = j$. Between these two asymptotes, the controller can show any positive phase slope from 0 to ∞, by properly setting integral and derivative parameters.

$$C_{pid}(s) = k_p + k_d s + k_i s^{-1} = \frac{k_p s + k_d s^2 + k_i}{s}, = k\frac{(s+a)(s+b)}{s}, \tag{2.1}$$

where $k_p = k_d(a+b)$, $k_i = k_d ab$ and $k = k_d$.

For this type of controller, the k_d parameter defines a static gain, as seen on the right side of (2.1), which affects only the magnitude plot, and the zeros define the phase curve, determined by k_p and k_i parameters. As the system must be feasible, only real or conjugate complex zeros can be used.

When the zeros are Real numbers, they define the frequencies where constant phase slope of $m = 1.1513$ rad/dec is obtained in the controller. For instance, the left Bode diagram in Fig. 2.1 shows the frequency response for a controller with $z_1 = 0.01$ rad and $z_2 = 100$ rad. As the zeros get closer, their slopes begin to add up, overtaking the constant slope of $m = 1.1513$ rad/dec to a maximum of $m = 2.3026$ rad/dec for the case of a repeated Real zero, shown in the right Bode diagram of Fig. 2.1.

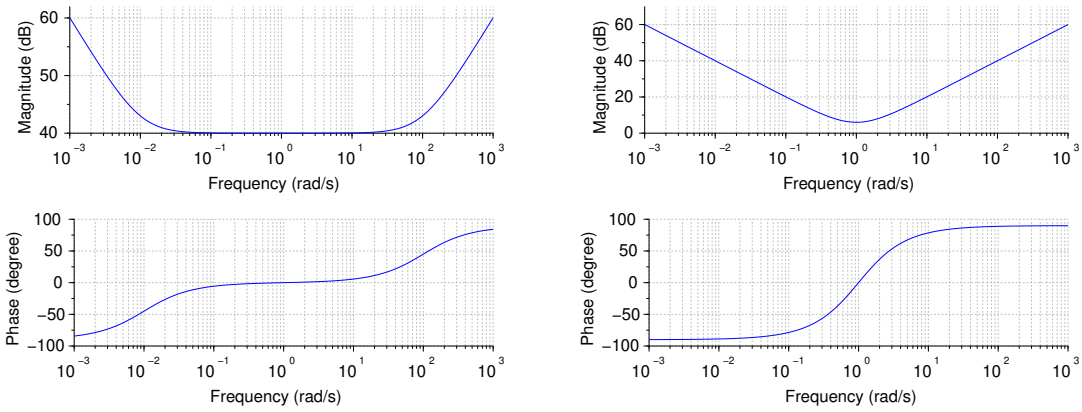

Figure 2.1: PID Controller Bode plots showing one pole at origin and two real zeros at different frequencies $\omega_1 = 0.01$ rad, $\omega_2 = 100$ rad (left), and repeated $\omega_1 = \omega_2 = 1$ rad (right).

When the zeros are complex conjugate numbers, their magnitude and angle define the phase frequency and slope. For example, Fig. 2.2 shows two controllers with $a = 1e^{i}$, $\overline{a} = 1e^{-i}$ (left), and $a = 1e^{1.5i}$, $\overline{a} = 1e^{-1.5i}$ (right). Note how a phase angle is related to the slope in the phase plot.

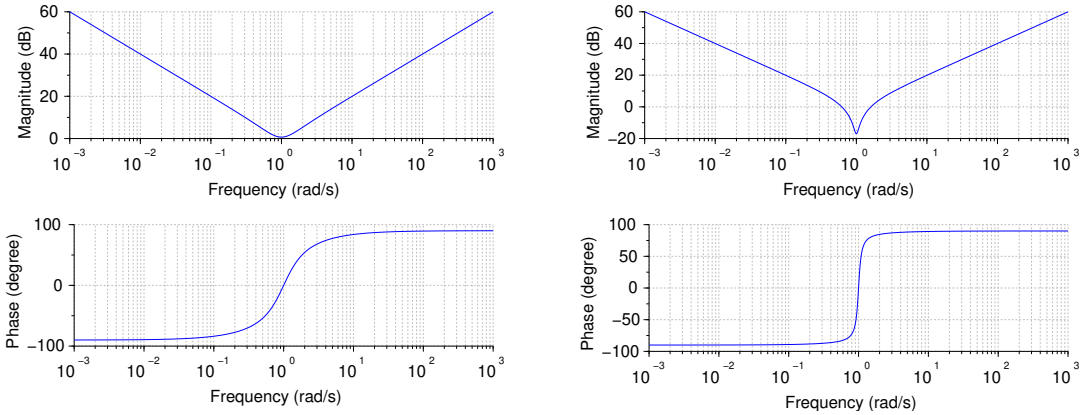

Figure 2.2: PID Controller Bode plots showing one pole at origin and two complex conjugate zeros with module one (frequency $\omega = 1$ rad), and different angles, 1 rad (left), and 1.5 rad (right).

Therefore, any plant slope can be canceled using a PID controller. When $s = j\omega$

in Eq. (2.1), the PID as a function of frequency is:

$$C_{pid}(\omega) = k_p + \frac{k_i}{j\omega} + k_d j\omega = k_p\left(1 + \frac{1}{\tau_i j\omega} + \tau_d j\omega\right) = k_p\left(1 - j\frac{1}{\tau_i\omega} + j\tau_d\omega\right), \quad (2.2)$$

that is a complex function where integral gain $k_i = k_p/\tau_i$ and derivative gain $k_a = k_p\tau_a$. Due to constant k_p is not related to phase, the following alternative can be used to compute phase equations:

$$\frac{C_{pid}(\omega)}{k_p} = 1 - j\frac{1}{\tau_i\omega} + j\tau_d\omega = 1 + j\left(\tau_d\omega - \frac{1}{\tau_i\omega}\right). \quad (2.3)$$

Taking arg at both sides of Eq. (2.3) results in:

$$\arg\left(\frac{C_{pid}(\omega)}{k_p}\right) = \arg\left(1 + j\left(\tau_d\omega - \frac{1}{\tau_i\omega}\right)\right), \quad (2.4)$$

and being k_p scalar,

$$\arg\left(\frac{C_{pid}(\omega)}{k_p}\right) = \arg(C_{pid}(\omega)) = \Phi_c(\omega). \quad (2.5)$$

According to Eqs. (2.4) (2.5), the phase depends on parameters τ_i, τ_d, and variable ω. The controller phase as a function of frequency is given by:

$$\Phi_c(\omega) = \arctan\left(\tau_d\omega - \frac{1}{\tau_i\omega}\right). \quad (2.6)$$

On the other hand, according to the second specification the controller must fulfill Eq. (1.9):

$$\arg\left(C(j\omega_{gc})G(j\omega_{gc})\right) = \arg C(j\omega_{gc}) + \arg G(j\omega_{gc}) = \Phi_C(\omega_{gc}) + \Phi_G(\omega_{gc}) = -\pi + \phi_m, \quad (2.7)$$

then,

$$\Phi_c(\omega_{gc}) = -\pi + \phi_m - \Phi_G(\omega_{gc}). \quad (2.8)$$

Therefore, since all values on the right side of Eq. (2.8) are specifications, $\Phi_C(\omega_{gc})$ is a known value. Now taking tan on both sides of Eq. (2.6) a better equation is found:

$$\tan\left(\Phi_c(\omega)\right) = \tau_d\omega - \frac{1}{\tau_i\omega}. \quad (2.9)$$

Putting Eqs. (2.9) and (2.8) together, and specifying for ω_{gc}, results in the first robust PID tuning equation:

$$\tan\Phi_c(\omega_{gc}) = \tau_d\omega_{gc} - \frac{1}{\tau_i\omega_{gc}} = \tan\left(\phi_m - \pi\right) - \tan\left(\Phi_G(\omega_{gc})\right) = T_{gc}, \tag{2.10}$$

where T_{gc} is used for reference simplification.

At the same time, the controller phase slope can be computed based on the derivative of $\Phi_c(\omega)$ in Eq. 2.6. As the Bode phase plot uses $\log_{10}$ scale for ω variable in abscissas axis, slope calculations will be simplified by the change of variable $x = \log_{10}(\omega)$. Taking the derivative with respect to $\log_{10}(\omega)$ on both sides of the equation results in:

$$m = \frac{d\Phi_c(\omega)}{d\log_{10}(w)} = \frac{d\phi(x)}{dx} = \frac{d}{dx}\arctan\left(\tau_d 10^x - \frac{1}{\tau_i 10^x}\right), \tag{2.11}$$

then, solving derivative and undoing the variable change:

$$m = \frac{\log(10)\left(\tau_d 10^x + \frac{1}{\tau_i 10^x}\right)}{1 + \left(\tau_d 10^x - \frac{1}{\tau_i 10^x}\right)^2} = \frac{\log(10)\left(\tau_d\omega + \frac{1}{\tau_i\omega}\right)}{1 + \left(\tau_d\omega - \frac{1}{\tau_i\omega}\right)^2} = \frac{\log(10)\left(\tau_d\omega + \frac{1}{\tau_i\omega}\right)}{1 + \tan(\Phi_c(\omega))^2}, \tag{2.12}$$

Again, specifying for ω_{gc} and rearranging, results in the second robust PID tuning equation:

$$m = \frac{\log(10)\left(\tau_d\omega_{gc} + \frac{1}{\tau_i\omega_{gc}}\right)}{1 + T_{gc}^2} \Longrightarrow \frac{m(1+T_{gc}^2)}{\log(10)} = \tau_d\omega_{gc} + \frac{1}{\tau_i\omega_{gc}} = M_{gc}, \tag{2.13}$$

where all known values are condensed into the constant value M_{gc}.

Therefore, the final result is a two equation deterministic system, which allows the parameter solution and the controller tuning based on the initial specifications:

$$\begin{cases} \tau_d\omega_{gc} + \frac{1}{\tau_i\omega_{gc}} = M_{gc} = \frac{m(1+T_{gc}^2)}{\log(10)} \\ \tau_d\omega_{gc} - \frac{1}{\tau_i\omega_{gc}} = T_{gc} = \tan\left(\phi_m - \pi\right) - \tan\left(\Phi_G(\omega_{gc})\right) \end{cases} \tag{2.14}$$

Solving (2.14) for τ_d and τ_i results in the following tuning equations for integral and derivative time parameters according to the desired specifications:

$$\begin{cases} \tau_d = \frac{1}{2\omega_{gc}}(M_{gc} + T_{gc}) \\ \tau_i = \frac{\omega_{gc}}{2}(M_{gc} - T_{gc}). \end{cases} \tag{2.15}$$

However, some restrictions have to be addressed prior to the implementation of this method. They are mainly due to the controller phase limits (-90 deg to 90 deg), and feasibility conditions.

Controller phase limits affect the range of possible phase margins; Since both, plant and controller add to the final phase, there will be possible minimum and maximum phase margins depending on the plant and crossover frequency. This is a minor concern, as most plants and controllers will fall in the possible range of phase margins.

Unfortunately, feasibility conditions are much more restrictive. This forces that both integral and derivative parameters are positive, and therefore, the feasible solutions for set of Eqs. (2.14) are reduced. If τ_d and τ_i must be positive, then $M_{gc}+T_{gc}$ and $M_{gc}-T_{gc}$ must be positive too, therefore:

$$\begin{cases} M_{gc}+T_{gc}>0 \quad \Rightarrow \quad M_{gc}>-T_{gc} \quad \Rightarrow \quad \frac{m(1+T_{gc}^2)}{\log(10)}>-T_{gc} \Rightarrow \quad \frac{m}{\log(10)}>\frac{-T_{gc}}{1+T_{gc}^2} \\ M_{gc}-T_{gc}>0 \quad \Rightarrow \quad M_{gc}>T_{gc} \quad \Rightarrow \quad \frac{m(1+T_{gc}^2)}{\log(10)}>T_{gc} \quad \Rightarrow \quad \frac{m}{\log(10)}>\frac{T_{gc}}{1+T_{gc}^2} \end{cases} \tag{2.16}$$

Using trigonometric identities and T_{gc} definition from (2.10), the restrictions result in:

$$\begin{cases} \frac{m}{\log(10)}>\frac{-\tan(\Phi_c(\omega_{gc}))}{1+\tan^2(\Phi_c(\omega_{gc}))} \quad \Rightarrow \quad \frac{m}{\log(10)}>\frac{-\sin(2\Phi_c(\omega_{gc}))}{2} \\ \frac{m}{\log(10)}>\frac{\tan(\Phi_c(\omega_{gc}))}{1+\tan^2(\Phi_c(\omega_{gc}))} \quad \Rightarrow \quad \frac{m}{\log(10)}>\frac{\sin(2\Phi_c(\omega_{gc}))}{2}, \end{cases} \tag{2.17}$$

which can be summarized as:

$$\begin{cases} m>\frac{-1}{2}\log(10)\sin(2\Phi_c(\omega_{gc})) \\ m>\frac{1}{2}\log(10)\sin(2\Phi_c(\omega_{gc})). \end{cases} \tag{2.18}$$

Since the controller phase ranges are $(-90, 90)$ deg, plotting the slope (m) as a function of $\Phi_c(\omega_{gc})$ for that range in Fig. (2.3) graphically shows the limitations of the controller. Both conditions must be fulfilled simultaneously, consequently, only the positive values are plotted.

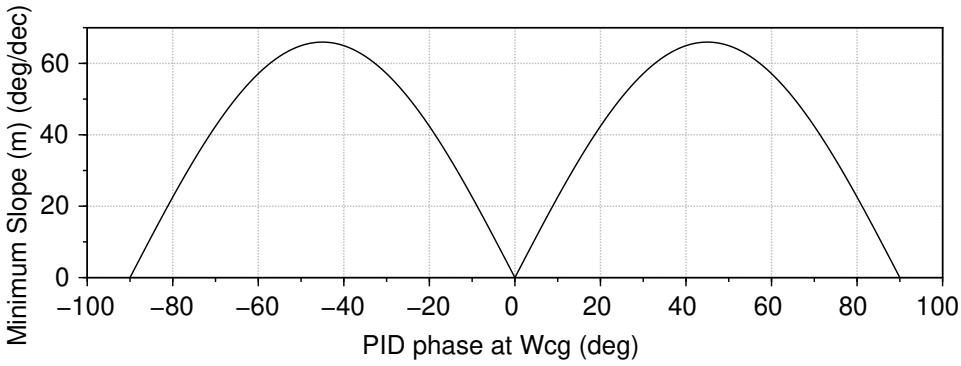

Figure 2.3: Minimum possible slope for a PID controller while complying with flat slope constraint in Eq. (1.7).

Notice how the ability of the controller to produce small slopes decreases near phase angles of -45 deg and 45 deg. For example, a 20 deg/dec phase slope can only be achieved with controllers that have phases in the ranges $(-90, -80)$ deg, $(-10, 10)$ deg and $(80, 90)$ deg. Looking now at Fig. (2.1) it becomes clear that those ranges match the lower slope parts of the phase plot.

This is a huge constraint, as the phase margin specification will be severely restricted when the required slope is small. As plant greater phase slopes are located close to their pole frequencies, this type of controller can be robust around them, but it cannot satisfy robustness constraints elsewhere, since pole distant frequencies have smaller slopes.

After slope cancellation (if possible), adjusting gain to fulfill Eq. (1.9) can be done through Eq. (2.19).

$$k = \frac{1}{|1 + 1/\tau_i j\omega_{gc} + \tau_d j\omega_{gc}||G(j\omega_{gc})|}. \tag{2.19}$$

2.2.2 Slope cancellation for fractional order controllers

A simple but powerful generalization of the PID controller that allows to overcome the previous limitations is based on fractional calculus. Since PID controllers contain integral and derivative operations, a generalization of these operator exponents, allowing them not only to be integers but also rational (hence fractional) or even real numbers, provides greater flexibility while retaining most PID controller simplicity.

The building blocks of integer order controllers are the binomial Laplace variable factors (usually called poles and zeros). Here, we will use an equivalent fractional factor to define the controllers.

The fractional order zero equivalent in fractional order calculus can be formulated as follows:

$$Z_a(s) = 1 + \left(\frac{s}{a}\right)^{\alpha} = \frac{a^{\alpha} + s^{\alpha}}{a^{\alpha}} = 1 + \tau_a s^{\alpha}, \tag{2.20}$$

where parameter α defines the fractional derivative exponent, and $\tau_a = 1/a^{\alpha}$. The parameter $a = 1/\tau_a^{(1/\alpha)}$ defines the cutoff frequency as will be shown.

In the same way, the definition of the fractional order pole is:

$$P_a(s) = \frac{1}{1 + \left(\frac{s}{a}\right)^{\alpha}} = \frac{a^{\alpha}}{a^{\alpha} + s^{\alpha}} = \frac{1}{1 + \tau_a s^{\alpha}}, \tag{2.21}$$

The Bode plot in Fig. (2.4) shows the frequency response for fractional zero (left) and pole (right) with example exponents $\alpha = 1.2$ and frequency $a = 1$.

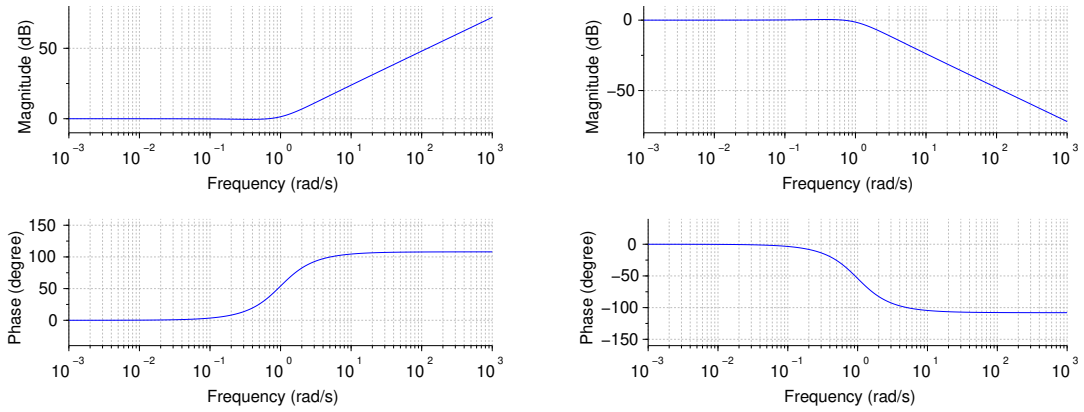

Figure 2.4: Example Bode plots for fractional zero (left) and pole (right) with exponents $\alpha = 1.2$ and parameter $a = 1$.

The left Bode diagram based on the fractional order zero, shows how singular phase values happen at frequencies DC ($\omega = 0$) and $w \to \infty$, resulting in the following asymptotic values:

- $\omega = 0$; $(\frac{1}{\tau_a \omega^{\alpha}} = \infty) \to \phi = 0\,\text{rad}$
- $\omega = \infty$; $(\frac{1}{\tau_a \omega^{\alpha}} = 0) \to \phi = \alpha\pi/2\,\text{rad}$,

and the cutoff frequency (ω_{co}):

- $\omega = \tau_a^{-1/\alpha}$; $(\frac{1}{\tau_a \omega^{\alpha}} = 1) \to \phi = \alpha\pi/4\,\text{rad}$.

A similar observation can be made for the pole, resulting in:

- $\omega = 0$; $(\frac{1}{\tau_a \omega^\alpha} = \infty) \rightarrow \phi = 0\,\text{rad}$
- $\omega = \infty$; $(\frac{1}{\tau_a \omega^\alpha} = 0) \rightarrow \phi = -\alpha\pi/2\,\text{rad}$,

and the cutoff frequency (ω_{co}):

- $\omega = \tau_a^{-1/\alpha}$; $(\frac{1}{\tau_a \omega^\alpha} = 1) \rightarrow \phi = -\alpha\pi/4\,\text{rad}$.

Further analysis will show how the exponent (α) is related to controller phase and maximum slope, while the time constant (τ_a) defines the cutoff frequency.

When $s = j\omega$ in Eq. (2.20) the exponent affects both terms j and ω, resulting in $s^\alpha = (jw)^\alpha = j^\alpha w^\alpha$. Then, Z_a is a complex function of the frequency, and can be written as:

$$Z_a(\omega) = 1 + \tau_a \omega^\alpha \cdot j^\alpha = 1 + \tau_a \omega^\alpha \cdot e^{(j\pi/2)\alpha}. \tag{2.22}$$

Now, finding the phase by taking arg of Eq. (2.22) results in:

$$\arg(Z_a(\omega)) = \arg\big(1 + \tau_a \omega^\alpha \cdot e^{(j\pi/2)\alpha}\big) = \Phi_z(\omega), \tag{2.23}$$

and computing the arg results:

$$\Phi_z(\omega) = arctan\left(\frac{\tau_a \omega^\alpha \sin(\alpha\pi/2)}{1 + \tau_a \omega^\alpha \cos(\alpha\pi/2)}\right) = \arctan\left(\frac{\sin(\alpha\pi/2)}{\frac{1}{\tau_a \omega^\alpha} + \cos(\alpha\pi/2)}\right), \tag{2.24}$$

Due to the logarithmic scale in the phase Bode plot, the slope derivative will be simplified using $x = \log_{10}(\omega)$ and $\tau_x = 1/(\tau_a 10^{x\alpha})$ variable changes, resulting in:

$$\Phi_z(x) = \arctan\left(\frac{\sin(\alpha\pi/2)}{\frac{1}{\tau_a 10^{x\alpha}} + \cos(\alpha\pi/2)}\right) = \arctan\left(\frac{\sin(\alpha\pi/2)}{\tau_x + \cos(\alpha\pi/2)}\right). \tag{2.25}$$

Being $\Phi_z(x)$ the phase, the slope as a function of x is found through the derivative of the previous expression:

$$m(x) = \frac{d\Phi_z(\omega)}{d\log_{10}(w)} = \frac{d\Phi_z(x)}{dx} = \frac{d}{dx}\arctan\left(\frac{\sin(\alpha\pi/2)}{\tau_x + \cos(\alpha\pi/2)}\right). \tag{2.26}$$

Therefore, solving (2.26), the slope equation is:

$$m(x) = \frac{\log(10)\alpha\sin(\alpha\pi/2)}{\left(\left(\frac{\sin^2(\alpha\pi/2)}{\tau_x + \cos(\alpha\pi/2)}\right)^2 + 1\right)(\tau_x \cos(\alpha\pi/2))^2} = \frac{\log(10)\alpha\sin(\alpha\pi/2)}{\tau_x + \frac{1}{\tau_x} + 2\cos(\alpha\pi/2)}. \tag{2.27}$$

Replacing $\tau_x + \frac{1}{\tau_x}$ for σ_x, the slope formula results in:

$$m(x) = \frac{\log(10)\alpha \sin(\alpha\pi/2)}{\sigma_x + 2\cos(\alpha\pi/2)} \quad , \quad \sigma_x = \tau_a 10^{-x\alpha} + \tau_a 10^{x\alpha}, \tag{2.28}$$

and removing the variable change:

$$m(\omega) = \frac{\log(10)\alpha \sin(\alpha\pi/2)}{\sigma_\omega + 2\cos(\alpha\pi/2)} \quad , \quad \sigma_\omega = \tau_a \omega^{-\alpha} + \tau_a \omega^{\alpha}, \tag{2.29}$$

Now, the highest slope (m_{max}) frequency, coincident with ω_{co} will be found. Only the σ_ω term depends on ω in Eq. (2.29), therefore, the extreme m_{max} value for the slope is bounded to σ_ω extreme values, more specifically, m_{max} matches the lowest σ_ω value.

The derivative of σ_ω results in the following equation:

$$\frac{d\sigma_\omega}{d\omega} = \sigma'_\omega = \frac{d}{d\omega}\left(\tau_a \omega^{\alpha} + \frac{1}{\tau_a \omega^{\alpha}}\right) = \frac{\alpha \tau_a \omega^{\alpha}}{\omega} - \frac{\alpha}{\omega \tau_a \omega^{\alpha}}. \tag{2.30}$$

Making the derivative equal to zero and solving for ω results in:

$$\tau_a \omega^{\alpha} = \frac{1}{\tau_a \omega^{\alpha}} \Longrightarrow \omega = \frac{1}{\tau_a^{(1/\alpha)}} = a. \tag{2.31}$$

While it is obvious from the phase curve that it is a maximum for the slope and a minimum for σ_ω, the second derivative can be used to find out.

$$\frac{d\sigma'_\omega}{d\omega} = \frac{d}{d\omega}\left(\frac{\alpha \tau_a \omega^{\alpha}}{\omega} - \frac{\alpha}{\omega \tau_a \omega^{\alpha}}\right) = \frac{\alpha[\tau_a^2 \omega^{2\alpha}(\alpha - 1) + \alpha + 1]}{\tau_a \omega^{(\alpha+2)}}. \tag{2.32}$$

When $\omega = a$, the second derivative is:

$$\left.\frac{d\sigma'_\omega}{d\omega}\right|_{\omega=a} = \frac{2\alpha^2}{a^2}, \tag{2.33}$$

that is always positive for any α, or a, making the point a minimum for σ_ω, and therefore a maximum for the slope (m_{max}). Using the value of $\omega = a$ in (2.29), the formula for maximum slope results:

$$m_{max} = \frac{\log(10)\alpha \sin(\alpha\pi/2)}{2 + 2\cos(\alpha\pi/2)} = \frac{\log(10)}{2} \cdot \alpha \tan(\alpha\pi/4). \tag{2.34}$$

Now placing $\omega = a$ in Eq. (2.24) the phase results in $\phi(\omega_{co}) = \alpha\pi/4$, as expected.

As a summary, when $\omega = a$ the plot shows its maximum slope, the phase value is exactly half of its asymptotic value, as defined for the cutoff frequency, and therefore $\omega_{co} = a$.

The same reasoning leads to the same result for the fractional pole, obviously with different sign. Since the slope must be negative for the pole, there is a minimum instead of a maximum.

Now these blocks can be used to create the fractional controller transfer function, allowing to use all the previous results to study and tune them.

The simplest integer controller could be a proportional differential (PD), composed by a zero and a static gain. The fractional counterpart should be defined by the same blocks. Hence, the fractional order proportional derivative controller (FOPD) will be defined with a zero and a static gain, as shown in (2.35).

$$FOPD(s) = k(1 + \tau_d s^{\delta}) = k_p + k_d s^{\delta}, \tag{2.35}$$

where $k_d = k\tau_d$, and $k_p = k$.

Adding an integrator to the above equation, the fractional order proportional integral (FOPI) controller is defined. Equation (2.36) shows the result.

$$FOPI(s) = \frac{k(1 + \tau_i s^{\iota})}{\tau_i s^{\iota}} = k_p + k_i \frac{1}{s^{\iota}}, \tag{2.36}$$

where $k_i = \frac{k}{\tau_i}$, and $k_p = k$.

Allowing negative values for the exponent, a single equation can define both FOPI and FOPD controllers. The usual derivative notation is positive while integral is negative, therefore, the first fractional order controller can be defined similarly to (2.35) by:

$$FOC_1(s) = k_p + k_a s^{\alpha} = k(1 + \tau_a s^{\alpha}), \tag{2.37}$$

where α is a fractional derivative exponent, $\alpha \in \mathbb{R} | -2 < \alpha < 2$, the proportional gain $k_p = k$ and the derivative gain $k_a = k\tau_a$.

A controller defined by Eq. (2.37) can show any phase slope and gain margin in the range $(0, \infty)$ depending on the gain k and the exponent α. Therefore, phase cancellation is always possible with this fractional controller for arbitrary target frequencies and gain margins, making fractional controllers the best option to overcome the PID limitations discussed above.

For example, Fig. (2.5) shows two controllers defined by (2.37) with different phases and slopes at the cutoff frequency $\omega_{co} = 1\,\text{rad/s}$ for the exponents $\alpha = 1.5$ and $\alpha = -0.5$. Notice how all the phase slopes are positive while the phase can be negative (FOPI) o positive (FOPD).

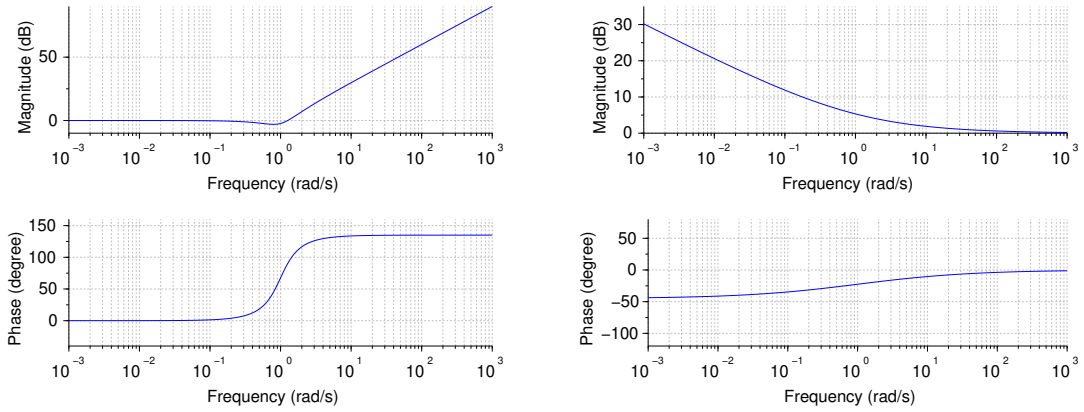

Figure 2.5: Examples of controller Bode plots for different α exponents (left: $\alpha = 1.5$, right: $\alpha = -0.5$), and crossover frequency $\omega_{gc} = 1$ rad/s. The slopes are positive in both but the phase can be negative (FOPI, right) or positive (FOPD, left).

Note that m_{max} does not depend on any parameter except α in Eq. (2.34). This could be used to cancel any known plant phase slopes simply by finding the proper exponent at the specified frequency.

Equation (2.34) cannot be solved for α, but plotting m_{max} versus α as in Fig. 2.6 can be used to graphically find the α exponent for any required slope. Another option is curve fitting. For example, Fig. 2.6 shows two fits using function $m = a\tan(b\alpha)^2$, hence the exponent can be obtained as $\alpha = b^{-1}\arctan(\sqrt{m/a})$.

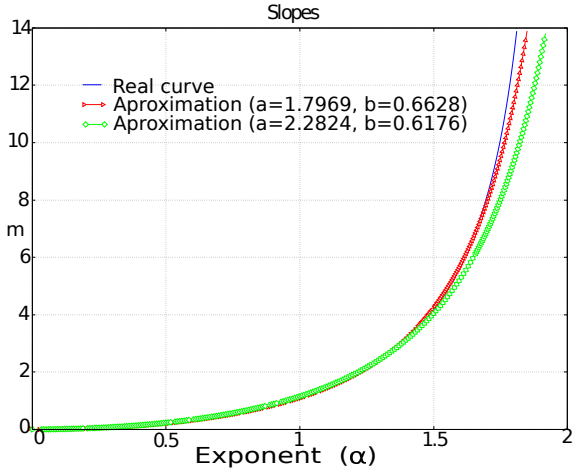

Figure 2.6: Maximum slope (m_{max}) versus α. Eq (2.34) direct values (solid line) and two approximations using the function $m = a\tan(b\alpha)^2$ with parameters a=1.7969, b=0.6628 (triangles), and a=2.2824, b=0.6176 (diamonds).

Therefore, this type of controller can show any slope, and would cancel any known plant phase slope using the correct exponent in the s Laplace variable. A flat phase area around the defined frequency is obtained by fulfilling the robustness constraint equation. This is not bad, but not much different from the previous PID controller, capable of canceling the slope, but unable to achieve a target phase margin. Fortunately, the method can still be improved by specifying the controller phase as before.

As in section 2.2.1, the controller phase is a known value, as it depends on the specifications (see (2.8)). The values for the controller phase do not depend on the static gain, and therefore, it will be equivalent to that of the fractional zero discussed earlier:

$$\Phi_c(\omega) = \arg(FOC_1(\omega)) = \arg\left(\frac{FOC_1(\omega)}{k}\right) = \arctan\left(\frac{\sin(\alpha\pi/2)}{\frac{1}{\tau_a\omega^\alpha} + \cos(\alpha\pi/2)}\right), \quad (2.38)$$

then using the crossover frequency specification (ω_{gc}) and taking the tan of Eq. (2.38) yields:

$$\tan(\Phi_c(\omega_{gc})) = \frac{\sin(\alpha\pi/2)}{\frac{1}{\tau_a\omega_{gc}^\alpha} + \cos(\alpha\pi/2)}. \quad (2.39)$$

Isolating $\frac{1}{\tau_a\omega_{gc}^\alpha}$ in Eq. (2.39), results in:

$$\frac{1}{\tau_a\omega_{gc}^\alpha} = \frac{\sin(\alpha\pi/2)}{\tan(\Phi_c(\omega_{gc}))} - \cos(\alpha\pi/2). \quad (2.40)$$

Then, for the specified frequency (ω_{gc}) the term $1/\tau_a\omega_{gc}^\alpha$ can be replaced in Eq. (2.29) as follows:

$$\sigma_w = \frac{\sin(\alpha\pi/2)}{\tan(\Phi_c(\omega_{gc}))} - \cos(\alpha\pi/2) + \frac{1}{\frac{\sin(\alpha\pi/2)}{\tan(\Phi_c(\omega_{gc}))} - \cos(\alpha\pi/2)}. \quad (2.41)$$

Replacing σ_ω in the slope Eq. (2.29) and simplifying, as shown in Eq. (2.42) gives m as a function of $\Phi_c(\omega_{gc})$ and α:

$$m = \log(10)\alpha\frac{1 - \frac{\tan(\Phi_c(\omega_{gc}))}{\tan(\alpha\pi/2)}}{\tan(\Phi_c(\omega_{gc})) + \frac{1}{\tan(\Phi_c(\omega_{gc}))}} = \frac{\log(10)}{\sin(\Phi_c(\omega_{gc}))}\alpha\left(1 - \frac{\tan(\Phi_c(\omega_{gc}))}{\tan(\alpha\pi/2)}\right). \quad (2.42)$$

Now it is possible to specify the controller phase (Φ_c) and solve for α. Remember that the phase in Eq. (2.42) is only the controller phase. To find a solution for the open loop phase margin specification in Eq. (1.9), the system phase must be known.

One of the options discussed above must be used to find a solution, as it is not possible to isolate the variable of interest.

2.3 Graphical method for exponent solution

For a graphical solution, figure 2.7 shows the resulting iso-slope (iso-m) curves relating the controller phase Φ_c in deg, the fractional order α and the slope m in deg/decade, both for positive and negative controller phase contributions (according to the control specifications).

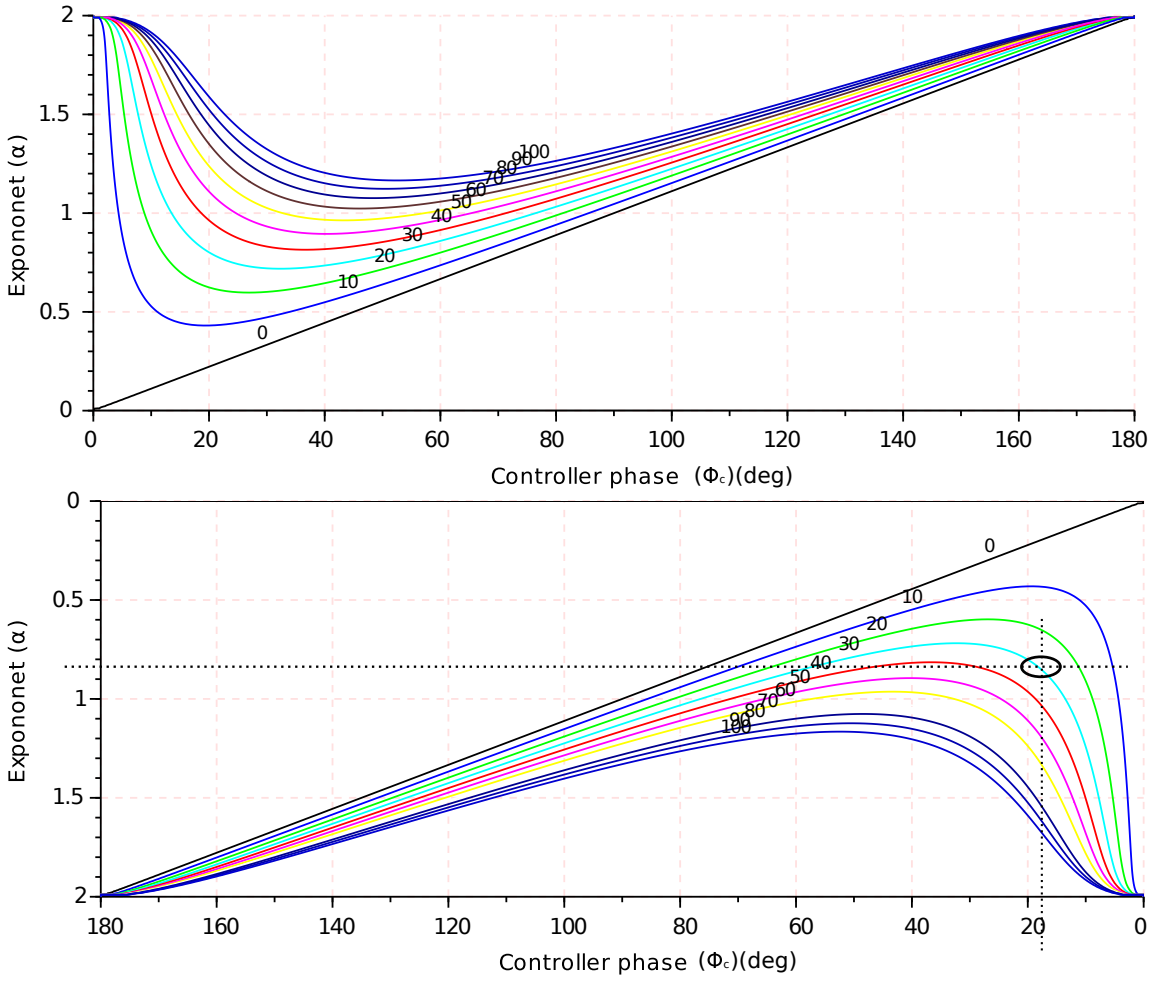

Figure 2.7: $Iso-m$ graph. Fractional order exponent α in ordinates and controller phase Φ_c [deg] in abscissas. Iso-m curves in [deg/decade].

Note that between both iso-m plots, all possible phases and slopes can be covered, offering a much better solution than the previous PID controller which failed to provide small slopes together with certain phase values according to Fig. 2.3. The phase is positive in the case of $FOPD$ (top) but negative in the case of $FOPI$

(bottom), then the controller phase in Fig. 2.7 will be subtracted instead of added, and will be in the region of negative exponents, as can be seen in the controller phase axis for the $FOPI$ curve.

2.4 Function approximations for exponent solution

Similar to the function approximations shown at Fig. 2.6, another option to approximate a solution to (2.42) is to find a curve with equivalent shape. Due to the higher complexity of that equation, finding that curve is much more difficult, and it lacks the advantages provided by the graphical method. Therefore, the graphical is preferred, as it offers a powerful tool for fractional order controller tuning that will be described next.

2.5 Controller parameters computations

Once the exponent is found, in order to cancel the phase slope of the system, the frequencies must match: the phase cancellation must occur at the specified crossover frequency. Knowing the exponent α and given ω_{gc}, τ_a can be calculated from Eq. (2.40) as follows:

$$\tau_a = \frac{1}{\omega_{gc}^{\alpha}\left(\frac{\sin(\alpha\pi/2)}{\tan(\Phi_c(\omega_{gc}))} - \cos(\alpha\pi/2)\right)}. \tag{2.43}$$

Using this equation, τ_a can be found so that the slope matches ω_{gc}, hence allowing to set the frequency where cancellation is planed. In the special case when $m = m_{max}$, Eq. (2.43) simplifies to $\tau_a = 1/\omega^{\alpha}$, and the exponent can be obtained from Fig. 2.6 or the fitted curve.

Finally, the crossover gain must meet the specifications, that is, the magnitude of the open loop must be exactly one at the crossover frequency. Using Eq. (1.8), k will be found as:

$$k = \frac{1}{|(1 + \tau_a(j\omega_{gc})^{\alpha})G(j\omega_{gc})|}. \tag{2.44}$$

Once all the parameters are solved for FC_1, a tuning based on initial Eqs. (1.8), (1.9) and (1.7) is found, thus meeting the design specifications while providing robust performance.

A summary of all the previous operations that ted to the order one controller tuning is detailed below.

2.6 Step by step iso-m controller design

The steps required for the fractional first controller (FOC_1) tuning with the new iso-m method are summarized below. Two values must be specified:

- Target crossover frequency ω_{gc}
- Target phase margin ϕ_m

Then, method implementation is as follows:
Step 1: Find the plant phase Φ_s and the slope m_s at the selected frequency. Having a system model or just frequency response data, the phase and its slope can be obtained. Their units are Φ_s deg and m_s deg/log(ω).
Step 2: Find the controller required phase and slope Φ_C and m_c . Knowing the system phase Φ_s and the target phase margin ϕ_m, the required controller phase is calculated from the equation $\Phi_c = (-\Phi_s + \phi_m - 180)$ deg. Then, the required controller phase slope is obtained as $m_c = -m_s$ deg/log(ω).
Step 3: Obtain the exponent α. Using these previous values (controller phase and slope), the exponent α is obtained, for instance, graphically from Fig. 2.7.
Setp 4: Compute τ_a from α and ω_{gc}. Using Eq. (2.43) the solution for τ_a is obtained, so the calculated controller has the correct slope at the specified frequency.
Step 5: Compute k according to ω_{gc}. To meet the specification in Eq. (1.8), k can be computed as in Eq. (2.44) so open loop system gain will be 0 dB at the crossover frequency ω_{gc}.
Step 6: Final solution. Once all the parameters are known, the controller is:

$$FOC_1(s) = k(1 + \tau_a s^\alpha) = k_p + k_a s^\alpha, \tag{2.45}$$

where α comes from Fig. 2.7, τ_a comes from Eq. (2.43), k comes from Eq. (2.44) and $k_a = k\tau_a$.

2.7 Examples of application of the iso-m tuning method

Next, the iso-m method will be applied to tune both example systems described in 1.1, following the step by step method shown at the previous section. Selected control specifications are:

- Desired crossover frequency $\omega_{cg} = 10$ rad/s
- Desired phase margin $\phi_m = 60$ deg

Using these values, the system response overshot will help to notice the iso-damping property caused by the flat phase of the open loop system around the crossover frequency (Eq. (1.7)).

The steps shown at the previous section will be followed in this example.

2.7.1 First order system

The first order system (G) was defined in chapter 1.3. The frequency response of Fig. 1.6 shows all required information needed from the plant for controller tuning. Using the above specifications and the method steps, a fractional controller will be tuned.

Step 1: The system phase and phase slope found at ω_{gc} are $\Phi_s = -84.26\,\text{deg}$ $m_s = -13.12\,\text{deg/log}(\omega)$ respectively. Note that a transfer function is not needed if the system frequency response around the desired ω_{cg} is available.

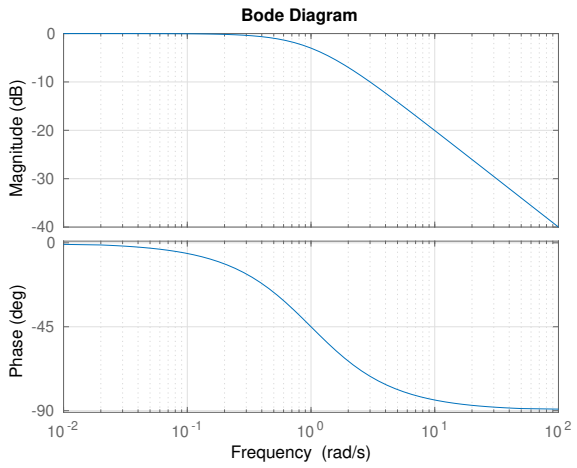

Figure 2.8: System phase and phase slope at the selected crossover frequency $\omega_{cg} = 10\,\text{rad/s}$ in the plant Bode diagram.

Step 2: The opposite of that system phase slope, is $m = 13.12\,\text{deg/log}(\omega)$, which is the controller phase slope required. The phase needed to achieve the phase margin specification at ω_{cg} is $\Phi_c = (-(-84.26) + 60 - 180)\,\text{deg}$, $\Phi_c = -35.74\,\text{deg}$.

Step 3: Based on that two values, the exponent resulting from Fig. 2.7 is $\alpha = -0.54$.

Step 4: Using these values, τ_a is computed using Eq. (2.43), resulting $\tau_a = 8.51$.

Step 5: Finally, k can be computed using Eq. (2.44), resulting $k = 3.12$, which makes open loop system gain to be 0 dB at $w_{cg} = 10\,\text{rad/s}$.

Step 6: Therefore, controller parameters are : $k_p = 3.12$, $k_a = 26.52$, $\alpha = -0.54$,

with the following transfer function:

$$C(s) = 3.12(1 + 8.51s^{-0.54}) = 3.12 + 26.52s^{-0.54}. \tag{2.46}$$

Frequency and time responses of the first order system using the iso-m fractional controller can be found at Fig. 2.9.

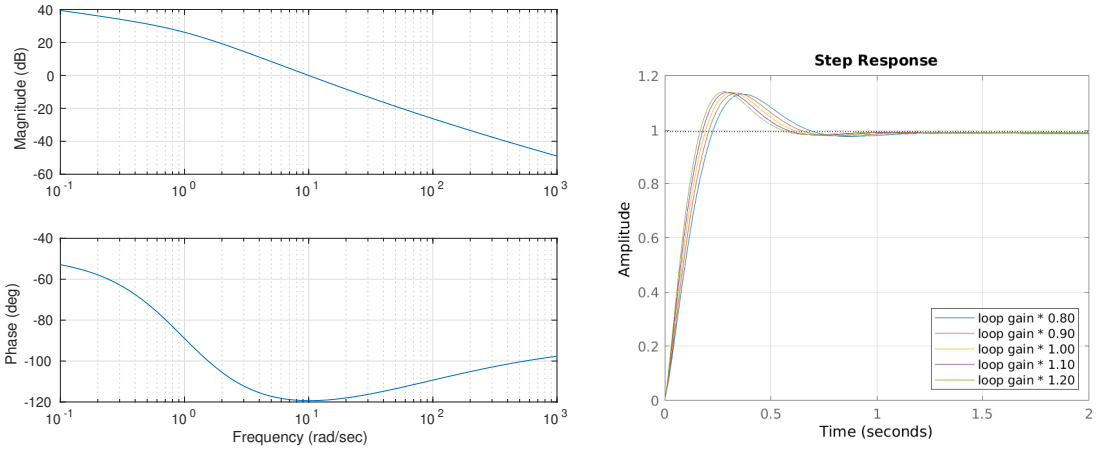

Figure 2.9: Open loop Bode diagram and step feedback response of the first order system with the fractional order controller designed using the iso-m tuning method.

Note how all specifications are fulfilled in the Bode diagram, including flat phase around $\omega_{cg} = 10\,\text{rad/s}$. Closed loop step responses for different system gains are drawn in this figure, evidencing the constant overshoot (iso-damping property). Note also the controller integrator effect due to the negative operator exponent resulting in a null stationary error.

The exponent results negative due to the combination of plant phase and specified phase margin. Given that the controller contribution to phase is negative, also the exponent is.

Let's see another example where the exponent required is positive.

2.7.2 Second order system

The second order system (G) was defined in chapter 1.3. The frequency response of Fig. 2.10 shows all required information needed from the plant for controller tuning. Observe how tiny is the phase for the original plant at $\omega_{cg} = 10\,\text{rad/s}$. This will force the exponent to be positive in order to increase its value according to the required phase margin. Therefore, Using the above specifications and the method steps, a fractional derivative controller will result.

Step 1: The system phase and phase slope found at ω_{gc} are $\Phi_s = -174.20\,\text{deg}$ $m_s = -13.52\,\text{deg}/\log(\omega)$ respectively.

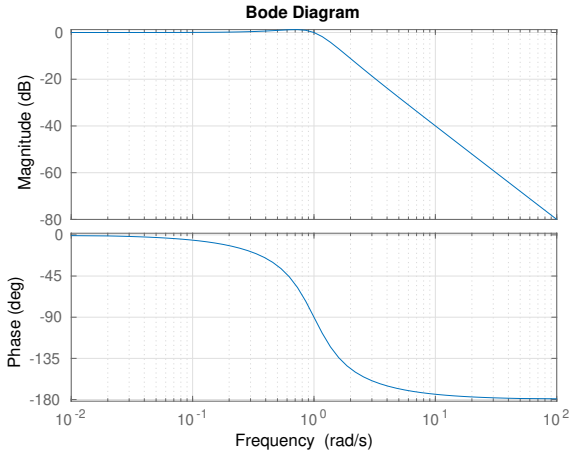

Figure 2.10: System phase and phase slope at the selected crossover frequency $\omega_{cg} = 10\,\text{rad/s}$ in the plant Bode diagram.

Step 2: The opposite of that system phase slope, is $m = 13.52\,\text{deg}/\log(\omega)$, and the controller phase slope required. The phase needed to achieve the phase margin specification at ω_{cg} is $\Phi_c = (-(-174.20) + 60 - 180)\,\text{deg}$, $\Phi_c = 54.20\,\text{deg}$.

Step 3: Based on that two values, the exponent resulting from Fig. 2.7 is $\alpha = 0.70$.

Step 4: Using these values, τ_a is computed using Eq. (2.43), resulting $\tau_a = 0.96$.

Step 5: Finally, k can be computed using Eq. (2.44), resulting $k = 18.50$, for an open loop system gain of 0 dB at $w_{cg} = 10\,\text{rad/s}$.

Step 6: Therefore, controller parameters are : $k_p = 18.50$, $k_a = 17.77$, $\alpha = 0.70$, with the following transfer function:

$$C(s) = 18.50(1 + 0.96s^{0.70}) = 18.50 + 17.77s^{0.70}. \tag{2.47}$$

Frequency and time responses of the second order system using results can be found at Fig. 2.11.

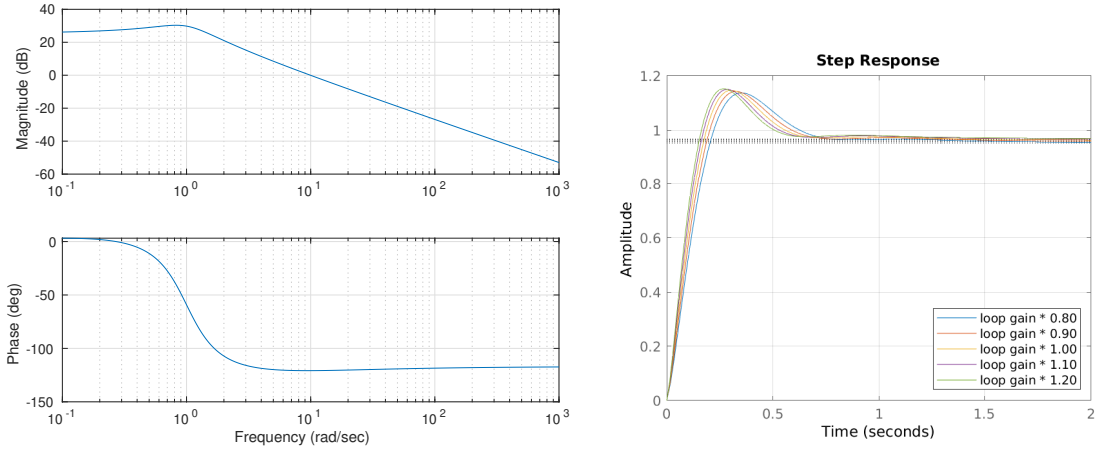

Figure 2.11: Open loop Bode diagram and step feedback response of the second order system with the fractional order controller designed using the iso-m tuning method.

Note how all specifications are fulfilled in the Bode diagram, including flat phase around $\omega_{cg} = 10\,\text{rad/s}$. Closed loop step responses for different system gains are drawn in this figure, evidencing the constant overshoot (iso-damping property). Observe how this time there is no integrator effect as the operator exponent is positive, resulting in a not null stationary error. Getting an integrator is possible at the cost of the system speed through crossover frequency reduction.

The exponent results positive due to the combination of plant phase and specified phase margin. The system needs a positive component in order to raise the phase value from $\phi = -174.20\,\text{deg}$ to $\phi = -120\,\text{deg}$ according phase margin. Another option could be to decrease the phase margin, although it is not a good option for this system, due to the very low value that would be needed.

Probably, a much better option for this system is to use an adaptive controller like shown in the next chapter as one of the major contributions of the thesis.

Chapter 3

Tuning approach for adaptive fractional order controllers

Although Robust controllers are useful in many cases, they still have limitations, notably, robustness is limited to a certain operating range. Adaptive control schemes allow these robust controllers to be adapted to plant changes, increasing their application range, usually known as adaptive robust control. In this chapter, the new tuning method described in Chapter 2 will be improved for its use in a wider set of scenarios through the use of adaptive methods.

3.1 Introduction

The iso-m method robust properties are based in the application of fractional order controllers. As discussed in chapter 1.2, the approach using a fractional order robust controller within an adaptive scheme is known in the literature as adaptive fractional order control.

Existing works have addressed the problem of fractional controller adaptation in very different ways, but most current approaches are based on implicit or direct adaptive control. However, the full potential of fractional order controllers for robust control is not achieved in these proposals. In most cases, the controller is either not part of the adaptation scheme, or even not a fractional order controller.

Explicit or indirect adaptive control provides a more complete approach to adaptive fractional order control. Using this scheme, plant system identification techniques are used in order to obtain an updated plant model. Then, the controller is tuned according to plant parameters and user specifications. Therefore, as they use an actual robust controller and a specification based tuning method, the full potential of the fractional order controllers is brought to the system. The result is a combination

of robust behavior for small quick plant variations, but with a controller always correctly tuned in the event of larger differences in the plant parameters thanks to the adaptive scheme.

Among the current proposals, the only approach near to explicit adaptive strategy is found in [38]. There, a self tuning method is used, in which the system identification runs during initial calibration. After the adaptation period, if plant parameters converge, the controller is tuned, which finish the adaptation and puts the system in production status.

In this scheme, usually known as STR, the adaptation is performed just during the initial stage, which is useful for LTI plants, but displays the same problems found with robust controllers for LTV or NLTI plants.

This kind of uncertain plants require different techniques, like, for instance, the continuous adaptation (CA) approach, which applies the adaptive scheme during the whole system operation. In this case, any changes detected in the plant will update the controller parameters according to the initial specifications.

Using this scheme, a fractional order control could be proposed for time varying plants. The inconvenience of CA methods is that they require very fast controller tuning methods, providing a result within a very small margin, usually less than a sampling period.

Classic fractional tuning processes are too slow for that, several times longer than plant time constants, and this makes the continuous adaptation approach unfeasible.

A possible solution is to use the tuning method described in Chapter 2, which is fast enough to work in-line within the control loop. In this way, new tuning parameters can be found for each iteration of the loop, turning the robust iso-m method into an adaptive CA system, and expanding the suitable plants to LTV or NLTI.

The new approach described here deals with fractional controller parameter continuous adaptation, including time constants, gains and fractional exponents. The same performance specifications defined previously for the iso-m method are used. The result is a robust and adaptable system, able to deal with plant changes and uncertainties at once.

The proposed fractional adaptive control scheme is basically composed of:

- Identification algorithm
- Iso-m tuning method
- Fractional order controller

Since these three items can run in a real time basis, the continuous adaptation approach is possible, resulting in the adaptive iso-m method described next.

3.2 Adaptive approach

As a continuous adaptive controller, the very first problem to be solved is the online system identification. Any real time method is applicable, but it must have the necessary features to be feasible in the adaptive control scheme.

Although model accuracy is important, algorithm speed is also significant. The fresher system information the better controller adaptation. Moreover, as an online identification algorithm, loop frequency could limit the speed of our system, reducing the frequency specification range.

Therefore, recursive Least Squares (RLS) is a suitable solution, as it offers a very fast algorithm, and a good accuracy for the required data, that is, the system phase and its slope for the cutoff frequency.

Empirical Transfer Function Estimate (ETFE) is another possibility, but the limitations are identical to those found with RLS, and its computation effort is much higher, since it includes matrix multiplication and Fourier transforms. On the other hand, such an implementation would have a clear advantage: a priori knowledge of the system order would not be necessary.

Given the real time constraint, the priority is a low computation effort, therefore, the closed loop RLS method will be used.

3.3 RLS system identification

The discrete RLS method consists of a series of sequential steps computed in a recursive loop, making the identification error tend to zero and thus allowing to track the changes in plant parameters during the execution of the algorithm.

Assuming zero delay for all the signals, a discrete domain SISO plant model can be described by the following transfer function:

$$\frac{Y(z)}{U(z)} = G(z) = \frac{b_1 z^{-1} + .. + b_{nb} z^{-nb}}{1 + a_1 z^{-1} + .. + a_{na} z^{-na}} = \frac{B}{A} \tag{3.1}$$

which can be expressed in a compact form as:

$$AY(z) = BU(z) \tag{3.2}$$

where A and B are polynomials in z^{-1} (delay operator), and $Y(z)$ and $U(z)$ are Z transform signals of plant output and input respectively. Equations (3.3) and (3.4) show the expanded polynomials with coefficients a_i and b_i.

$$A = a_0 z^0 + a_1 z^{-1} + .. + a_{na} z^{-na}, \tag{3.3}$$

$$B = b_0 z^0 + b_1 z^{-1} + .. + b_{nb} z^{-nb}. \tag{3.4}$$

Note that the polynomial exponents can not be positive due to the assumption of a deterministic environment. Putting Eqs. (3.2), (3.3) and (3.4) together:

$$a_0Y(z)+a_1z^{-1}Y(z)+..+a_{na}z^{-na}Y(z) = b_0U(z)+b_1z^{-1}U(z)+..+b_{nb}z^{-nb}U(z). \quad (3.5)$$

Then, finding the Z^{-1} transform of Eq. (3.5) together with the time shift property $Z^{-1}[z^{-i}Y(z)] = y(t-i)$ and $Z^{-1}[z^{-i}U(z)] = u(t-i)$, results in:

$$a_0y(t) + a_1y(t-1) + .. + a_{na}y(t-na) = b_0u(t) + b_1u(t-1) + .. + b_{nb}u(t-nb), \quad (3.6)$$

where $y(t)$ is the plant output variable at time t, and $u(t)$ is the plant input variable at the same instant.

Usually $a_0 = 1$ to show the current system response as a function of past inputs and outputs, otherwise all coefficients can be divided by a_0 and renamed, so $a_0 = 1$ can be considered without any loss of generality. It is also common that plants lack of a direct term, therefore $b_0 = 0$ (so they are out of scope as of now). Replacing and rearranging results in Eq. (3.7).

$$y(t) \; = \; -a_1y(t-1) - .. - a_{na}y(t-na) + b_1u(t-1) + .. + b_{nb}u(t-nb), \quad (3.7)$$

that can be packed in a matrix form:

$$y(t) = \theta\phi'(t-1), \quad (3.8)$$

where $\theta = [a_1, .., a_{na}, b_1, .., b_{nb}]$ is the plant parameters array, while the values in $\phi(t-1) = [-y(t-1), .., -y(t-na), u(t-1), .., u(t-nb)]$ store all previous system inputs and outputs.

Equation (3.8) represents the output prediction of the model based on past inputs and outputs ($\phi(t-1)$), and model parameters (θ).

Recursive identification methods use Eq. (3.8) as a predictor for the next system output, just advancing the index one position:

$$\hat{y}(t+1) = \hat{\theta}(t)\phi'(t), \quad (3.9)$$

therefore, a predicted system output $\hat{y}$ is available for a known set of past inputs and outputs based on the current model estimate ($\hat{\theta}$). Notice that the hat notation ($\hat{y}$, $\hat{\theta}$) means estimated values in contrast to the real ones without any marking. A time index ($\hat{\theta}(t)$) is introduced to show that $\hat{\theta}$ could change during identification, or if the system is time variable. Figure 3.1 shows the basic scheme for the implementation of the identification method.

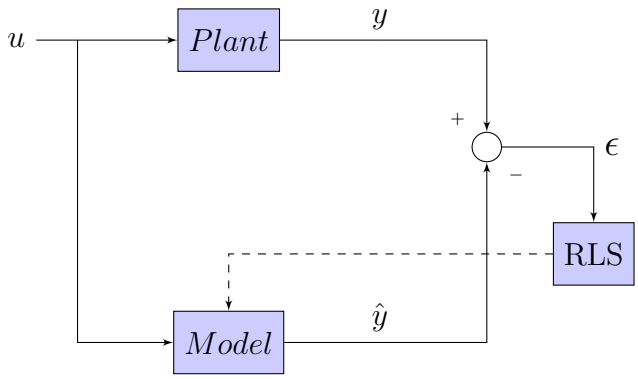

Figure 3.1: Block diagram of a simple RLS identifications system. The model error (ϵ) is used by the RLS algorithm to update (dashed line) the estimated model.

The difference between predicted ($\hat{y}$) and real (y) system output is the prediction error (ϵ), as shown in Fig. 3.1 and Eq. (3.10).

$$\epsilon(t) = y(t) - \hat{y}(t) \Rightarrow \epsilon(t+1) = y(t+1) - \hat{y}(t+1) \tag{3.10}$$

When $y(t+1)$ becomes available, this error will be used to compute $\hat{\theta}(t+1)$, that is an improved plant estimate while the error is reduced. Here, each identification method uses the error in a different way. For example, in the least squares, the squared error of all the previous identification data is considered. The algorithm is summarized in the following equations:

$$\hat{\theta}(t+1) = \hat{\theta}(t) + F(t+1)\phi(t)\epsilon(t+1), \tag{3.11}$$

$$F(t+1) = F(t) - \frac{F(t)\phi'(t)\phi(t)F(t)}{1+\phi(t)F(t)\phi'(t)}, \tag{3.12}$$

$$\epsilon(t+1) = y(t+1) - \hat{\theta}(t)\phi'(t), \tag{3.13}$$

where $\epsilon(t+1)$ is the prediction error according to Eqs. (3.10) and (3.9), making the algorithm a function of known input and output data $\phi(t)$ and the immediate previous model estimate($\hat{\theta}(t)$).

At this point, RLS method is only applicable to LTI systems, because all past identification data is stored in the gain matrix (F) giving naturally more weight to the (more numerous) previous inputs over the current ones.

Therefore, some modifications are needed for LTV system identification. As will be shown during stability analysis, the most suitable method for this case is time variable forgetting factor, described in [27], which introduces one parameter and one equation that shape the algorithm in order to change the impact of past identification data. Variable forgetting factor RLS is summarized in the following revised equations:

$$\hat{\theta}(t+1) = \hat{\theta}(t) + F(t+1)\phi(t)\epsilon(t+1), \tag{3.14}$$

$$\lambda_1(t)F(t+1) = F(t) - \frac{F(t)\phi'(t)\phi(t)F(t)}{\lambda_1(t) + \phi(t)F(t)\phi'(t)}, \tag{3.15}$$

$$\epsilon(t+1) = y(t+1) - \hat{\theta}(t)\phi'(t), \tag{3.16}$$

where $\lambda_1(t)$ is the forgetting factor.

For $\lambda_1(t) = 1$ the basic RLS method is obtained, giving preference to past values (more precisely to the large sets of data). In order to reduce the effect of past values towards more current ones, forgetting factor method requires $\lambda_1(t) < 1$, where the smaller $\lambda_1(t)$, the greater preference for current values (stronger forgetting factor). When $\lambda_1(t) = 0$, $1/\lambda_1(t) = \infty$, $F(t+1)$ can not be computed, therefore the method requires $0 < \lambda_1(t) < 1$.

Using this factor, the adaptation speed can be changed according to different approaches, from basic filters to specific functions, depending on how $\lambda_1(t)$ is computed.

An interesting option for continuous identification systems is to modify the adaptation speed based on the PE content of the input signal. In the function shown in (3.17) λ_1 decreases for uncorrelated $\phi(t)$ values, and the estimate parameters are updated more often when the input signal is PE. Otherwise, λ_1 increases.

$$\lambda_1(t) = 1 - \frac{\phi(t)F(t)\phi'(t)}{1 + \phi(t)F(t)\phi'(t)} \tag{3.17}$$

With this method, we can ensure that the system identification is only updated when a sufficiently rich spectrum is available, which ensures that the estimations converge asymptotically (see [109] and [27]) while avoiding the corruption of plant estimates in a sustained steady state. This feature is also critical for stability analysis.

All previous identification techniques are based on the assumption that inputs and outputs are not correlated, as in open loop configuration, but this is not true for feedback systems, where input and output signals are combined. Therefore, further analysis is needed when the adaptive system is to be used in a feedback configuration.

The control scheme for RLS applied in a feedback system is shown in Fig. 3.2.

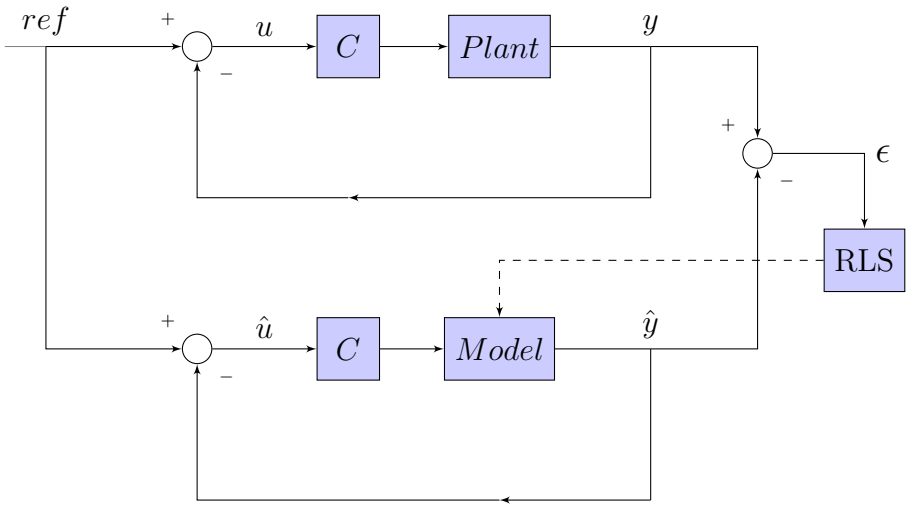

Figure 3.2:

Again, the modeling error is obtained from the difference of the current system (y) and the model ($haty$) outputs.

$$\epsilon_{cl}(t) = y(t) - \hat{y}(t) \Rightarrow \epsilon_{cl}(t+1) = y(t+1) - \hat{y}(t+1). \tag{3.18}$$

Therefore, the error prediction is similar to RLS, and Eq. (3.10) can be used with a remark, a new equation that relates u and y arises from the feedback loop ($u(t) = ref(t) - y(t)$). During closed loop operation, the system inputs are correlated with the outputs, resulting in a poor PE input signal.

Åström showed in [110] how to solve the correlation problem by filtering both signals with a filter that includes the estimation of the closed loop system poles, and the inverse of the controller, as follows:

$$L = \frac{C^{-1}}{(C^{-1}\hat{A} + \hat{B})} = \frac{1}{(\hat{A} + C\hat{B})}. \tag{3.19}$$

Therefore, using that filter in the inputs and outputs solves the correlation problem. Note that while $\hat{A}$ and $\hat{B}$ are the plant estimate parameters, C is the actual controller. Since the above expression matches the feedback model poles, and these will tend to the design poles when the error tends to zero, it is common practice to use the design poles. In our case, the closed loop poles are not defined, but we can find a filter based on the target open loop system response.

As shown in section 1.1, our target open loop system is a Bode's ideal transfer function defined by crossover frequency and phase margin specifications, $CG = (\omega_{gc}/s)^{\mu}$,

the closed loop function results in:

$$\frac{CG}{1+CG} = \left(\frac{\omega_{gc}^{\mu}}{s^{\mu}+\omega_{gc}^{\mu}}\right), \tag{3.20}$$

where $\mu = (\phi_m/90 - 2)$ and the phase margin (ϕ_m) is given in deg.

Note that the closed loop poles are fractional too, so the filter L should also be. Several approaches to L definition are valid here, from an integer invariant filter approximation roughly similar to closed loop poles, to update L with each new C, $\hat{A}$ and $\hat{B}$ obtained in tuning and plant identification. During the stability analysis it will be shown that first option is more suitable, but the tuning method will be described first.

3.4 Real time controller tuning

Once the plant is identified, these parameters are used for controller tuning through the method described in chapter 2.

The controller definition used in the iso-m method has three adjustable parameters, k_p, k_a, and α. Finding the controller parameters that meet all these constraints is the problem to be solved for fractional robust controller tuning. In order to find these parameters using the iso-m method, the specifications defining the performance of the resulting system must be established.

The described method's frequency specifications used for fractional controller tuning are:

- ϕ_m: Phase Margin relative stability.
- ω_{cg}: Crossover frequency system dynamics.
- Flat phase specification defined in Eq. (1.7).

The first, (ϕ_m), is related to stability and overshoot while the second (ω_{gc}) specifies the system responsiveness (rise time). To apply these specifications, Eqs. (1.8) and (1.9) are used in chapter 2 to solve the controller parameters for a known plant.

Flat phase specification ensures that plant changes will not affect the open loop phase margin (ϕ_m), therefore, the feedback response will show a constant overshoot despite plant variations (iso-damping).

We defined RLS in the previous section with a forgetting factor as a function of the signal PE content. This ensures that plant identification converges to a reliable solution if the conditions are met. Therefore, an updated plant model ($\hat{G}$) must be available to be used in the controller tuning.

Also, according to 2, the required information from the system model is the phase and the slope at the specified gain crossover frequency. The plant estimate discrete transfer function can be obtained from online identification parameters, which provides phase and slope estimates for any frequency, considering that $z = e^{Tj\omega}$. These terms can be computed for the crossover frequency as follows. First, the phase and magnitude of the plant can be found as:

$$\hat{\phi}_G = tan\left(\frac{\Im(\hat{G}(e^{Tj\omega_{gc}}))}{\Re(\hat{G}(e^{Tj\omega_{gc}}))}\right), \tag{3.21a}$$

$$|\hat{G}| = \sqrt{\Im(\hat{G}(e^{Tj\omega_{gc}}))^2 + \Re(\hat{G}(e^{Tj\omega_{gc}}))^2}, \tag{3.21b}$$

then the plant slope can be computed as follows:

$$\hat{m}_G = \frac{d(G(e^{Tj\omega_{gc}}))}{d\log_{10}\omega}. \tag{3.22}$$

Once the phase and slope of the plant are obtained and the control specifications are defined, the controller can be tuned according to the iso-m method. Thanks to the online identification described above, the phase and slope of the plant are obtained in a continuous basis, and a fractional controller can be tuned according to the iso-m method for each update of the estimates of the plant parameters.

Then, using these values, the phase and slope required by the controller are obtained by Eqs. (3.24) as follows:

$$\phi_C = \phi_m - \hat{\phi}_G - 180, \tag{3.23}$$

$$m_C = -\hat{m}_G. \tag{3.24}$$

Note that ϕ_m is known from the controller specifications.

Then, similarly to Eq. (2.42), the following Eq. (3.25)

$$m_C = \frac{\log(10)}{\sin(\phi_C)}\alpha\left(1 - \frac{\tan(\phi_C)}{\tan(\alpha\pi/2)}\right), \tag{3.25}$$

can be used to calculate the exponent (α). Although it can not be solved directly for α, several options were previously proposed as solutions, including the plot shown in figure 2.7, a lookup table, and the fit function.

As controller tuning needs to be done in real time, the lookup table or the fit function are the best options for the adaptive iso-m exponent computation.

Having α exponent and crossover frequency (ω_{gc}), τ_a can be calculated using Eq. (2.43).

$$\tau_a = \frac{1}{\tau_x {\omega_{gc}}^{\alpha}} \quad ; \quad \tau_x = \frac{\sin(\alpha\pi/2)}{\tan(\phi_C)} - \cos(\alpha\pi/2) \tag{3.26}$$

Finally, controller gain is computed using Eq. (1.8), fulfilling the crossover frequency specification.

$$k = \frac{1}{|1 + \tau_a(j\omega_{gc})^{\alpha}||\hat{G}|} \tag{3.27}$$

Once all three parameters are found and the controller is tuned according to the specifications, it can be used in our adaptive scheme after the identification step. These two steps will be repeated alternatively during the continuous adaptation operation.

Thanks to the robustness of the system, performance will not change for the operating point, and thanks to the adaptability of the system, plant changes will update the controller tuning to obtain the same specifications of the original operating point. To have a functional adaptive system, stability must be ensured, which is discussed in the next section.

3.5 Stability analysis

The most important part of the adaptive control applied to LTV plants is the stability analysis. It is challenging because, even though the tuning method is known, controller tune depends on identification, which is uncertain because of the time varying nature of the plant. Therefore, re-tuning can result in an unstable system.

The immediate solution to this problem is to verify that all possible controller tuning results are within a stability range. To ensure this, the following conditions must be met:

- Identification error decreases asymptotically
- Plant parameter estimates ($\hat{\theta}$) are bounded and converge to a value
- Controller tuning method results are bounded and stabilize the system

For the first condition, Landau demonstrated in [95] that, if the a posteriori error can be written as a filtered function of the measured error:

$$\epsilon(t+1) = H[y(t+1) - \hat{\theta}(t)\phi'(t)], \tag{3.28}$$

then the sufficient condition for the error to decrease asymptotically is that the expression $H(z) - \lambda_2/2$ must be strictly positive real, where $1 \leq \lambda_2 < 2$ and $H(z)$ is the H filter discrete transfer function.

Note that filtering the observation vector ϕ through the filter L defined at Eq. (3.19), as described in the previous section, is equivalent to Eq. (3.28), therefore we can choose $L = H$, solving both problems at once. That makes the filter update option not feasible for L, so a static filter is the best option, since all previous conditions can be met.

For the second stability condition, there is an additional requirement. The gain matrix F has to be strictly positive as well, which in our case is given by the chosen computation method for λ_1, which avoids updating the gain matrix (F) when the input is not rich enough in frequency.

Therefore, both first and second stability conditions are granted if the filter L is chosen correctly.

Regarding the third condition, since the tuning inputs are specifications and plant model, both are bounded if the first two conditions are met.

As tuning is done using the iso-m method described, and knowing that plant identification converges to reliable phase and slope data, we can check the tuning output range to verify the final stability of the system. Figure 2.7 shows how, for any possible phase and slope value, the exponent alpha is bounded in the interval $(-2, 2)$, so we can be sure that the controller parameters are all correct numbers, although it does not mean that the resulting controller stabilizes the system.

About the final system's stability, given the way we defined the specifications, it will be implicitly ensured if the controller is properly tuned. Note that, since the phase margin is among the initial specifications, once the method is implemented correctly, we can accurately guarantee how good the system stability is, or even change through this parameter if it is not suitable. In short, when using the iso-m method for controller tuning, stability is not only granted, but specified.

Experimental results

Having robust and adaptive schemes completely specified, it is time to validate the results in real platforms.

Iso-m and adaptive iso-m methods experimentation results are discussed in the following chapters. Previously described control strategies will be used in different platforms with varying degrees of uncertainty and non-linearity for testing and validation.

These experiments are intended to assess the performance of proposed methods and compare the results with other control schemes. For this purpose, iso-m (robust and adaptive variants) will be compared with diverse fractional order (FOC) and an integer order (IOC) controllers.

First, an iso-m robust autonomous driving car experiment is discussed in Chapter 4. Next, a set of robust control experiments are shown for the case of a humanoid robot arm in Chapter 5. Finally, robust and adaptive iso-m controllers are tested in the soft neck control system developed in [7] and equipped with an MPU-9250 sensor as in [8] in Chapter 6.

Chapter 4

Experimental Results: Autonomous car

This chapter presents and discuss the results obtained in the robust iso-m method application to the control of a Hybrid Honda Accord 2014 autonomous vehicle shown in the figure 4.1.

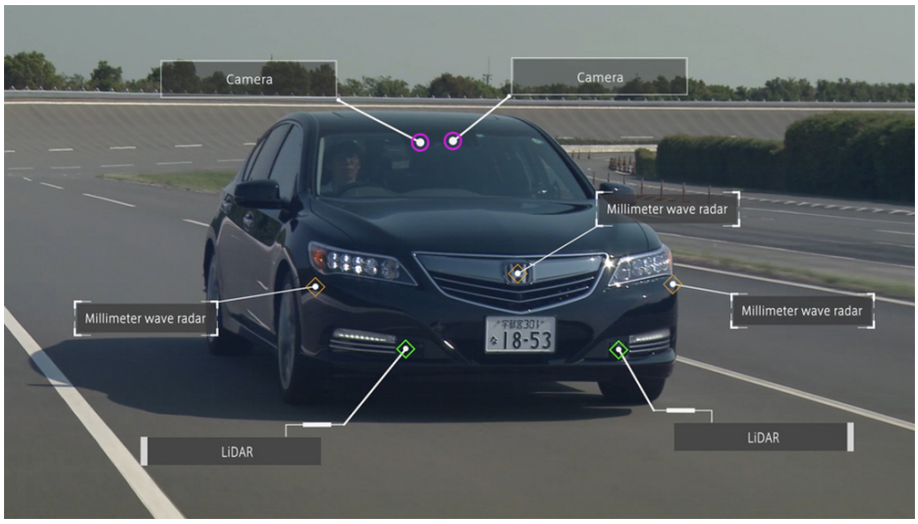

Figure 4.1: Front image of the autonomous car proposed as a test platform, showing front sensors.

The sensors available for control applications mounted in the car are:

- Five RADAR, three front and two back.
- Five LIDAR, two front and three back.

- Two RBG 2D cameras at front.
- One GNSS, with its antenna on top.

The locations of these sensors are shown in Figs. 4.1 and 4.2.

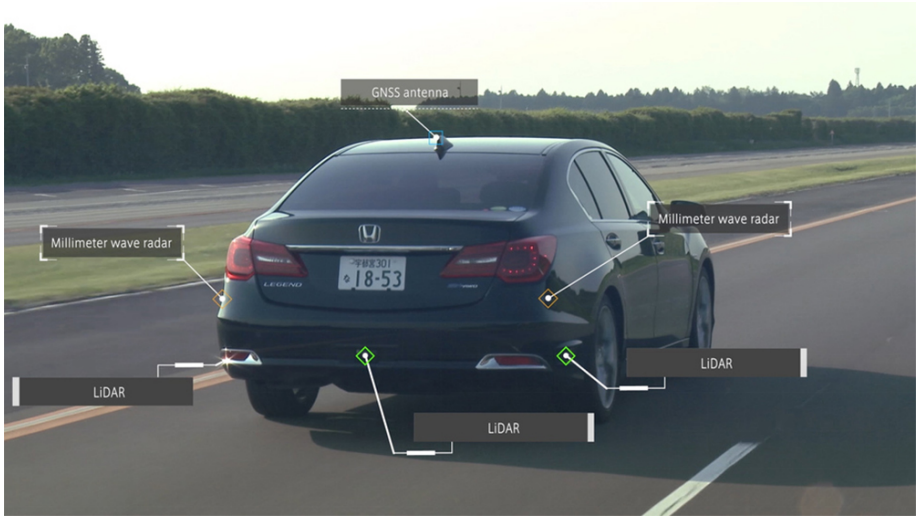

Figure 4.2: Back image of the autonomous car, showing back sensors.

Among the control applications in ground transport, usually known as advanced driving assistance systems (ADAS), we can find the adaptive cruise control (ACC). This application deals with the throttle and brake pedals management in order to maintain a constant velocity while keeping a safety distance to next vehicle.

This ACC functionality must ensure that, in the event of a detected object in the driving direction, the speed will be reduced in order to maintain a safe distance at all times as shown in Fig. 4.3. See [111] for a survey on different ACC systems.

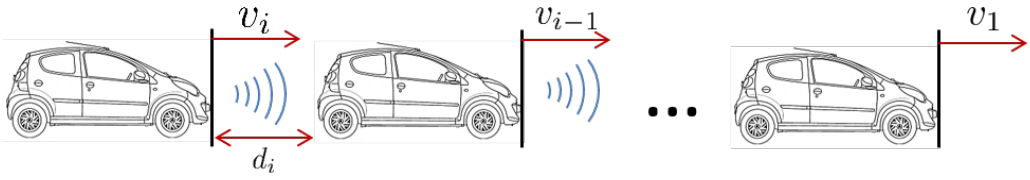

Figure 4.3: String of ACC-controlled vehicles.

This spacing, applied to all vehicles on the road, may provide additional safety and reduce emissions, as stated in [112]. Nevertheless, current ACC applications are still only available as a comfort feature for high-end vehicles, probably due to the

expensive control equipment required in order to avoid known issues. Therefore, their impact on overall safety and pollution is very low, as shown in [113]. A cheap, robust control ACC application may help in the widespread adoption of these systems.

4.1 Current approaches

As seen in Chapter 1, many industrial control systems use standard PID controllers. ACC proposals are not the exception, and available systems are normally based on PD or PI controllers. Although these first systems show a correct performance (see [114], [115] and [116]), recent studies as [57] have demonstrated that production systems still exhibit some performance limitations when coping with all ACC control requirements. Therefore, more advanced control structures are needed to deal with the increasing demanding specifications.

For example, approaches like the Model Predictive Control (MPC) described in [117], which improves the car-following performance, or the H_∞ robust control applied in [118], have been used to mitigate the effects of the plant uncertain dynamics.

A major shortcoming of these methods is the added complexity, which requires non-standard equipment, resulting in a fundamental issue when considering real-world platform applications. As shown before, fractional order controllers are an excellent solution to these issues, allowing a simple but powerful control design.

In the field of intelligent transport systems (ITS), the fractional order control has been applied to both lateral and longitudinal motion problems of autonomous vehicle control. For example, in [58] a FOPID algorithm is presented for lateral control in parking maneuvers, and in [119], the speed of the vehicle is used to compute the order of a fractional controller. Regarding vehicle longitudinal speed control, a FOPI controller is proposed in [60] for the cruise control system in gas powered vehicles, and later, Hosseinnia et al. implemented a hybrid fractional controller in [61] for cruise control at low speeds.

In this chapter, the fractional order iso-m control design methodology described in Chapter 2 is applied to the ACC control of the autonomous vehicle as in [3]. The plant considered, and the control scheme implemented is described next.

4.2 Plant model

The proposed ACC scheme is shown in Fig. 4.4. It is composed of two main blocks, the fractional order controller and the set of actuators and low-level control systems. Therefore, robust control is applied in the high level system, considering the other low level systems as a compact block.

This high level control is designed to regulate the distance to the preceding vehicle.

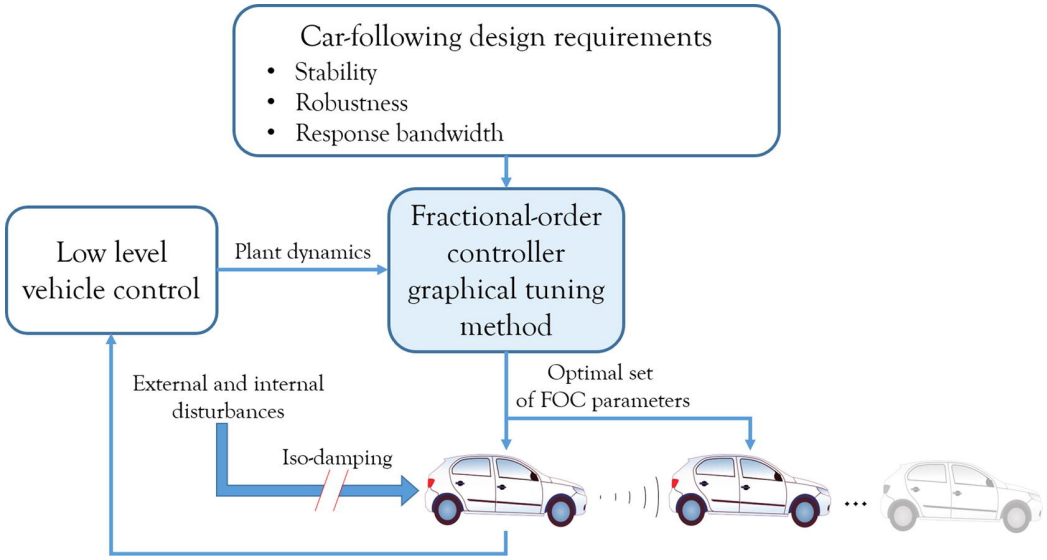

Figure 4.4: ACC proposed control scheme.

A more detailed diagram of the loop shown in Fig. 4.4 is provided in Fig. 4.5. Note that indices are used in the figure to differentiate between cars, where $i \in [1, N]$ is the currently considered car index, being N the vehicle string size, as in Fig. 4.3.

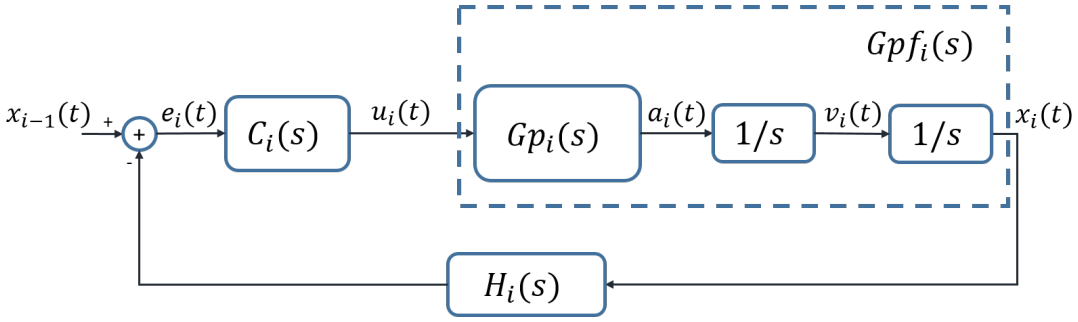

Figure 4.5: High level control loop.

The system acting on the throttle and brake is considered as $Gp_i(s)$. This subsystem has its own loop and performance specification, and is designed to deliver the reference acceleration required by the top layer. Therefore, changes in the speed and position of the vehicle depend on its performance. At the high level, the desired distance is obtained through a feedback loop with a reference established by the spacing policy, which in our case is a constant time gap as in [120].

The constant time gap technique consists of calculating the required distance as the product of the vehicle speed (position time derivative) by a time gap h, adding

a minimum safety distance, resulting in the expression $H_i(s) = hs + 1$. The benefits of this approach are a greater loop stability, thanks to the addition of a zero in the feedback loop, and a closer resemblance to the usual ways of a human driver.

The difference between the measured and the desired gap is the spacing error $e_i(s)$, which is fed to the controller $C_i(s)$ producing a high-level control action $u_i(t)$ based on this error. The control signal then corrects the longitudinal speed of the vehicle by means of the acceleration set by the low level control loop $Gp_i(s)$. Note that this block is made up of subsystems and loops needed to control vehicle acceleration, therefore the input and output signals must be the same (DC gain of 1) after the transient period. Find a more detailed description of this block below.

4.3 Low level control layer

The acceleration tracking block $Gp_i(s)$ design specifications are the following:

- Acceleration reference precision tracking.
- Robustness to changing road conditions.

The low level control layer loop must fulfill these specifications in order to allow the high level layer to perform correctly. In order to design the control loop, the following vehicle longitudinal acceleration $a_i(t)$ model is used:

$$M_v a_i(t) = \frac{\tau_{th,i}(t) - \tau_{br,i}(t)}{r_w} - F_a(\dot{x}_i(t)) - F_g(\theta_r) - F_r(\theta_r, \mu), \tag{4.1}$$

where M_v is the vehicle mass, r_w the wheel radius, θ_r is road steepness, and μ is the friction. Motor and brake torques, are, respectively $\tau_{th,i}(t)$ and $\tau_{br,i}(t)$, see [121] for a detailed discussion on this model. Disturbances are produced by the aerodynamic resistance F_a, the gravitational force F_g and the rolling resistance force F_r.

The low level layer should track the reference acceleration using the throttle and brake system torques, $\tau_{th,i}(t)$ and $\tau_{br,i}(t)$. An extensive set of tests were conducted in open loop configuration on the Honda Accord for dynamic modeling. Mapping the effects of control signals on acceleration as a function of the vehicle speed allows robust control of the throttle or brake pedals required to apply the desired acceleration using the current measured speed. The structure of this low level control layer is shown in Fig. 4.6.

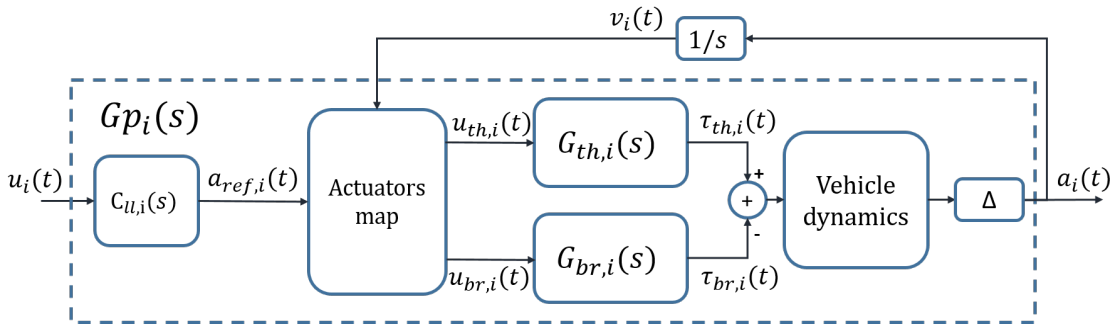

Figure 4.6: Low level control layer block diagram ($Gp_i(s)$)

Coming from the high level control loop, the required acceleration $u_i(t)$ enters the block $Gp_i(s)$ through the controller $C_{ll,i}(s)$, which grants a low sensitivity for the disturbances. Although this controller is a good candidate for robust control techniques, its design is left out of this work to be treated in future developments.

The $C_{ll,i}(s)$ controller output is the control signal $a_{ref}(t)$. This reference, combined with the current speed measurement, is used to decide the necessary action to achieve the required acceleration. This is done by means of the previously discussed mapping, resulting in the desired throttle ($u_{th,i}$) or brake ($u_{br,i}$) command levels that are applied to the vehicle.

These maps are designed to provide the low-level control block with unitary DC gain, and are specific to the vehicle being mapped, in this case the Hybrid Honda Accord 2014. The specific torque commands obtained by mapping are introduced into the propulsion and brake systems, which provide the necessary torques to accelerate the vehicle as required by the high-level loop. These systems are shown in Fig. 4.6 as the throttle and brake transfer functions $G_{th,i}(s)$ and $G_{br,i}(s)$, defined by the following functions:

$$\begin{aligned} G_{th,i}(s) &= \frac{\tau_{th,i}}{u_{th,i}} = \frac{K_{th}}{s/\omega_{th} + 1}; \\ G_{br,i}(s) &= \frac{\tau_{br,i}}{u_{br,i}} = \frac{K_{br}\omega_{br}^2}{s^2 + 2\xi_{br}\omega_{br}s + \omega_{br}^2}; \end{aligned} \tag{4.2}$$

The last two blocks in Fig. 4.6 represent the vehicle dynamics defined in Eq. (4.1). Disturbances F_a and F_r are speed related, and therefore, they have been considered previously in the mapping. Their effects are included in the vehicle dynamics block. However, the disturbance F_g is caused by changes in vehicle mass and road slope, which are uncertain at the controller design time. Given their low frequency, they can be modeled by a DC gain parameter Δ. Therefore, the last block shown as Δ in Fig. 4.6 represents F_g and other uncertain plant disturbances.

In order to find a dynamic model for the low level loop, a test profile, especially designed for modeling and analysis, was performed to obtain the real system response. The results are shown in Fig. 4.7, where correct stabilization times are found after positive (throttle) and negative (brake) acceleration targets. This is important for the closed loop stability, and prove that the maps used in this case are working correctly.

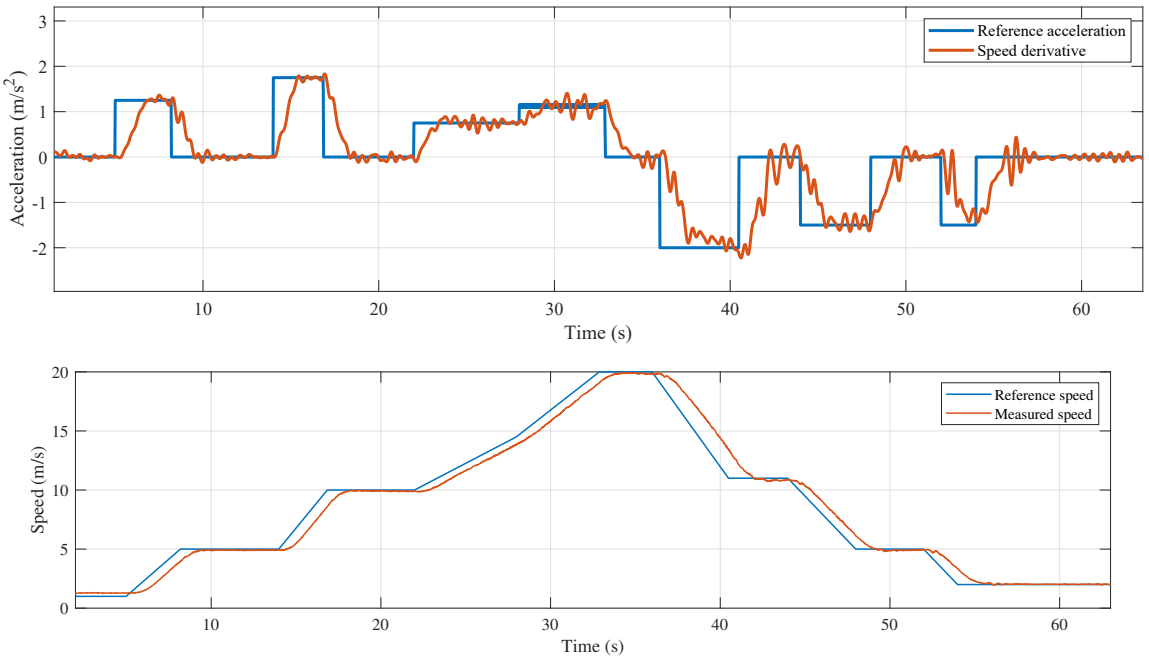

Figure 4.7: Acceleration (top) and speed (bottom) modeling profiles and system responses used in the empirical model of low level block $Gp_i(s)$

The data captured from this profile response was used to find an empirical model for the low level control dynamics through system identification $Gp_i(s) = A_i(s)/U_i(s)$, resulting in:

$$Gp_i(s) = \frac{A_i(s)}{U_i(s)} = \frac{\Delta \cdot 4.51}{s + 3.717}, \tag{4.3}$$

where Δ represents the possible DC gain disturbances of the plant. Considering a default value of $\Delta = 1$, the resulting frequency and time responses are shown in Fig. 4.8.

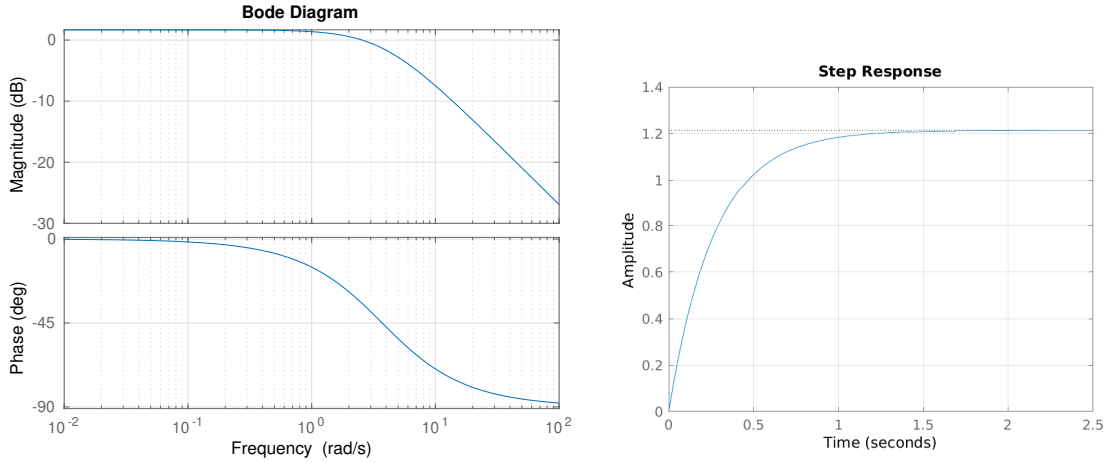

Figure 4.8: Bode diagram of the open loop system $Gp_i(s)$

Note how the low level loop DC gain is not unitary as it should, probably due to unmodeled dynamics, leading to small inaccuracies in the speed tracking results. This error can be considered within the DC gain disturbances of the low level loop, modeled by Δ parameter in Eq. (4.3).

Once the low level $Gp_i(s)$ loop layout has been found, the plant considered for the robust control inside the high level loop can be defined. The high level loop shown at Fig. 4.5 has the following open loop expression:

$$L_i(s) = C_i(s)Gpf_i(s)H_i(s), \tag{4.4}$$

where $Gpf_i(s) = Gp_i(s)/s^2$ corresponding to the dashed line block in that figure.

The purpose of the high level $C_i(s)$ robust controller design is robustness to these uncertainties, as well as other specifications, such as stability or response bandwidth requirements. The desired frequency response shape for this high level loop is a high gain at low frequencies, stable response at medium frequencies, and low gain at high frequencies granting noise rejection, as described in [122].

The transfer function $H_i(s)$ is a problem in the robust design, because changes in the gap policy will change the plant response, affecting robustness. In addition, the Bode's ideal function based robust scheme, requires the feedback to be unitary. In order to solve these problems, $H_i(s)$ function is introduced as a pole in the C_i controller, resulting in:

$$C_i(s) = \frac{FOPD(s)}{H_i(s)}, \tag{4.5}$$

where $FOPD(s)$ is the fractional order controller proposed.

The result of the feedback control shown at Fig. 4.5 in that case is:

$$F_i(s) = \frac{\frac{FOPD(s)}{H_i(s)} Gpf_i(s)}{1 + FOPD(s)Gpf_i(s)}, \tag{4.6}$$

or, rearranging in order to have a unitary feedback loop:

$$F_i(s)H_i(s) = \frac{FOPD(s)Gpf_i(s)}{1 + FOPD(s)Gpf_i(s)}, \tag{4.7}$$

As we can not get $F_i(s)$ to be robust, but we can get $F_i(s)H_i(s)$, we will adjust the controller for that system. Then, to get a robust behavior in the high level loop, it is enough filter the input using $H_i(s)$ transfer function.

Therefore, the robust control design for the loop in Fig. 4.5 proposed is based on the unitary feedback of the loop defined by $Lr_i(s) = FOPD(s)Gpf_i(s)$. The plant model used in the iso-m tuning method is then:

$$Gpf_i(s) = \frac{\Delta \cdot 4.51}{s + 3.717} \cdot \frac{1}{s^2}. \tag{4.8}$$

Frequency response of this model is shown at Fig. 4.9

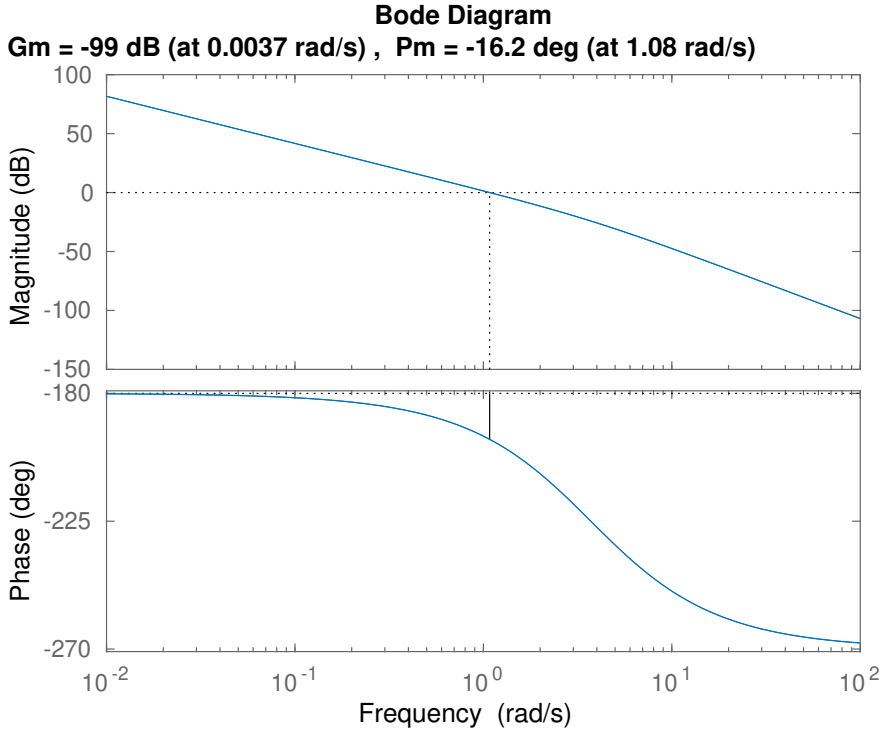

Figure 4.9: Bode diagram of the open loop system $Gpf_i(s)$

4.4 Fractional order controller

Once the plant model is defined, specifications ω_{gc} and ϕ_m must be selected for iso-m tuning. Some overshoot will help to compare the responses in order to evaluate the robustness. According Fig. 1.2, the phase margin required for a damping factor of $\xi = 0.5$ is 50 deg, enough for an acceptable overshoot. A closed loop system bandwidth of 1 rad/s or higher is required to grant a fast response. Using Fig. 1.2, and Fig. 4.9 it is checked that the closed loop bandwidth will be higher than ω_{gc}, therefore, a value of 1 rad/s is valid. As a summary, the specifications chosen are:

- $\omega_{gc} = 1$ rad/s
- $\phi_m = 50$ deg

Therefore, the considered open loop transfer function is $Lr_i(s) = (k_p + k_a s^{\alpha})Gpf_i(s)$ as discussed above. The term $H_i(s)$ is not considered for controller design, but included after solving the parameters k_p, k_a, and α as the pole $1/H_i(s)$.

Controller tuning according iso-m method is described next.

Given the plant description and the Fig. 4.9 Bode diagram, the phase slope at the gain crossover frequency is $m_s = -33$ deg/log(ω), and the phase $\phi_s = -195$ deg. As flat phase is granted using iso-m method, just the following steps are needed for the robust controller tuning:

Step 1: Plant phase slope and phase are $m_s = -33\,\text{deg}/\log_{10}(\omega)$ and $\phi_s = -195$ deg respectively at $\omega_{gc} = 1$ rad/s, as found through Eq. (4.3) or Fig. 4.9.

Step 2: Plant's opposite phase slope is used as controller phase slope, resulting $m = 33\,\text{deg}/\log_{10}(\omega)$. Also, the controller phase required to achieve the phase margin specification at ω_{gc} is $\phi_c = (-(-195) + 50 - 180)$ deg, $\phi_c = 65$ deg. Therefore, using Fig. 2.7 an exponent $\alpha = 0.91$ is found.

Step 3: From these results, τ_a value is found through Eq. (2.43), resulting $\tau_a = 2.964$.

Step 4: Finally, k is found using Eq. (2.44), which results in $k = 0.2607$, making the open loop system gain to be 0 dB at $w_{cg} = 1$ rad/s.

Step 5: Resulting controller parameters are:

k_p	k_a	α
0.2607	0.7741	0.91

Table 4.1: Iso-m FOPD controller parameters for the autonomous car.

Given the positive exponent, we can say it is a fractional proportional derivative controller (FOPD), with a transfer function as follows:

$$FOPD_i(s) = 0.2607(1 + 2.964s^{0.91}) = 0.2607 + 0.7741s^{0.91} \tag{4.9}$$

Based on that, the resulting controller is:

$$C_i(s) = 0.2607\frac{(1+2.94s^{0.91})}{hs+1} = \frac{0.2607+0.7741s^{0.91}}{hs+1}. \tag{4.10}$$

The frequency response of the $Lr_i(s)$ open loop using this controller is shown in Fig. 4.10.

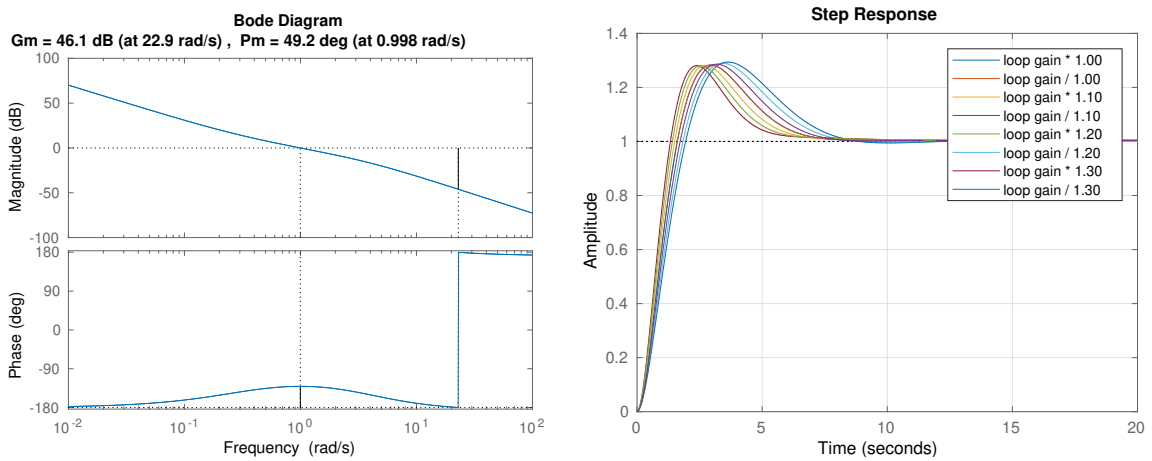

Figure 4.10: Frequency (left) and time (right) responses using FOPD controller tuned with iso-m method.

Observe how fulfilled phase and frequency specifications are shown, presenting a flat phase slope around the crossover frequency, and how step response overshoot is preserved despite the different system gains (iso-damping).

4.5 Integer order controller

The performance obtained with the robust controller will be compared with an integer order PD controller (IOPD), designed with the same phase margin and crossover frequency specifications. The obtained IOPD controller results $PD_i(s) = 0.373 + 0.7662s$.

The open loop response of the system using this controller is shown at Fig. 4.11.

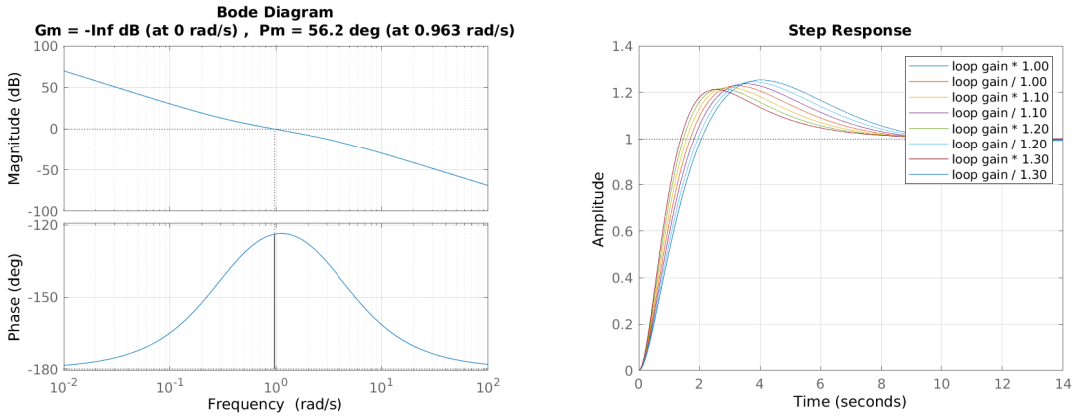

Figure 4.11: Frequency (left) and time (right) responses using IOPD controller.

Now the specifications are not completely fulfilled, presenting a certain phase slope around the crossover frequency. Therefore, step response overshoot is not the same for the different system gains.

The reason for this difference is that integer controller is unable to meet the robustness requirements, as shown in Fig. 4.12. The IOPD (blue line) and the FOPD (red line) fulfill the phase margin and crossover frequency requirements, but only the later shows a flat phase at the crossover frequency.

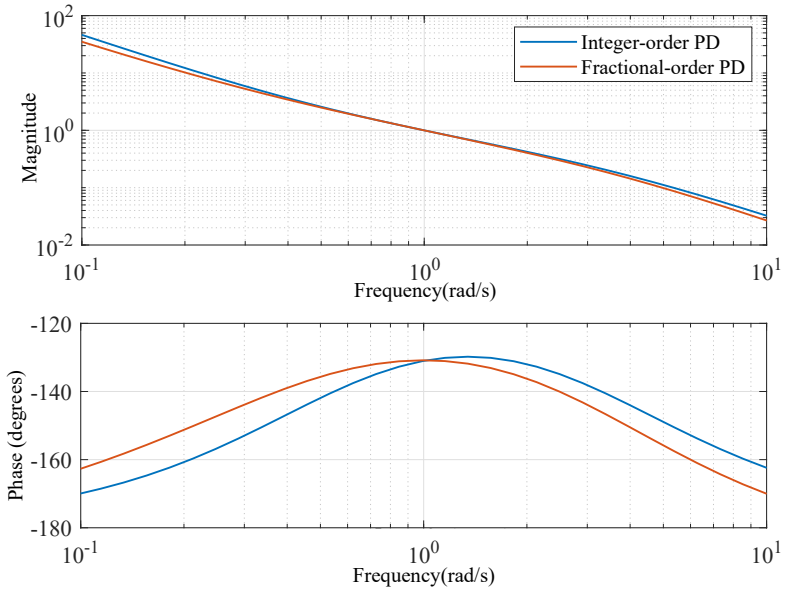

Figure 4.12: Frequency response comparison of the IOPD and FOPD controllers.

4.6 Simulation results

A simulation including plant gain variations was carried out to analyze the performance of the controller. The system responses are shown in Figure 4.13 for the proposed controller and the plant model. Observe how the performance is greatly improved, showing a constant overshoot in the interdistance plot (bottom).

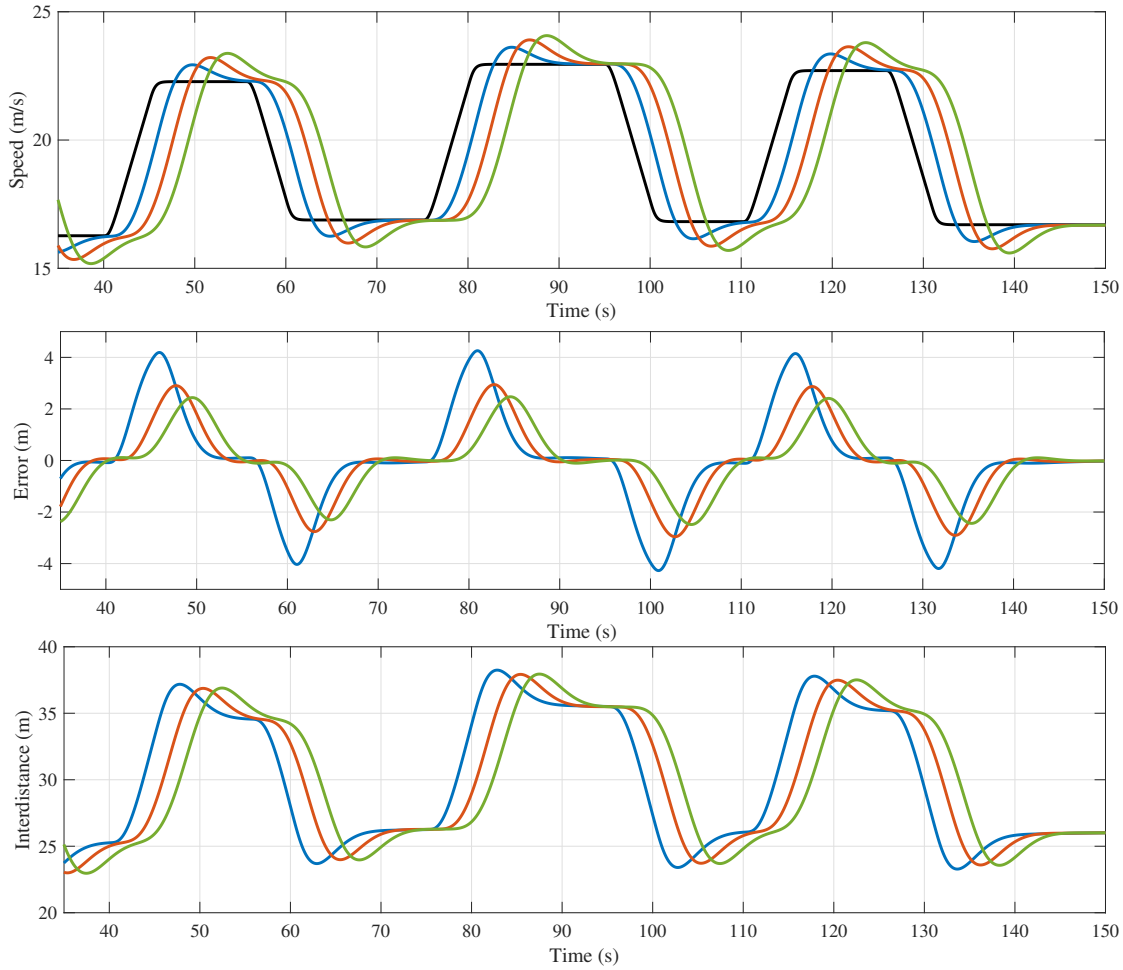

Figure 4.13: Simulation results including plant DC gain variations. Plots of leader and controlled vehicles with index 2, 3 and 4 (black, blue, red and green lines, respectively).

This simulation shows the analysis of a 4 vehicle chain. The first vehicle is commanded to follow an acceleration profile (in black), while the followers are tracking the leader using the designed ACC controller with a time gap of $h = 1.5s$. The

graph on the top shows the speed of all vehicles, the middle shows the evolution of the spacing error and the bottom figure presents the distances between vehicles. The vehicles in the chain are set with different DC gain disturbances, where the index 1, 2, 3 and 4 vehicles are set with $\Delta = [1.0, 0.76, 1.1, 1.3]$, respectively.

Speed changes introduced by the leader are correctly followed by the entire chain, according the desired policy of constant time gaps. It is important to note the iso-damping property achieved, resulting in the same stability and overshoot of closed loop response for all vehicles despite the different DC gains. This robustness feature is highly desirable for automated vehicle tracking systems, since a difference in road slope, vehicle mass, or powertrain dynamics can produce unwanted results.

Another simulation showing the response comparison for the case of a vehicle in the string equipped with either the IOPD (blue line) or the FOPD (red line) controller is provided in Fig. 4.14.

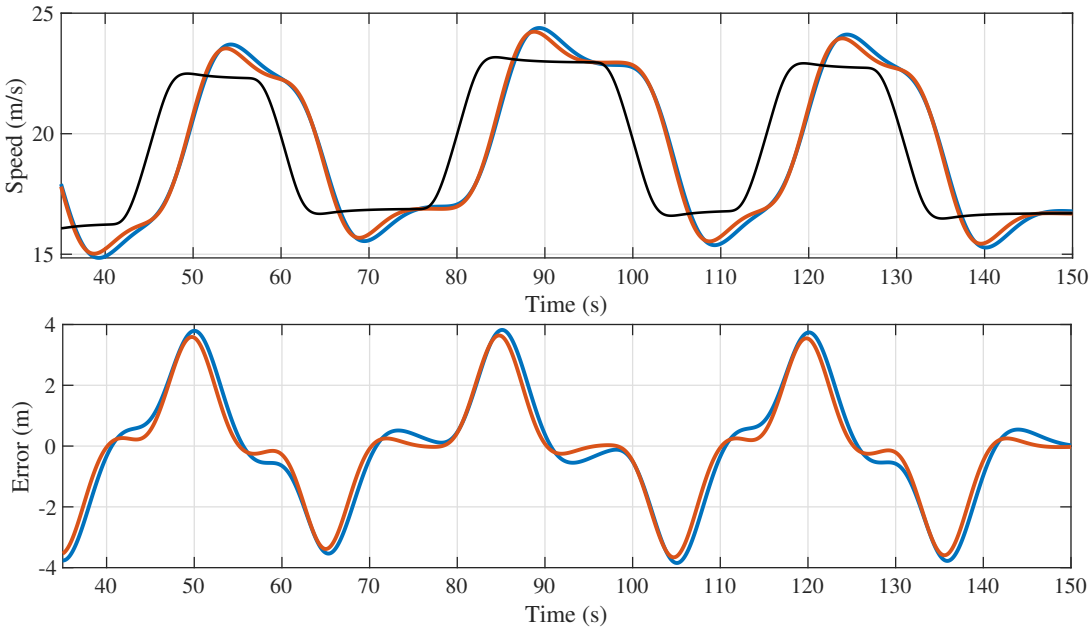

Figure 4.14: Comparison showing the last vehicle (index 4) ACC-control response in the cases of IOPD (blue line) and FOPD (red line) controllers.

The leader vehicle follows the same speed profile presented in Fig. 4.13, and the graphs shows speed (top) and distance error (bottom). A slightly higher overshoot can be observed for the IOPD vehicle, due to the gain change produced by the *Delta* disturbance. Using the fractional order controller instead of the IOPD, not only the spacing error is more stable, but the absolute error is reduced by 17%. This feature is especially useful when dealing with heterogeneous dynamics chains. The iso-damping

property would play a key role to ensure a consistent tracking performance of the different vehicles ACCs.

4.7 Experiment description

The controller designed using the iso-m method was approximated with a six (integer) order transfer function. It was later discretized using Tustin's method with a 0.05s sampling period in order to transfer to the vehicle's real time computer. The discrete high-level controller transfer function results in:

$$C_i(z) = \frac{0.3621z^6 - 1.193z^5 + 1.087z^4 + 0.4256z^3 - 1.301z^2 + 0.7669z - 0.1482}{z^6 - 3.53z^5 + 3.937z^4 - 0.2446z^3 - 2.575z^2 + 1.788z - 0.3746} \tag{4.11}$$

This controller was set on the Hybrid Honda Accord 2014 platform in Fig. 4.1 and evaluated on a highway scenario. The target vehicle was tracked using front radar, and the time gap set to $h = 1.5s$.

4.8 Results

The preceding (leading) and subject (following) vehicle measured speeds are shown in Fig. 4.15. Observe how the controlled vehicle tracks the speed oscillations with a good accuracy. In addition, the speed changes are tracked without amplification, showing the controller's capacity to provide stable tracking of the chain's next vehicle.

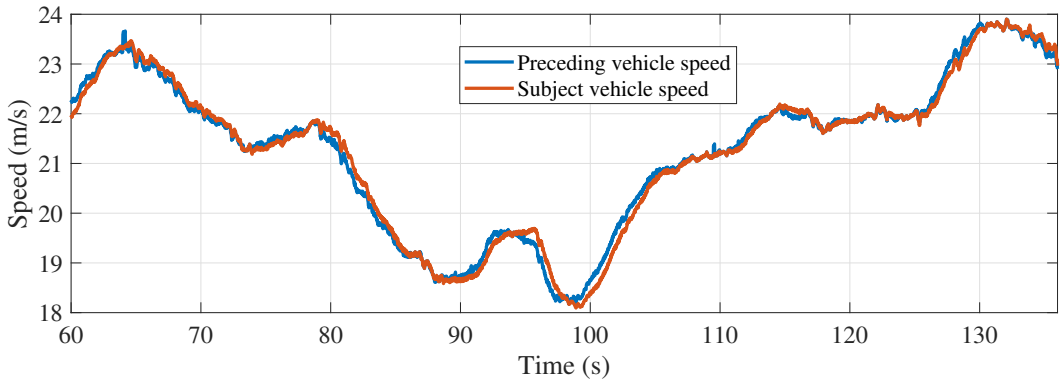

Figure 4.15: Preceding (leading) and controlled (following) vehicle speeds

According to the $1.5s$ time gap spacing policy, the distance to preceding vehicle must evolve proportionally to the subject vehicle's speed. The experiment measured

spacing gap is plotted at Fig. 4.16, showing a correct evolution compared to the Fig. 4.15.

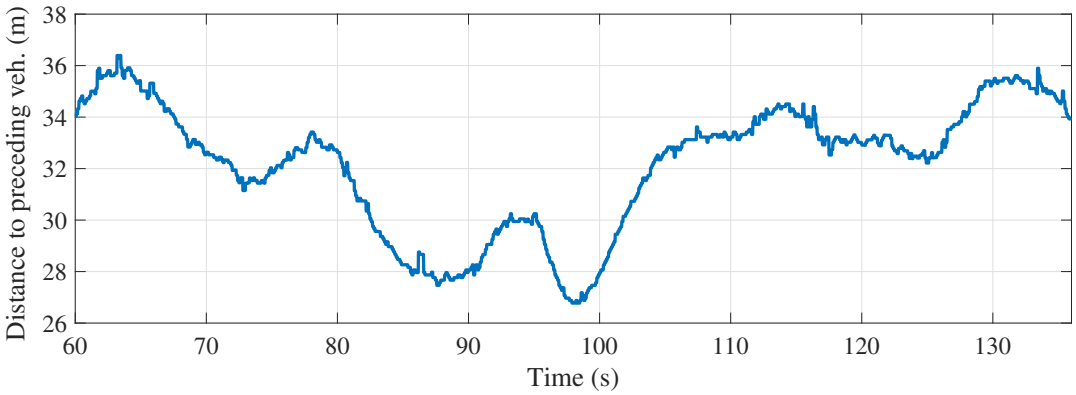

Figure 4.16: Measured distance towards preceding vehicle

The spacing error through the experiment is shown in Fig. 4.17. Note the absolute value lower than $1.8m$ and under $1.8m$ most of the time.

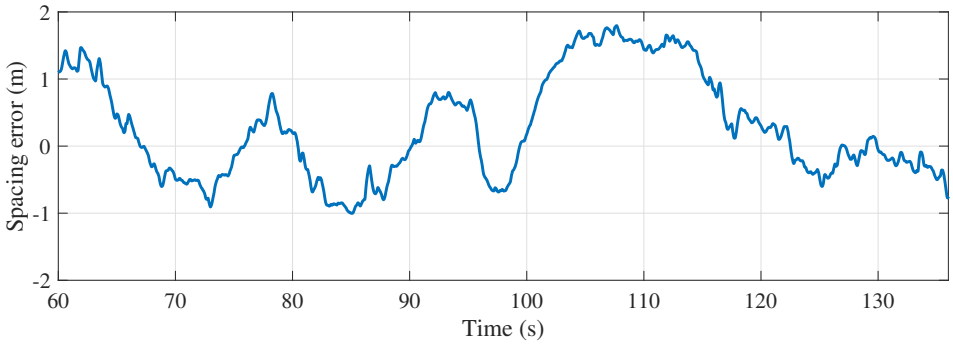

Figure 4.17: Spacing gap error used for feedback control

These results show the proposed control method potential to grant a safe and stable tracking ACC system, even at highway speeds and despite possible changes in road slope or other disturbances affecting the low-level system gain.

It is important to note that the experimental results obtained are coherent with the previously presented simulation results, in terms of speed propagation and spacing error magnitudes. This confirms the feasibility of the approach and its benefits added to real-world applications.

Chapter 5

Experimental Results: Humanoid robot TEO

The second platform considered is the elbow joint of TEO, a full-size humanoid robot developed by the Robotics Lab team of Carlos III University of Madrid [108], shown in Fig. 5.1.

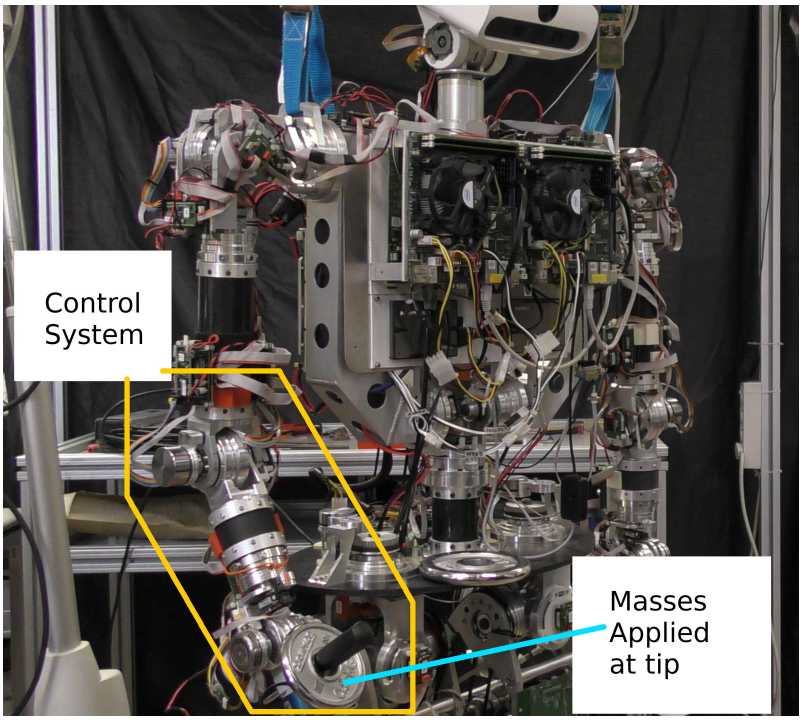

Figure 5.1: Humanoid robot TEO. Control system (yellow) and applied masses (blue).

It is an improved version of its predecessor RH1. TEO (RH2) has six joints on each limb, making a total of 24 DOF for all four limbs. The joints for the trunk and head pitch-yaw add four DOF, resulting in a combined 28 DOF robot.

The system to be controlled will be the forearm (see Fig. 5.1). Since the other joints are kept static, the system can be modeled as a solid of 8 cm diameter and 20 cm length, rotating around the joint axis.

During this experiment, several integer and fractional controllers will be tested and compared to validate the proposed control methods.

5.1 Similar approaches

Many works have addressed similar problems using fractional order controllers. A significant number of papers, especially when motion control is involved, focus on the derivative controller. This scheme considers the position sensor as an integrator that enables the cancellation of steady state errors while simplifying the controller to a PD. For example, in [52] Dorcak proposed this scheme, and later, in [35], a FOPD controller was used for the first time for the control of a DC motor. This approach is also proposed in [123] and [63], and has been successfully applied in the field of robotics. For example, in [36] this strategy was applied for a robot joint control, and in [64] for the control of a legged robot.

5.2 Plant model

A plant model is required for the design and simulation of the controller. The joints of the robot, including the elbow, are made up of a driver-motor-gear system:

- Driver: Technosoft iPOS3604 MX-CAN; 400 W, 12-50 Volt, 8 Amp (intelligent motor driver).
- Motor: Maxon EC 45; flat 42.8 mm, brushless, 70 Watt.
- Gear: Harmonic Drive™ (of different ratios).

Since the motor velocity is managed through the iPOS3604 intelligent driver, featuring a micro-controller with an existing motion profile, the velocity response of the joint is different from a standard DC motor. The existing velocity profile was trapezoidal, as shown in Fig. 5.2, which means that the speed change is made through a ramp (therefore trapezoidal), allowing only two possible acceleration values (currently $\pm 10\,\mathrm{deg/s^2}$), with a software limited velocity (saturation at 24 deg/s). The

benefit of this profile is a good balance of current input, but it makes the plant nonlinear and makes modeling more difficult.

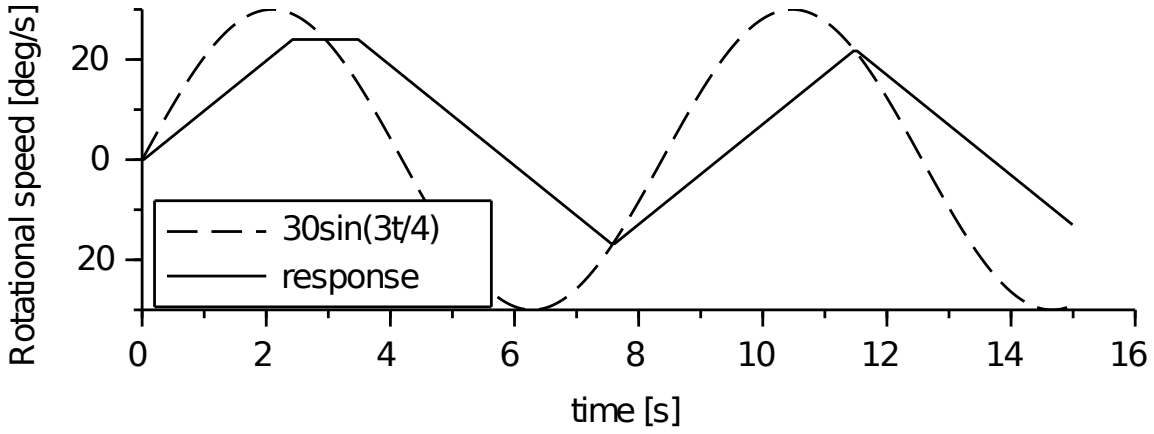

Figure 5.2: Velocity system response to a sinusoidal input, showing constant acceleration and saturation at 24 deg/s. Although the frequency is the same for the input and the output, their wave forms are different.

The model that best fits the described behavior is shown in Fig. 5.3 and is based on a constant acceleration constraint.

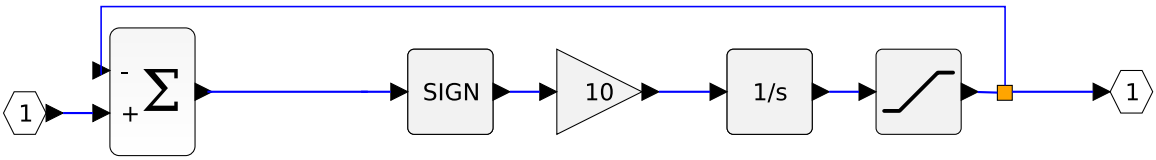

Figure 5.3: Block diagram of the system. Left to right: Input, Difference, Sign, Gain, Integrator, Saturation, Output.

The sign block makes linear modeling not possible. Therefore, an approximation model will be used. The proposed alternative is a unit feedback system with a gain and an integrator, with a closed loop transfer function $G(s) = 1/(0.1s + 1)$, similar to the plant described in Fig. 5.3, with saturation and sign blocks removed.

Therefore, as long as the operation stays below the saturation levels of this model, the approximation will be valid for design and simulation. To check the model, a unitary step was introduced in the linear and non-linear models using a simulation tool (scilab xcos), resulting in the plot shown in Fig. 5.4. Given the similarity of the response curves (97.4%), the use of the linear model for controller design purposes may be acceptable.

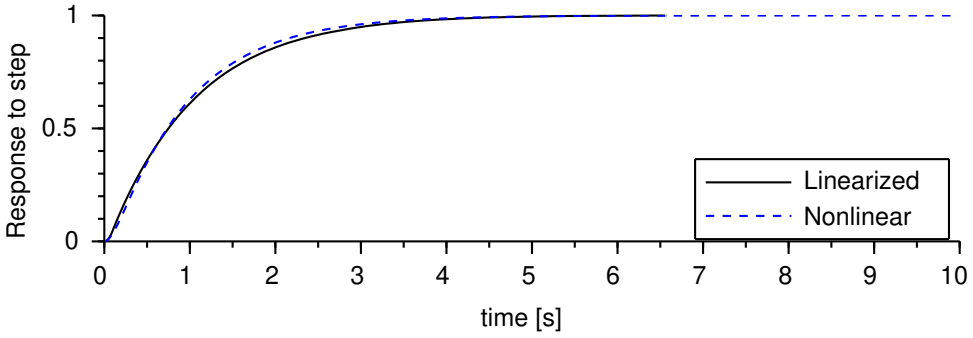

Figure 5.4: Response to a feedback unit step in deg/s showing the difference between linearized and nonlinear models.

Although there is obviously a difference between the two systems, it will be neglected given the robustness properties of the proposed control schemes. It is assumed that the differences between the model and the plant will not be significant for control tasks, as will be proven in the experimental results section.

Therefore, the motor will be modeled as a first order system, with velocity input and joint velocity output. The plant gain is one because the motor is commanded from the intelligent driver, where all ratios, (including gear ratio) are already considered, making velocity targets to be expressed in joint units.

If the encoder signal is used for the control loop, the angular position must be considered as the system output. In this case, if the target velocity is used as the system input, an integrator must be considered in the transfer function, resulting in Eq. (5.1).

$$G(s) = \frac{1}{(0.1s+1)s} \tag{5.1}$$

The frequency response of the plant model is shown in Fig. 5.5, where a phase margin of $\phi_m = 84.3\,\text{deg}$ and a gain crossover frequency of $\omega_c = 0.995\,\text{rad/s}$ can be observed.

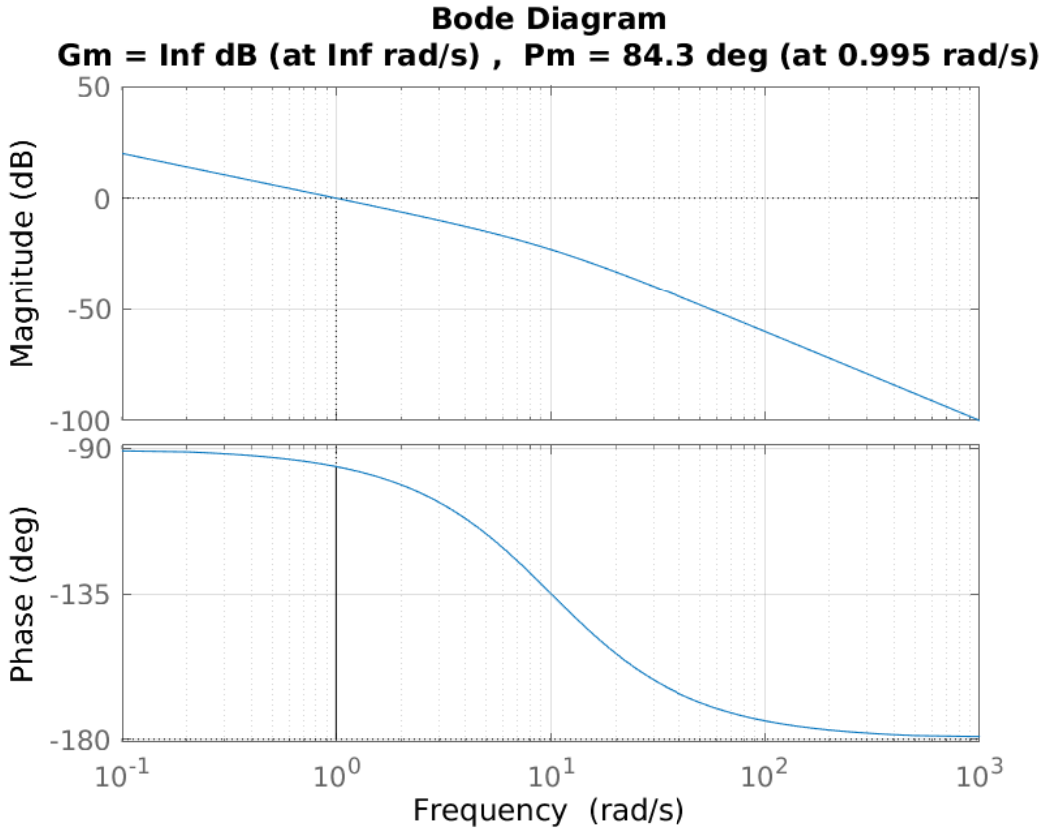

Figure 5.5: Bode diagram for the system model with transfer function in Eq. (5.1).

Given the actuator described, the plant model for TEO's elbow joint, considering the same velocity input and joint position output, is similar to the described system, but presents a changing gain, due to the inertial properties and the effects of gravity.

During the experiments, different payloads will be attached to the robot's hand, in order to verify the robustness properties of each controller. The time response for each method will be studied in order to analyze the robustness of the system to mass changes. Also, to include the effects of gravity, the input reference will be a negative step moving the arm down. In this way, the system performance in the presence of modeling uncertainties will be tested.

The proposed controllers are FOPD and FOPI. Both can be defined by the same equation as follows:

$$C(s) = k_p + k_a s^{\alpha}, \tag{5.2}$$

since the derivative fractional order α can have negative values. The parameter k_p is the proportional gain and k_a is the derivative/integral gain.

The control specifications to meet are defined in Eqs. (1.8), (1.9), and (1.7). The first two specifications define performance in the usual sense of stability (overshoot) and responsiveness (peak time), and the third gives robustness to:

- Plant gain changes
- Model uncertainties

The gain of the plant is mainly affected by its payload, as demonstrated in [124]. Therefore, meeting the third specification will make the system robust to payload changes.

The gain crossover frequency should be lower than the plant cutoff frequency to avoid saturation, but there is no reason to use a lower frequency. Then, the maximum available $\omega_{gc} = 1\,\text{rad/s}$ is specified.

The plant phase margin at that frequency is 84.3 deg, therefore, the plant phase is $\Phi_s = -95.7\,\text{deg}$. The derivative controller specifications must be above this phase margin, since they add phase to the final system, and in the same way, the integral controllers specifications must be below that margin. Therefore, the following specifications are considered:

- FOPD: $\phi_m = 110\,\text{deg}$
- FOPI: $\phi_m = 70\,\text{deg}$

Given these specifications, the controller tuning is done using three different methods to compare.

5.3 Monje's fractional order controller

The first method considered is the one described in [31]. According to the Monje's method, the following specifications will be used:

1. Phase margin ϕ_m at crossover frequency ω_c:
   - $|C(j\omega_c)G(j\omega_c)|_{dB} = 0\,\text{dB}$
   - $\arg\left(C(j\omega_c)G(j\omega_c)\right) = -\pi + \phi_m$
2. Plant gain changes robustness:
   - $\left(\frac{d(\arg F(s)}{d\omega}\right)_{\omega=\omega_c} = 0$, F(s) being the open loop system.

Using numerical methods like [125] and [126], a solution was obtained that met the above constraints for the following controller parameters: $k_p = 0.463$, $\tau_d = 0.621$, $\mu = 0.495$. The Bode diagram of the open loop system with this controller and the step response are shown in Fig. 5.6, where the specifications are clearly met. It can be verified that the phase slope is flat at the selected frequency ($\omega_c = 1\,\text{rad/s}$), and that $\phi_m = 110\,\text{deg}$.

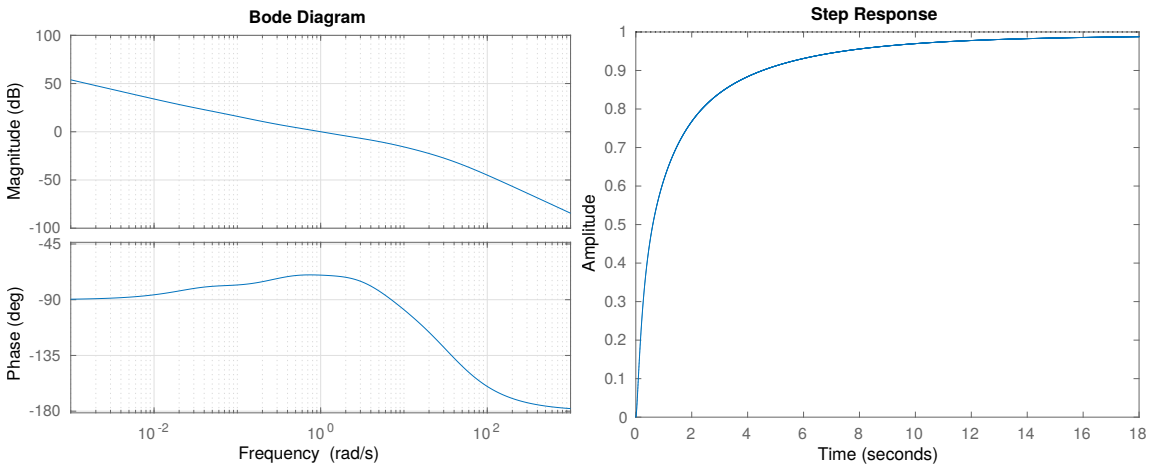

Figure 5.6: Frequency and step responses for the FOPD based on Monje's method.

Notice how the specifications are met in terms of phase margin and crossover frequency.

5.4 Artificial Bee Colony (ABC) algorithm

Using the ABC algorithm as in [44], with the following parameters:

- employed: 50,
- onlookers: 50,
- iterations: 100,
- acceleration coefficient upper bound: 1,

the following controller parameters were found: $k_p = 0.009$, $\tau_d = 0.996$, $\mu = 0.99$. The results are shown in Fig. 5.7.

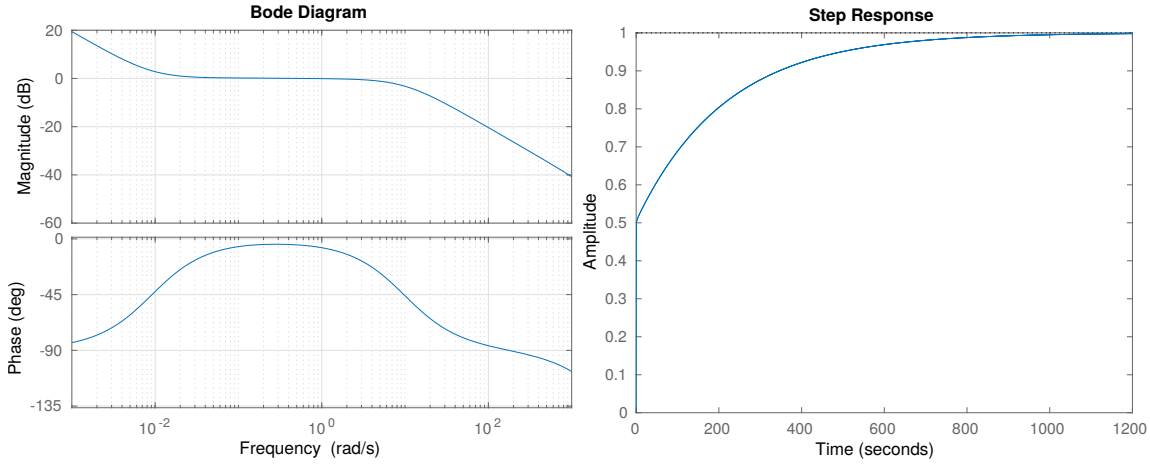

Figure 5.7: Frequency and step responses for the FOPD controller based on the ABC algorithm.

Note how the specification of the gain crossover frequency $\omega_c = 1\,\text{rad/s}$ is achieved, but with $\phi_m = 175\,\text{deg}$, much higher than desired. It is a common problem in optimization methods, while one of the specifications is met, the other gets stuck at local minima.

5.5 Fractional order controller based on the iso-m method

Given that the flat phase specification in Eq. (1.7) is granted automatically using the iso-m method, which provides robustness to parameter variations, just the following steps are to be taken:

Step 1: The plant phase slope at $\omega_{gc} = 1\,\text{rad/s}$ is $m_s = -12.94\,\text{deg}/\log_{10}(\omega)$, and the phase is $\Phi_s = -95.7\,\text{deg}$, as found through Eq. (5.1) or in the frequency response shown in Fig. 5.5.

Step 2: The controller phase slope is then $m = 12.94\,\text{deg}/\log_{10}(\omega)$, which is the opposite of the plant, and the controller phase required to achieving the specification of the phase margin at ω_{gc} is $\phi_c = (-(-95.7) + 110 - 180)\,\text{deg}$, $\phi_c = 25.7\,\text{deg}$. Therefore, using Fig. 2.7 we find an exponent $\alpha = 0.49$.

Step 3: According to these values, τ_a value is found using Eq. (2.43), resulting in $\tau_a = 1.31$.

Step 4: Finally, k can be computed using Eq. (2.44), resulting in $k = 0.4671$, which makes the open loop system gain to be 0 dB at $w_{cg} = 3\,\text{rad/s}$.

Step 5: The resulting controller parameters are:

k_p	k_a	α
0.4671	0.6120	0.49

Table 5.1: Iso-m FOPD controller parameters for the elbow of TEO.

Given the positive exponent, we can say it is a fractional proportional derivative controller (FOPD), with the following transfer function:

$$C(s) = 0.4671(1 + 1.31s^{0.49}) = 0.4671 + 0.6120s^{0.49} \tag{5.3}$$

The resulting Bode diagram is shown in Fig. 5.8. A flat slope is observed at the specified frequency, as well as a crossover frequency according to the requirements. The step response of the controlled system is also shown on the right side of figure.

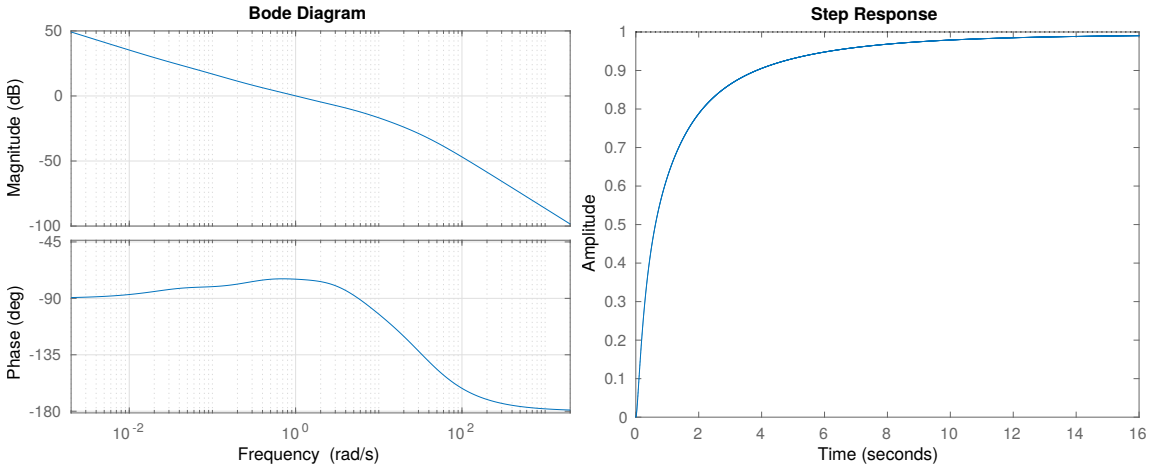

Figure 5.8: Bode diagram (left) and step response (right) for the FOPD controller based on the iso-m method.

5.6 Experiment description

Once the different controllers have been tuned, they will be implemented and tested in the real platform, and the results will be discussed.

For the controller implementation, an integer order approximation for s^α, based on an iterative algorithm described in [127], will be used for each exponent. Then, the transfer function for s^α will be discretized, using Tustin's method with a sampling period of $t_s = 0.01$.

During the experiment, the robot is standing with all joints blocked, except the fourth joint of the right arm, which will receive a -30 deg step input starting from the position of 60 deg. The arm will move following a downward trajectory, going through

the worst case of uncertainty, since the gravity force is opposite to the control effort. Different masses will be attached to the tip to test the robustness of each controller. The masses will vary from 0 kg to 2 kg in steps of 500 g, which gives a forearm weight variation of 64.5%, since its total weight is 3.1015 kg

5.7 Results

The same performance and robustness specifications have been set for all controllers, but not all specifications were met for the ABC controller. Therefore, a clear advantage of the fractional order controllers obtained using the iso-m and Monje's method is observed in Fig. 5.9, where the system performances are shown for the case of no load at the tip.

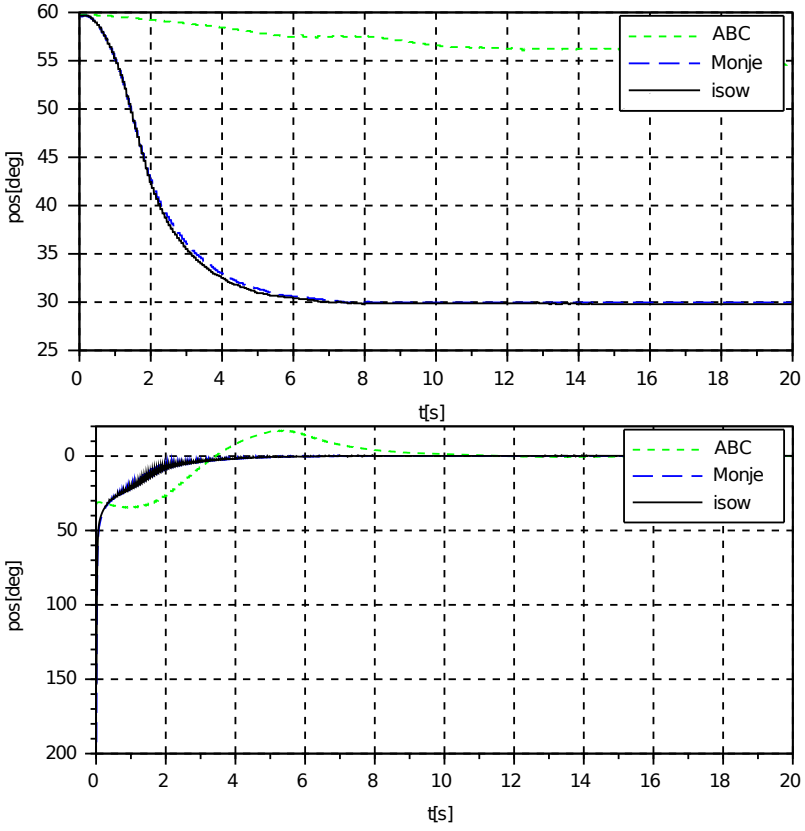

Figure 5.9: Comparison in the case of zero payload for all controllers, showing time response (top), and control signal (bottom). Step input of −30 deg.

The robustness of the different controllers is shown in Fig. 5.10. Note that the response is invariant for Monje's and iso-m methods despite the different loads at

the tip, starting with 500 g and reaching 2000 g. Again, the results are worse for the ABC-based control system, since the phase is not flat around ω_{gc}.

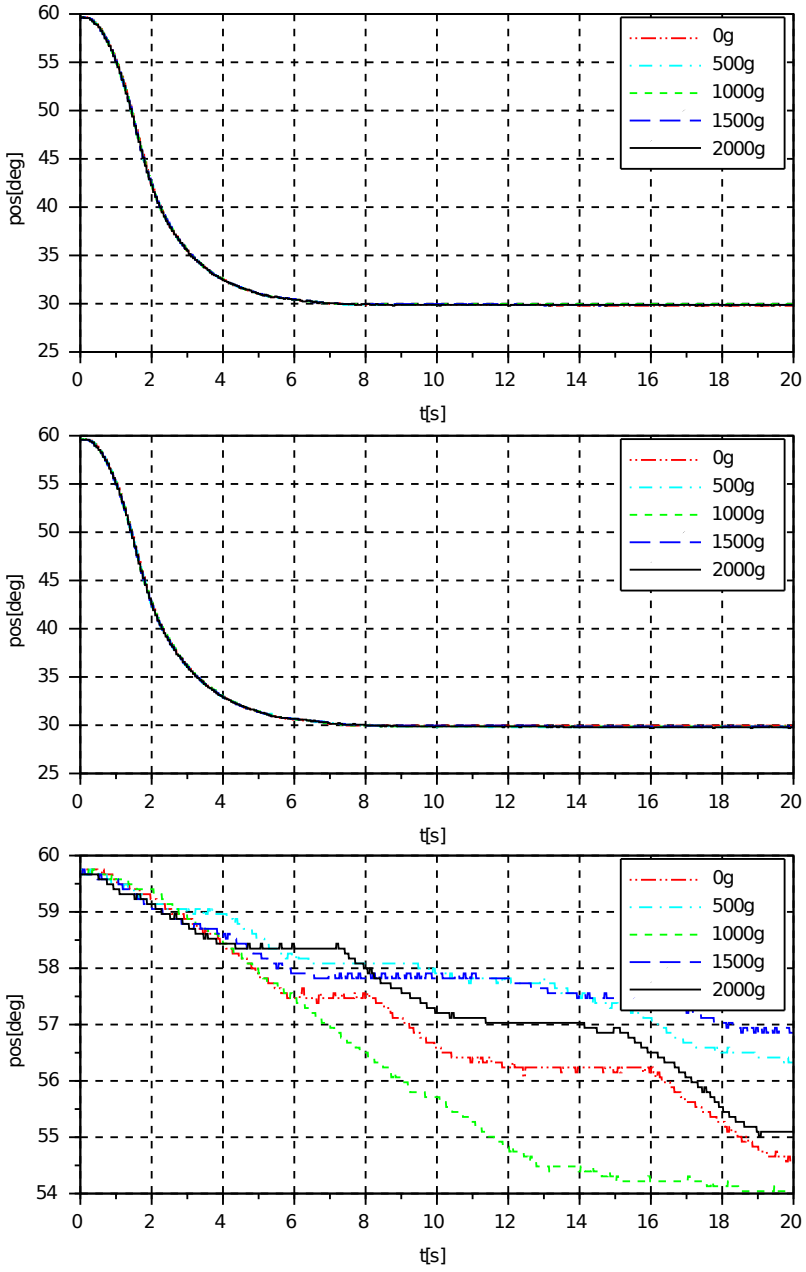

Figure 5.10: Comparison of the responses of all controllers for different masses at the tip. Step input of −30 deg. Iso-m (top), Monje's (middle) and ABC (bottom) methods.

Regarding performance, both iso-m and Monje's methods show very similar results, the former showing a slightly faster response. The results of the ABC method are worse, presenting a very high settling time (800 s). The steady state error is zero for Monje's and iso-m control systems. The ABC controller should cancel the error as well, but the system is too slow. Table 5.2 shows detailed performance data for each method from Fig 5.10.

Method	Overshoot	Rise t. s	Sett. t. s	ΔO
Monje's	0	4.94	6.35	0
iso-m	0	4.64	5.83	0
ABC	0	≥ 20	≥ 20	-

Table 5.2: Performance comparison results including overshoot variation (ΔO) for TEO robot

5.8 Fractional order controller after joint replacement

After the first set of experiments, during some maintenance works, the elbow motors and other parts were replaced, making it necessary to obtain a new plant model. A frequency identification was performed on the real system, and then the result was approximated by Levy's method for complex curve fitting [127]. The result is shown in Eq. (5.4).

$$G(s) = \frac{1}{s + 1.25} \tag{5.4}$$

Based on this approximation, the Bode plot shown in Fig. 5.11 was obtained. The original frequency response of the system is also shown in the figure.

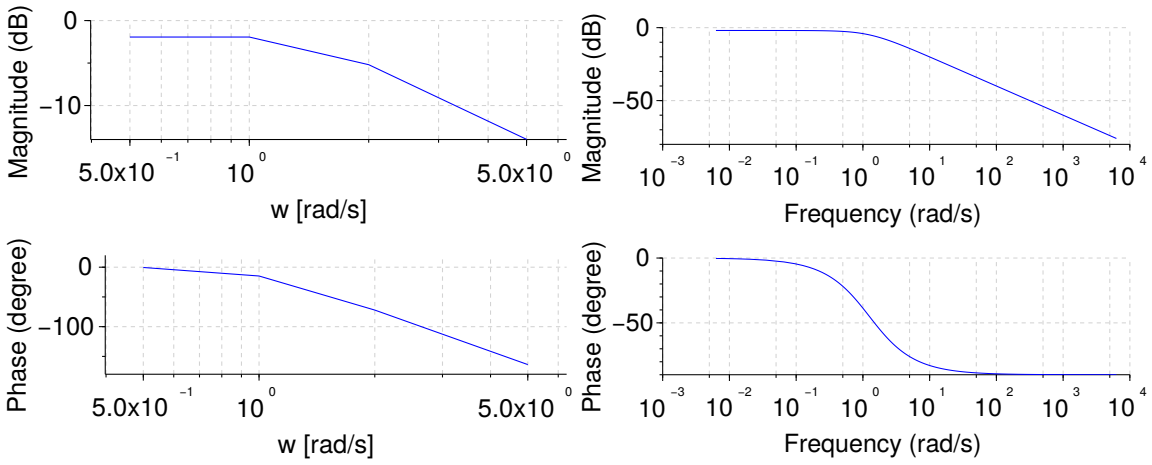

Figure 5.11: Frequency system identification results. Bode diagrams of the measured system (left) and approximate model (right).

Therefore, a first order system was approximated using Levy's method, and considering the encoder output (additional pole at the origin), the resulting model is shown in Eq. (5.5). This new model will be used for the FOPI controller tuning.

$$G(s) = \frac{1}{(s + 1.25)s} \tag{5.5}$$

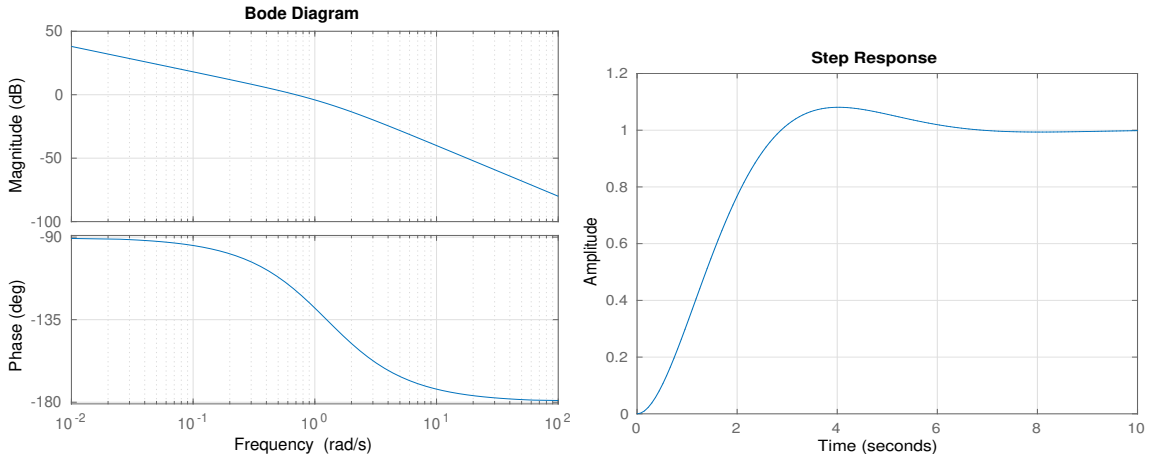

Figure 5.12: Bode diagram for the new system model with transfer function in (5.5) (left) and unitary feedback step response in deg (right).

Using the model in Eq. (5.5), a fractional FOPI controller was tuned and tested on the real robot.

Comparison with the results presented in the previous sections is not possible because the plant models are different; therefore, more convenient control specifications have been used:

- $\omega_c = 0.5\,\text{rad/s}$
- $\phi_m = 35\,\text{deg}$

Note the very low phase margin that is needed in order to make the controller FOPI (i.e. negative exponent). This is the reason why FOPD is preferred for this type of plants that include an integrator. Now, we will apply the iso-m method to tune the controller.

Given the system slope of $-45\,\text{deg}/\log_{10}(\omega)$ found in the Bode diagram of the system in Fig. 5.12 and according to Fig. 2.7, clearly $\alpha = -0.858$. Then, using Eq. (2.43), a value of $\tau_a = 0.5517$ is found.

Finally, $k = 0.43385$ is computed using (2.44), making the magnitude 0 dB at $\omega_{gc} = 0.5\,\text{rad/s}$. Therefore, the result is the following:

$$C(s) = 0.43385(1 + 0.5517s^{-0.858}) = 0.43385 + 0.2394s^{-0.858} \tag{5.6}$$

The resulting open loop Bode diagram and unitary feedback step response are shown in Fig. 5.13. A null slope is observed at the specified frequency, as well as a gain crossover frequency according to the requirements.

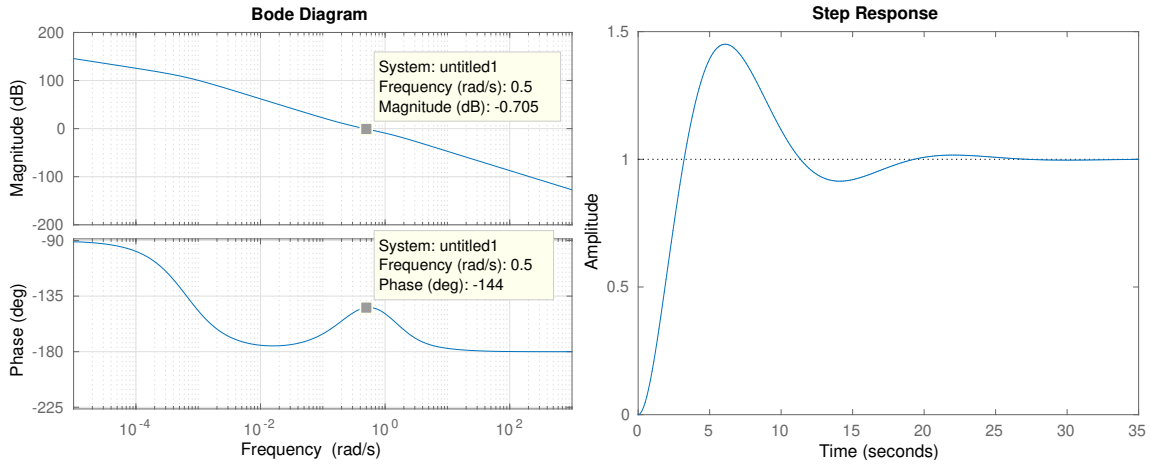

Figure 5.13: Bode diagram and step response for FOPI controller based on the counter-slope method.

The defined controller was tested on the robot arm. A setup similar to the other experiments was used for the FOPI. A downward trajectory was used, starting at 50 deg with a target of 40 deg.

In Fig. 5.14 a robust response is shown despite the different masses. Notice how the overshoot is invariant for variable loads at the tip, starting with 0 g and reaching 2000 g.

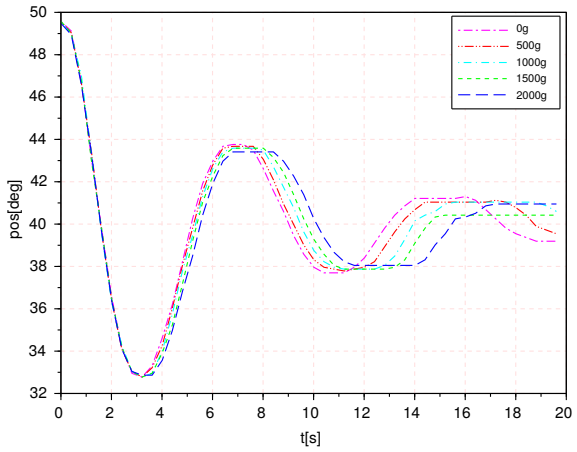

Figure 5.14: Comparison of the time responses of the FOPI controller for different masses at the tip. Step input of -10 deg.

Table 5.3 shows the performance results data for the FOPI experiment.

Method	Overshoot	Rise t. s	Sett. t. s	ΔO
iso-m (FOPI)	0.45	5.85	16.6	0

Table 5.3: FOPI performance data including overshoot variation (ΔO) for TEO robot

Chapter 6

Experimental results: Soft robotic neck

Another platform considered in this thesis is the bio-inspired robotic soft neck developed in the works of [7] and [9]. Given the non-linear and variable properties of this platform, it provides an excellent test bench for this type of controllers.

Some current modeling and control approaches are discussed below.

6.1 Current soft robotic designs

Soft robotics is an emergent field showing non-linearity problems that need to be solved. Trying to address these new non-linearity problems, soft robots have received a lot of attention in the recent years.

Some efforts are devoted to improving soft material models to allow a better understanding of soft robotics systems, for example as in [128] where three characterizations (Ecoflex 00-30, Mold Max 14NV, and Smooth-Sil 950) are provided for different soft robotics materials.

At the same time, in the field of robot modeling, new proposals have been studied, such as [129], modeling a soft robotics gripper for different actuation valves and pressures, or the soft neck model proposed in [65], where a two tendon actuator system was used to tilt a soft material in a single direction.

Regarding control, model accuracy is less important than feasibility in a control scheme. As discussed above, a simple system identification algorithm may be preferred for control due to convergence and stability properties. For example, in [130] a characterization of the frequency response of a self healing material pouch actuator is used for PID controller tuning, using a dual control scheme where compression and relaxation are treated separately with a different controller each, and in [131] a simple

feed-forward compensation rule following a friction model inverse is enough to control tension in a wearable robot.

However, more advanced control schemes have also been used in soft robotics, for example, in [132] a neural network is trained using finite element simulations, and later used to control a multi-segment soft tentacle robot made of a Nitinol needle inside a Helmholtz coil, or the embodied intelligence proposal from [133] where the robot shape is exploited for kinematic resolution in a bio-inspired octopus robotic arm. For a reference on other older soft robotics proposals and solutions, find a survey in [134].

In this chapter, the two novel controllers will be used to control the soft neck prototype based on the works in [7], showing how these type of systems can be controlled using robust and adaptive fractional controllers.

The system to be controlled is the robotic soft neck shown in Fig. 6.1. The purpose of the neck is to tilt any system such as cameras and sensors mounted on the humanoid's head to arbitrary orientations. This design features a central soft link, which acts as a spine, and a parallel cable driven mechanism (CDPM), which acts as tendon actuators. The three tendons are configured to bend the central link, causing the upper platform to reach different inclinations and orientations within a range.

Its main components, shown in Fig. 6.1 are:

1. Base.
2. Moving platform.
3. Soft link.
4. Tendons.
5. Actuators.
6. Tilt sensor.

Each of the three actuators located on the base consist of:

- Driver: Technosoft iPOS4808 MX-CAN; 400 W, 12-50 Volt, 8 Amp (intelligent motor driver).
- Motor: Maxon RE 16, 16 mm, Graphite Brushes, 4.5 Watt.
- Gear: Maxon planetary gear head GP16A $(24 : 1)$.
- Encoder: Maxon MR Type M, 128–512 CPT (2048 positions).

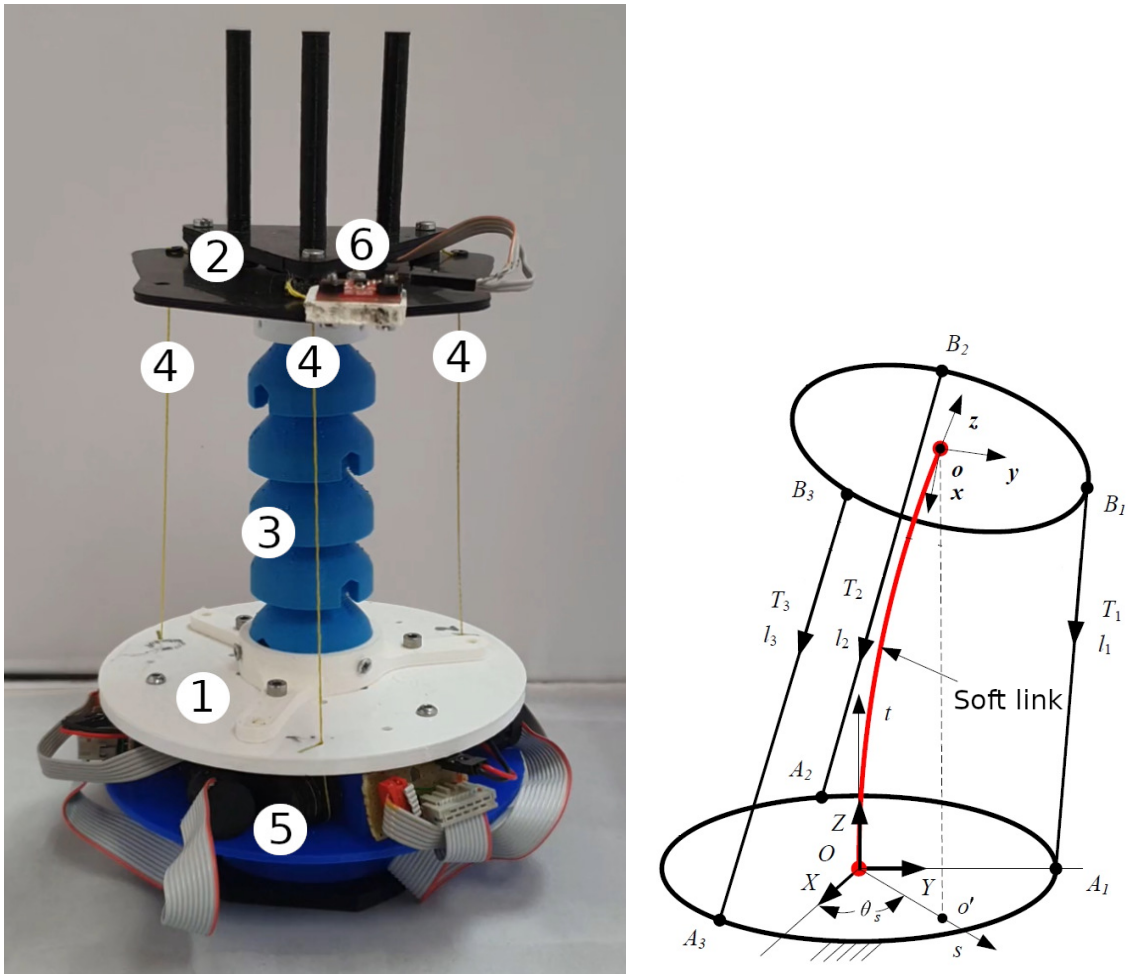

Figure 6.1: Robotic soft neck prototype (left) and kinematics model (right). *1. Base; 2. Moving platform; 3. Soft link; 4. Tendons; 5. Motors; 6. Tilt sensor.*

This prototype was made from 3D printed materials, including the central soft link weighing 125 g, designed to hold 1000 g at the tip, resulting in a payload-mass ratio of 800%. The target neck positions are fully defined by the tilt and orientation of the upper platform, which in turn depends on the tendon arrangement. Therefore, the problem of neck control is reduced to finding the correct action for each tendon in order to achieve the expected outcome.

A first control approach was made in [7], where inverse kinematics is used to find the length of each tendon to reach the platform targets. Due to the winch mechanism, each cable length takes a specific motor angular position, therefore, servo-control is necessary to reach and hold the desired platform inclination and orientation.

Later, in [8] it was discussed how open loop kinematics configuration tends to

result in positioning errors, and a feedback loop was proposed as future work. This section follows that approach, using a feedback configuration for both the proposed robust and adaptive iso-m methods.

To design and tune these robust and adaptive controllers, a model is needed, which will be discussed next.

6.2 Plant model

The soft neck is non-linear and time variant from various perspectives. First, the different neck inclinations place a changing load on the motor, which means that gain depends on the neck inclination, resulting in plant parameter uncertainty and time variation. In addition, the material of the central link is a polymer with unknown viscoelastic behavior, which adds non-linearity and more uncertainty. Therefore, we are facing a time varying system with uncertainty and non-linearity.

The proposed control schemes are known to address these problems, but some a priori knowledge of the system is needed for controller design. Knowing that controllers can deal with the non-modeled plant dynamics, a simple model is proposed. Let's first analyze the inputs and outputs of the system.

The actuators are managed from an intelligent driver, therefore, the input possibilities are the acceleration (torque), velocity and position references for each motor. The state for these variables can also be obtained from the driver, which offers velocity and position measurement outputs, and a rough estimate of torque through coil current for each motor, resulting in a total of nine inputs and the same number of outputs. These variables are time derivatives of one another, so the number of degrees of freedom (DoF) remains three for the actuation system.

Additionally, the tilt sensor provides the actual neck inclination and orientation so that speed and acceleration of the upper platform can also be obtained through their time derivatives, adding another six output variables to our plant.

Now the system variables must be set to define the control scheme. In [65], a possible approach was proposed using torques, bending the central soft link to the desired inclination and orientation. Another approach based on tendon lengths was used in [8].

Both proposals show good results, but to obtain a compact system, only integrated torque sensor, with rather rough available precision, could be considered, ruling out the first option.

Therefore, tendon lengths or velocities can be used as control variables. Considering that the actuators are based on DC motors, a good choice for the control variable is velocity. Additionally, the tilt sensor data readings provide tip inclination, which is more related to velocities than torques, resulting in a simpler model. Therefore,

the experiment approach is based on feedback control of the tilt sensor signal using tendon velocity actuators.

Since the main cause of the uncertainty and non-linearity of the neck is the bending angle of the central soft link, which depends on the tilt, but not on the orientation, we will focus on the inclination movement of the neck. Therefore, as the experiment only involves inclinations, the neck can be actuated using a single tendon, simplifying the model input to motor velocity. As a result, the plant model is based on velocity inputs and neck inclinations outputs.

An integrator is expected to emerge from this configuration, due to the relationship between tendon velocity and platform inclination, therefore, a pole located at $z = 1$ must be found during identification. Also, since the plant is considered as the target velocity input to the inclination output, dc motor dynamics, soft link behavior, and sensor measurements are included in the system. This leads to the introduction of an additional pole to capture this dynamics, resulting in a second order plant model estimate. Any additional plant behavior is neglected, as it is expected to be many orders of magnitude below.

Once the variables have been defined, the neck kinematics will be considered to find a convenient correlation between the inputs and outputs of the system, making identification easier.

A neck kinematic model was proposed in [7], but a dynamic model is not provided, therefore, a modeling technique will be applied at first. Given the control methods that are being tested, the RLS identification described in chapter 3 is the best choice, as it can be used in both schemes. Required plant model phase and slope at gain crossover frequency can be obtained from the resulting RLS model.

Due to the properties of the neck, the model is expected to change for different inclinations, making it a time varying system. Although the iso-m tuning method is applicable only to invariant systems, considering we are talking about a robust control method, an average steady plant model will be used for tuning.

To find this steady plant parameters, RLS identification was performed for a 10 deg step reference and 0 g payload during 150 s. The input and output variables of the system used for identification are shown in Fig. 6.2.

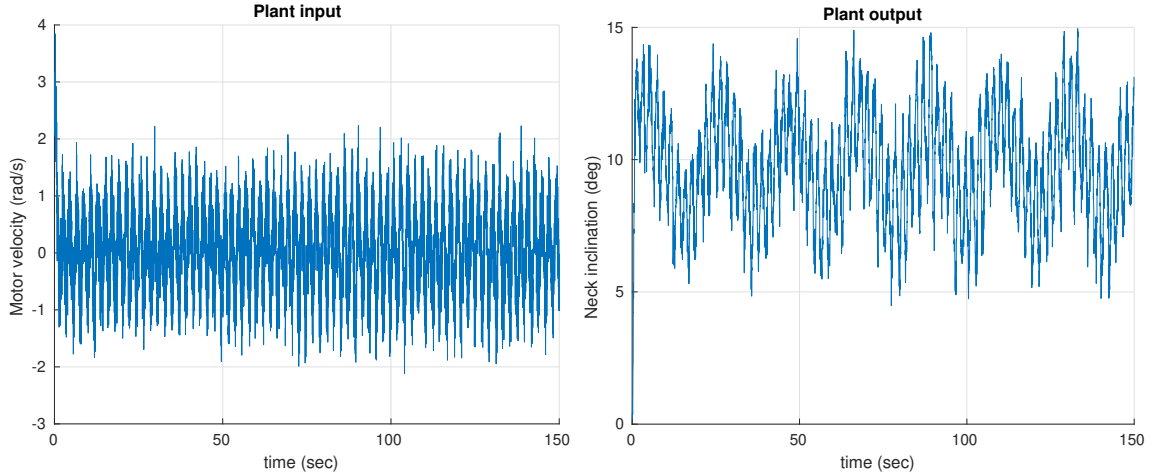

Figure 6.2: Capture data used for RLS system identification. Motor velocity input (left) and tip inclination output (right).

The results of the RLS identification of the input and output signals in Fig. 6.2 are shown in Fig. 6.3. Parameter convergence is correct after a few seconds of RLS identification, where the evolution with time of the parameters of the system transfer function (left) and the pole-gain model (right) are shown for the 0 g case. Notice how the pole located at $z = 1$ converges immediately, and how the second pole and the gain are stable throughout the experiment.

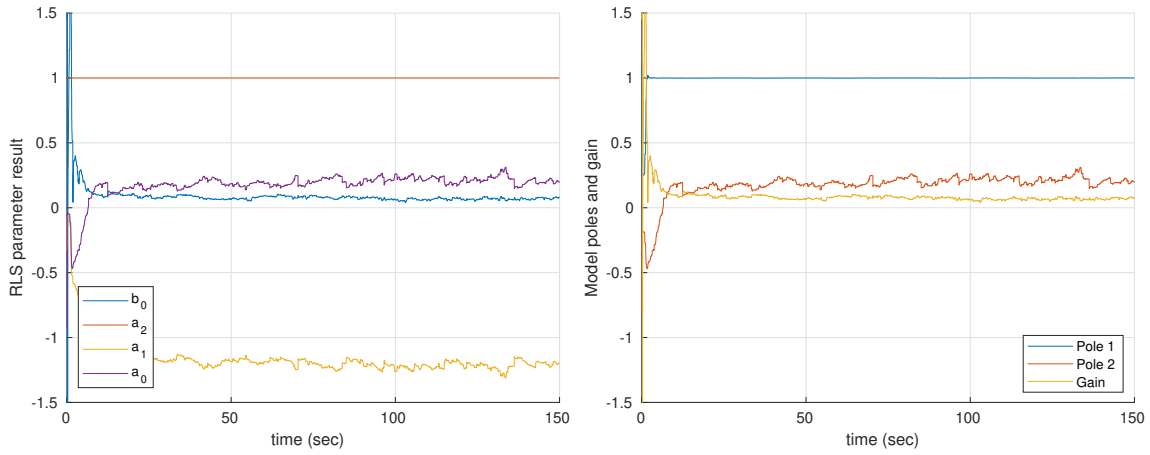

Figure 6.3: Convergence of system parameters (left) and pole-gain model (right) during system identification for the case of 0 g payload.

Using the average of stable values (those after 20 s) shown in Fig. 6.3, the following

transfer function was obtained:

$$G(z) = \frac{0.08207}{z^2 - 1.184z + 0.1838} \approx \frac{0.08207}{(z-1)(z-0.184)}, \tag{6.1}$$

and the time and frequency responses of this system are as follows:

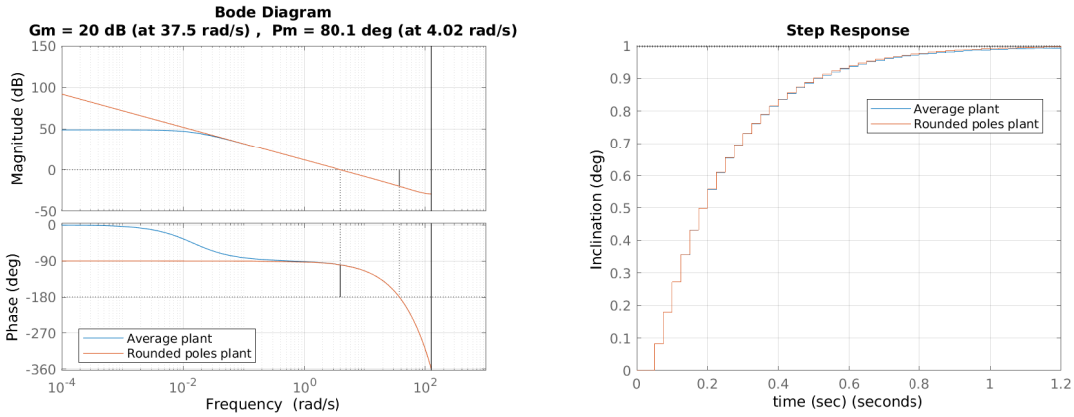

Figure 6.4: Open loop frequency response and unit feedback step response plots.

This model is the result of a recursive online identification method, therefore, the integrator pole is not located at $z = 1$, but very close. It is not important for iso-m controller tuning, as long as the specified crossover frequencies are kept above 1 rad/s. The figure 6.4 shows the difference between the RLS result and the same system with the pole forced to be exactly at $z = 1$ by rounding the pole value to three decimal digits.

6.3 Fractional order controller

The system to be controlled is the described soft neck, so the specification will be chosen close to a real human neck. In clinical works such as [135], it is possible to find that normal speed of neck motion is around 150 deg/s, and considering the artificial neck mechanics, a crossover frequency of $\omega_{gc} = 3$ rad/s will give similar speed and good reference tracking, while remaining slightly below the original system bandwidth, avoiding saturation.

Next the soft neck system will be tuned step by step using the iso-m method described previously in chapter 2. Given the intention of evaluating the robustness of the system, a low phase margin is chosen to force a time response overshoot.

According to Fig. 1.2, the phase margin required for a damping factor of $\xi = 0.5$ is 50 deg, enough for an acceptable overshoot.

A closed loop system bandwidth of 3 rad/s is required as discussed before. Using Fig. 1.2, it is observed that the closed loop bandwidth will be very similar to ω_{gc}, therefore, a value of 3 rad/s is valid.

Therefore, the experiment control specifications are:

- Desired crossover frequency $\omega_{gc} = 3\,\text{rad/s}$
- Desired phase margin $\phi_m = 50\,\text{deg}$

The open loop crossover frequency flat phase is also inherently granted through this tuning method (using Eq. (1.7)), which provides robustness to parameter variations. The following steps are needed for tuning:

Step 1: Plant phase slope at ω_{gc} is $m_s = -14\,\text{deg/log}(\omega)$, and phase $\phi_s = -95\,\text{deg}$. It can be found through Eq. (6.1) or in the frequency response shown in Fig. 6.4.

Step 2: Controller phase slope is then $m = 14\,\text{deg/log}(\omega)$, which is the opposite of the plant, and the controller phase required to achieve the specification of the phase margin at ω_{gc} is $\phi_c = (-(-95) + 50 - 180)\,\text{deg}$, $\phi_c = -35\,\text{deg}$. Therefore, looking at Fig. 2.7 an exponent $\alpha = -0.55$ is found.

Step 3: According to these values, τ_a is found using Eq. (2.43), resulting in $\tau_a = 3.9523$.

Step 4: Finally, k can be computed using Eq. (2.44), resulting in $k = 0.2037$, which makes the open loop system gain 0 dB at $w_{cg} = 3\,\text{rad/s}$.

Step 5: The resulting controller parameters are:

k_p	k_a	α
0.2037	0.8052	-0.55

Table 6.1: Iso-m controller parameters for the soft neck.

Given the negative exponent, we can call it a fractional proportional integral controller (FOPI), with the following transfer function:

$$FOPI(s) = 0.2037(1 + 3.9523s^{-0.55}) = 0.2037 + 0.8052s^{-0.55}. \tag{6.2}$$

The frequency (open loop) and time (feedback) simulation responses of the system with this controller are shown in Fig. 6.5. You can see how the specifications are met in the Bode diagram. This figure also shows the closed loop step responses for different system gain multiples (MxG) and fractions (G/D), showing constant overshoot (iso-damping property).

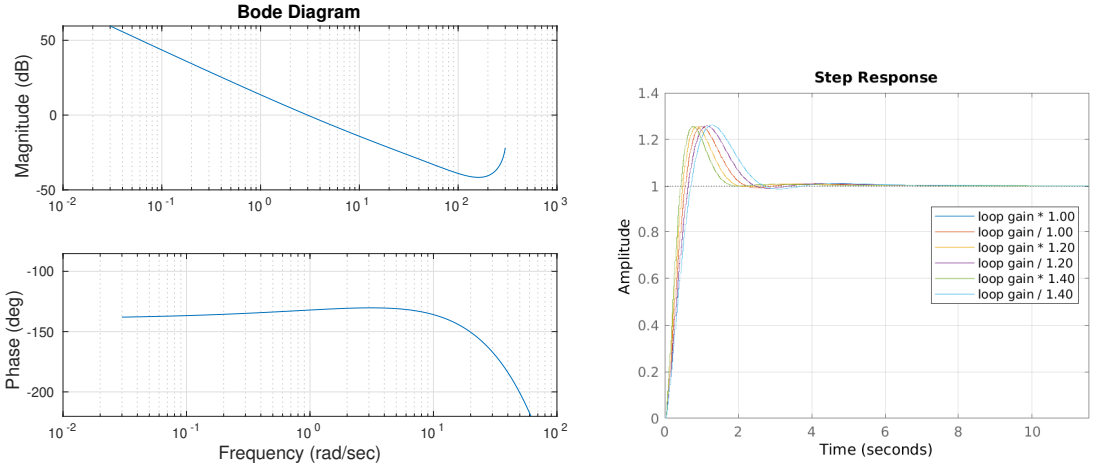

Figure 6.5: Iso-m resulting open loop Bode diagram (left) and step feedback response (right). Specifications: $\omega_{gc} = 3$ rad/s, $\phi_m = 50$ deg. Gain range ($gain*1.3$, $gain/1.3$).

6.4 Integer order controller

Now, to compare the robustness of the system, an integer controller will be applied with the same parameters obtained by the iso-m method, with the exponent brought to the nearest integer order (-1). Although a better tuning of this controller can be achieved, the goal is a robustness comparison, hence the tuning method is not relevant.

Considering an integer order PI (IOPI) controller that has the same parameters found above, the following values are obtained:

k_p	k_a	α
0.2037	0.8052	-1

Table 6.2: IOPI controller parameters for the soft neck.

The integer controller transfer function is as follows:

$$IOPI(s) = 0.2037(1 + 3.9523s) = 0.2037 + 0.8052s. \tag{6.3}$$

In Fig. 6.6 the frequency (open loop) and time response are shown for different payload configurations using the integer controller. Note that the flat phase specifications are not met in the Bode diagram and iso-damping is not shown in the time response plots.

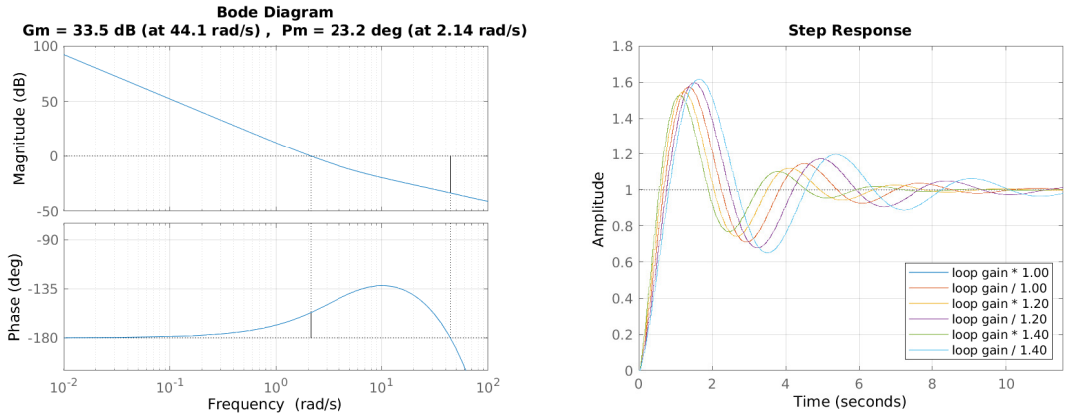

Figure 6.6: Open loop Bode diagram (left) and step feedback response (right) of the system with integer PI controller used to compare robustness. Parameters $k_p = 0.2037$, $k_i = 0.8052$. Gain range $(gain * 1.3, gain/1.3)$.

Once the FOPI and PI parameters are found, the last controller considered in this experiment is described.

6.5 Adaptive fractional order controller

The third control scheme tested in the soft neck is the adaptive iso-m. As described in chapter 3, the performance specifications are the same as in the robust iso-m method, which means that the phase margin and crossover frequency must be provided. Using the specifications from the previous sections, a more meaningful comparison is obtained, hence the specifications are:

- Phase Margin: $\phi_m = 50$ deg
- Gain crossover frequency: $\omega_{gc} = 3$ rad/s

According to chapter 3, the phase and slope information is obtained through Eqs. (3.21) at a specified gain crossover frequency, based on plant parameters estimate $(\hat{G})$. Therefore, before the iso-m tuning, the updated plant estimation is found using RLS including a PE signal in the system input to ensure parameter convergence. After that, the plant phase and slope estimates $(\hat{\phi}, \hat{m}_G)$ are computed using Eqs. (3.21) and (3.22) and plant estimate $(\hat{G})$.

Next, as described in chapter 3, the required phase and slope of the controller are obtained using Eqs. (3.24):

$$\phi_C = 50 - \hat{\phi}_G - 180, \tag{6.4}$$

$$m_C = -\hat{m}_G. \tag{6.5}$$

To obtain the controller exponent (α) a solution to Eq. (3.25) must be found. In chapter 2 several options are proposed as solutions, including the plot shown in figure 2.7, a lookup table, and the fit function. The second option was implemented in the real system for its simplicity and accuracy.

Having found α exponent and knowing the crossover frequency ($\omega_{gc} = 3\,\mathrm{rad/s}$), τ_a can be calculated using Eq. (2.43).

$$\tau_a = \frac{1}{\tau_x 3^\alpha} \quad ; \quad \tau_x = \frac{\sin(\alpha\pi/2)}{\tan(\phi_C)} - \cos(\alpha\pi/2) \tag{6.6}$$

Finally, using Eq. (3.21) and the plant estimate ($\hat{G}$) gives the magnitude at crossover frequency ($|\hat{G}|$), and then, the controller gain is computed using Eq. (2.44), fulfilling Eq. (1.8) for crossover frequency specification:

$$k = \frac{1}{|1 + \tau_a(j \cdot 3)^\alpha||\hat{G}|} \tag{6.7}$$

Once all three parameters are found and the controller is tuned according to the specifications, it can be used in the feedback loop of the adaptive scheme. As plant identification is done seamlessly, as well as controller tuning based on the latest estimate, the system will keep the specifications unchanged despite plant variations. These two identification and tuning steps will be repeated alternately during the continuous adaptation operation.

Stability was discussed in chapter 3, where parameter convergence and specifications were found to be the keys. Their importance will be shown below through experimentation.

6.6 Experiment description

First, in order to compare the theoretical and actual performances, step responses are presented under different payload conditions for the FOPI and the IOPI controllers.

Then, knowing that the plant parameters are variant, a second experiment will be carried out, aimed at determining how the plant changes depend on the neck inclination. This experiment has varying target inclinations to check system variability versus inclination for the case of zero payload. Target inclinations are set twice (upwards and downwards) to verify that equivalent results are obtained for similar input conditions.

Finally, the main experiment consists of a series of inclination targets in the range of 10 deg to 30 deg, following the same pattern as the previous experiment. A sequence of step inputs will be programmed to push the plant to different working conditions.

This sequence of target positions used in the last two experiments is shown in Fig. 6.7 for reference.

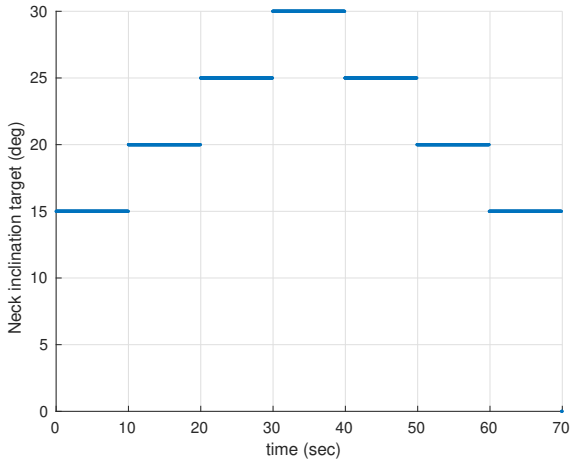

Figure 6.7: Target positions during the main experiment.

Using this trajectory, all three controllers, FOPI, IOPI and then the adaptive iso-m controller will be tested. All experiments will be repeated using four different payload configurations from 0 g to 600 g, in order to discuss the effects of mass variation on the system.

In the adaptive controller experiment, an initialization period is required. This initial phase is intended to populate the identification system matrices and vectors, in order to offer an adequate and stable model estimate when continuous adaptation begins. The input signal at this stage is a frequency rich sinusoidal linear combination, designed to have sufficient PE order to ensure good initial identification. After this twenty seconds stage, the system enters continuous adaptation mode.

6.7 Results

The first experiment performed is a step response similar to that modeled in Figs. 6.8 and 6.9. The step height is 10 deg to get a valid output signal, and different masses will be set to verify robustness to mass changes. The results of this experiment are shown in Fig. 6.8 for the case of IOPI controller and in Fig. 6.9 for the case of FOPI controller.

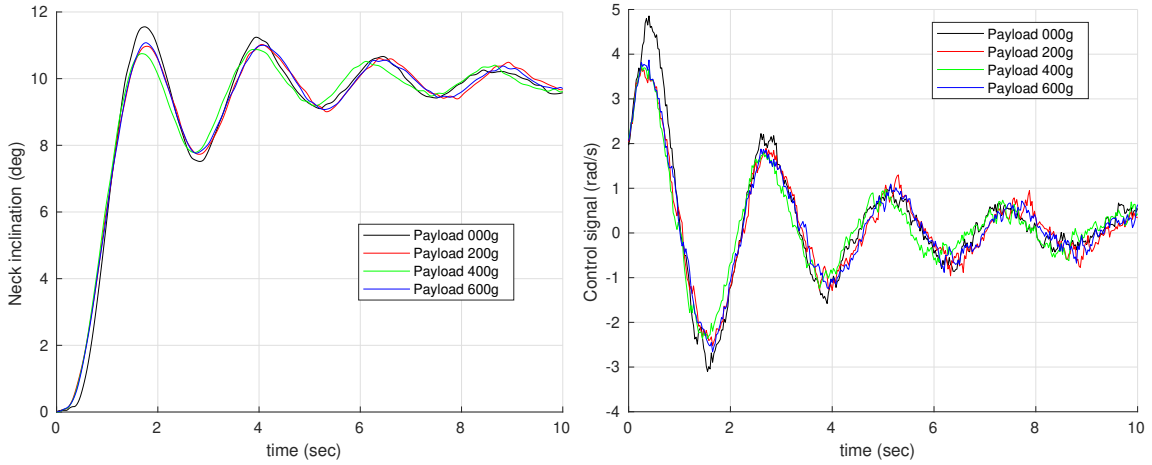

Figure 6.8: Integer controller (IOPI) neck step response (left) and control signal (right) for different payloads.

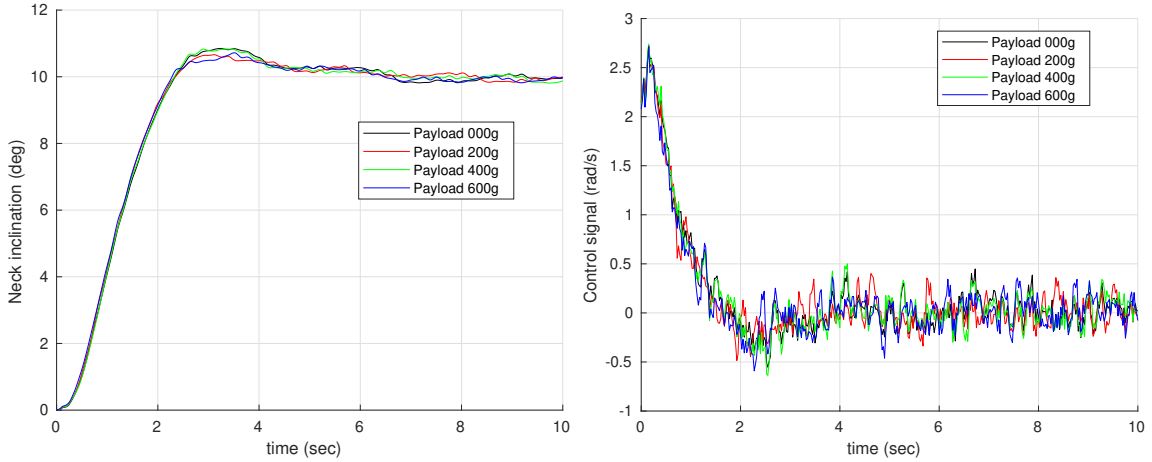

Figure 6.9: Iso-m fractional controller (FOPI) neck step response (left) and control signal (right) for different payloads.

The integer PID controller, although highly oscillating, as expected from the presence of an integer order integral, is stable for the identified model and for the set of payloads considered.

Compared with the theoretical results, a certain degree of similarity can be observed. Notice how the impact of the payload variation is not that important in the experiment, revealing that the plant gain is not as dependent on the payload as expected, probably due to the neck geometry.

Now, a second experiment is analyzed, aimed at determining the variations in the parameters of the plant depending on neck inclination. This experiment was performed using the sequence of target inclinations previously described in Fig. 6.7.

The time response and control signal results are shown in Fig. 6.10.

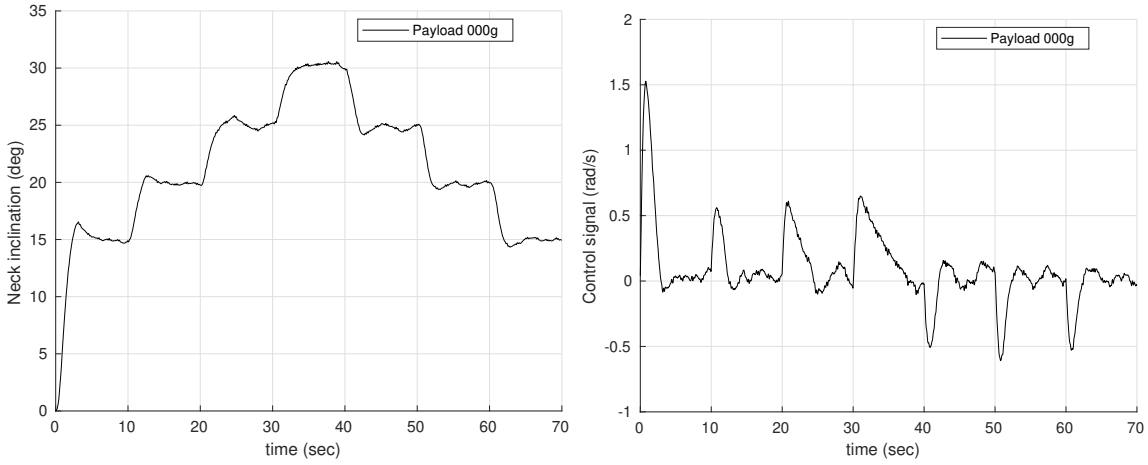

Figure 6.10: Step response (left) and control signal (right) for zero payload in the case of varying inclinations during system identification.

System identification was performed during this experiment producing the results shown in Fig. 6.11, where a greater response variability is observed.

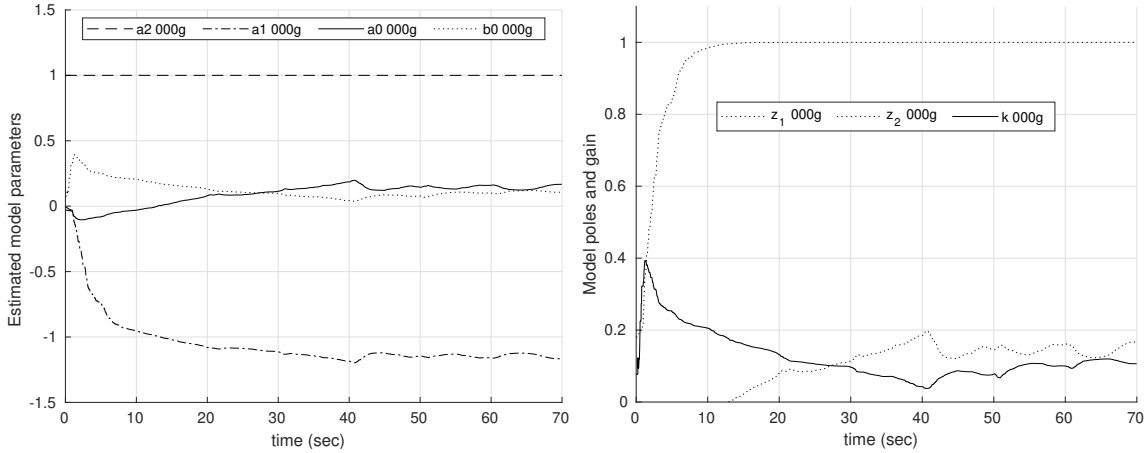

Figure 6.11: System identification results of the experiment with varying inclinations. Evolution with time of transfer function parameters (left) and model poles and gain (right).

Notice how the change in plant parameters is most noticeable at different inclinations. For example, regarding system gain, it can be clearly seen how its values decrease to a minimum coinciding with the highest inclination, and then increase again to values similar to those obtained for the same inclination. The opposite behavior can be observed in the pole z_2, which means that the response of the system becomes slower at higher inclinations, probably due to the elastic behavior of the soft link. Again, the pole at $z = 1$, shown in the figure as z_1 converges very quickly showing good stability.

Based on these results, greater variability due to changing inclinations than payloads is expected in the next experiment. Since the test is designed to examine the influences separately, it is possible to assess the effect of each factor on the final result.

At first, the result of the integer controller experiment is shown in Fig. 6.12, where, as expected, variability is mainly influenced by neck inclination, except from the 600 g payload, leading to instability in some cases.

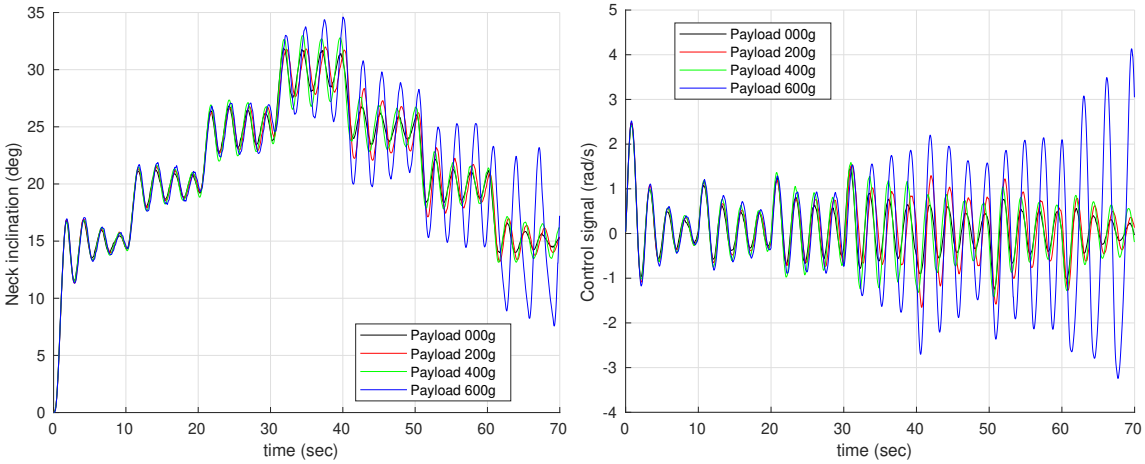

Figure 6.12: Step response (left) and control signal (right) for different payloads in the case of varying inclinations for the integer IOPI controller.

You can see how stability is significantly reduced at high inclinations, which is not surprising knowing that system gain decreases as inclination increases. Looking at the Bode diagram in Fig. 6.6 you can see how the phase tends to -180 deg at low frequencies. Given the shape of the magnitude curve, a gain decrease will inevitably reduce crossover frequency, thereby shortening the phase margin.

This behavior was already predicted by the time response simulation in Fig. 6.6, where the amplitude of the sine wave increases for those cases where the gain decreases, and reaches its maximum in the case of minimum gain ($gain/1.3$). Therefore, the predicted variability is noticeable in the system time response as seen in Fig. 6.12 due to target inclination.

Note one of the integer controllers drawbacks regarding system phase. The problem here is that the double integrator of the system will always result in a -180 deg phase for low frequencies. Fractional controllers avoid that problem by featuring exponents greater than -1. See for example, the $\alpha = -0.55$ of the FOPI controller, raising the phase and avoiding the instability area as shown in 6.5.

The second controller tested in this experiment is the previously designed fractional FOPI. The results for the step input sequence are shown in Fig. 6.13, with a substantially more robust performance compared to the previous case.

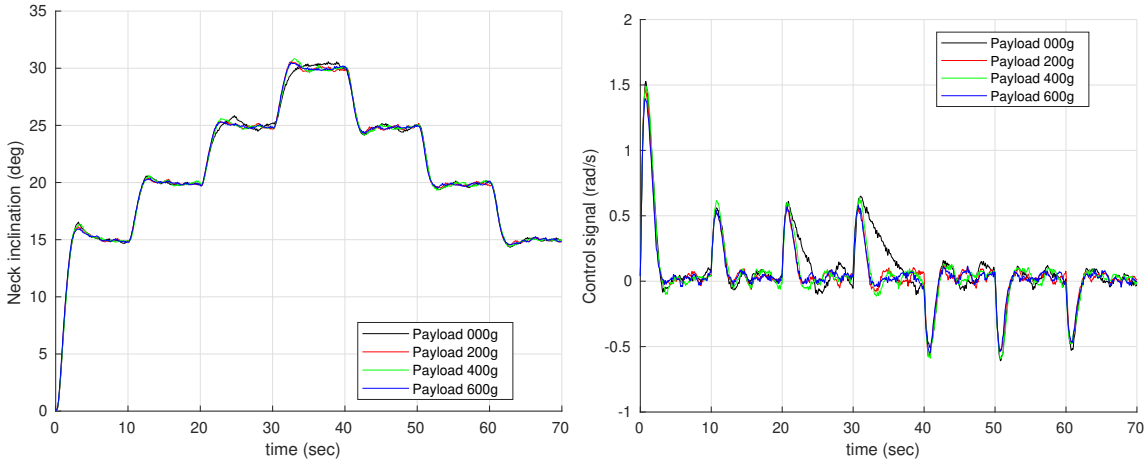

Figure 6.13: Step response (left) and control signal (right) for different payloads in the case of varying inclinations for the fractional FOPI controller.

As expected, the robust controller shows similar performances for the different mass configurations, and a small difference can be observed for different inclinations. Again, the impact of payload on performance is not significant, except for the case of zero payload, where a clear difference in overshoot is shown at 30 deg inclination. As discussed earlier, the robust controller is designed for an operation range, which in our case can be considered centered at 10 deg inclination, where the system identification was done. To explain this behavior, it is necessary to observe the system parameters throughout the experiment.

Figure 6.14 shows the evolution over time of the system identification parameters. Notice how the plant gain reaches the lowest value coincident with the top inclination, which explains the performance differences in the time response plot. Since the controller gain is constant, a plant gain decrease leads to open loop gain reduction, up to the saturation point, causing the system to be unable to achieve the required control signal velocities. On the right side of Fig. 6.13 you can see how the control signal remains high for a longer time, which shows the saturation of the system.

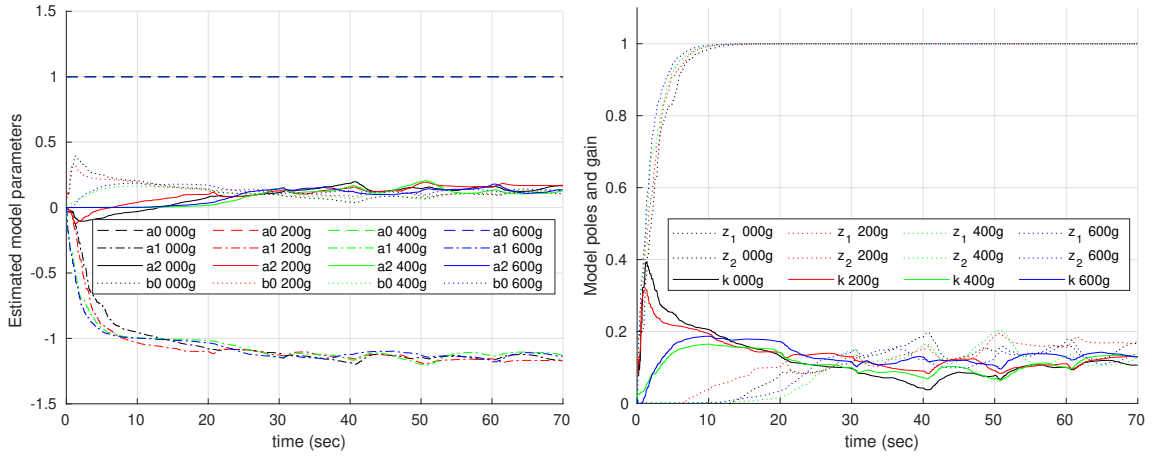

Figure 6.14: System identification results for different payloads during the step sequence experiment. Evolution of transfer function parameters (left) and model poles and gain (right) for the fractional FOPI controller.

Once the payload increases, it causes the system gain to recover the values of the lower inclinations, as seen in Fig. 6.14, solving the saturation problem. The reason is that the inclination causes a neck mass dislocation that contributes to the central link bending. It is interesting to note how the gain variation with payload is smaller for lower inclinations, as the weight is less off-centered.

Apart from the first case, the three remaining payload configurations have similar performances and the overshoot is almost invariant for the iso-m method despite mass differences or inclinations, starting from 0 g and reaching 600 g; therefore, robustness is achieved with this tuning methods for the proposed payload configurations also reaching a zero steady state error.

In contrast, the integer controller response shows how performance is affected by both, mass and inclination, leading to instability in some cases, mainly in decreasing inclination trajectories. Once the plant parameters change, the performance deteriorates. Note how overshoot and oscillations increase as inclination angle decrease.

With the fractional order controller, the integral action is alleviated by its fractional order, allowing the system to achieve zero steady state error but with a much less oscillatory response. Also, another benefit of the fractional controller is that, thanks to the non-integer exponent of the integrator, the system phase never reaches the value of -180 deg at low frequencies, as can be seen in Fig. 6.5, thus avoiding the aforementioned problem with low plant gains using the integer controller.

The results of the third controller, adaptive iso-m, are shown in figure 6.15. You can see how the system response is preserved for varying payloads and inclinations.

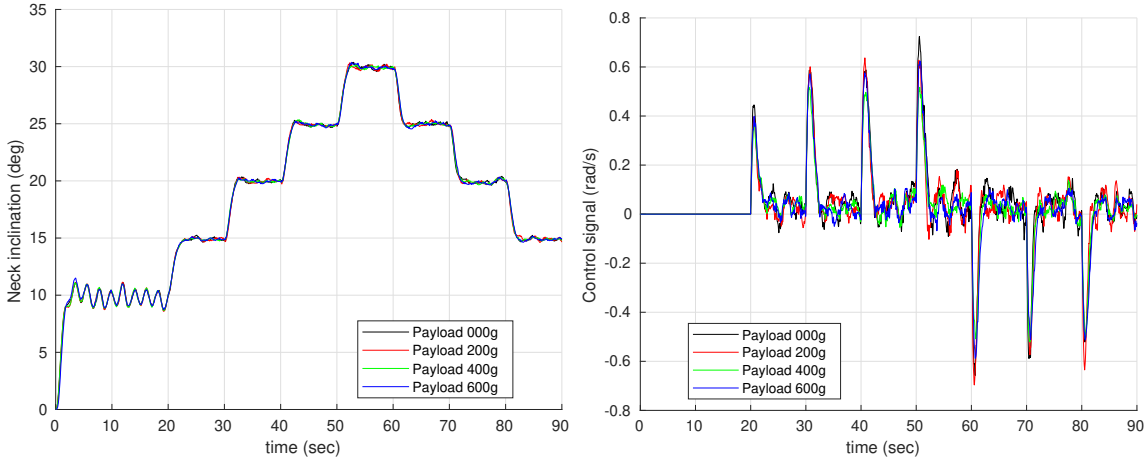

Figure 6.15: Step response (left) and control signal (right) for different payloads in the case of varying inclinations for the adaptive iso-m controller.

Note how this time the same performance is maintained throughout the experiment. Control signals are now invariant for different payloads, meaning that no saturation is reached at any point. Figure 6.16 shows the estimated parameter values of the plant during the experiment, where a correct parameter convergence is observed for all mass configurations.

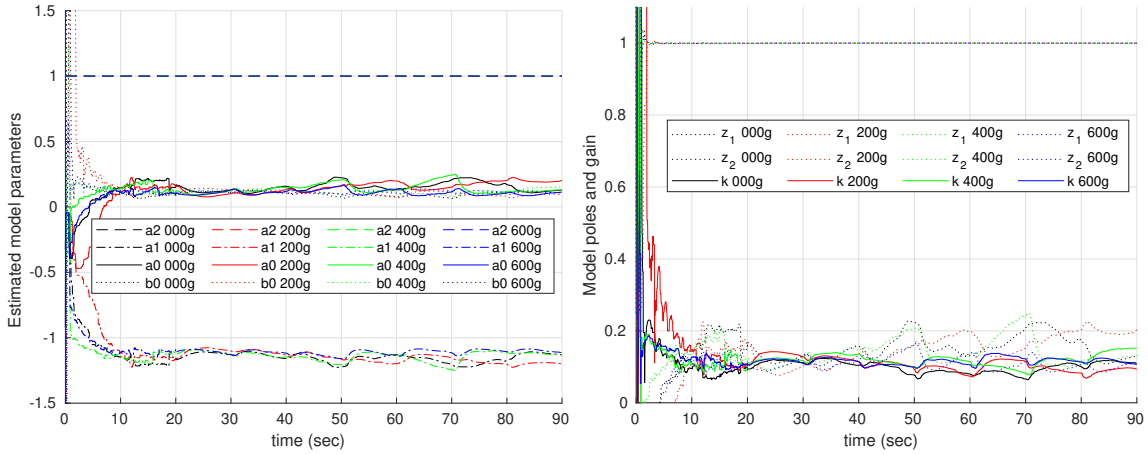

Figure 6.16: System identification results for different payloads during the step sequence experiment. Evolution of transfer function parameters (left) and model poles and gain (right) for the adaptive iso-m controller.

Note how the convergence of the system parameters is correct on the plot, while the identification is still able to track plant changes, and how the pole located at

$z = 1$ convergence is very fast, and the other pole and the gain evolve through the experiment. As is known, slightly lower gains and slower system responses are obtained for high inclinations.

Figure 6.17 shows all the parameters of the adaptive controller parameters obtained during the experiment (left) and the values of plant phase and magnitude at the crossover frequency according to the plant estimates (right). It is interesting to see how the adaptive controller parameters evolve during the experiment.

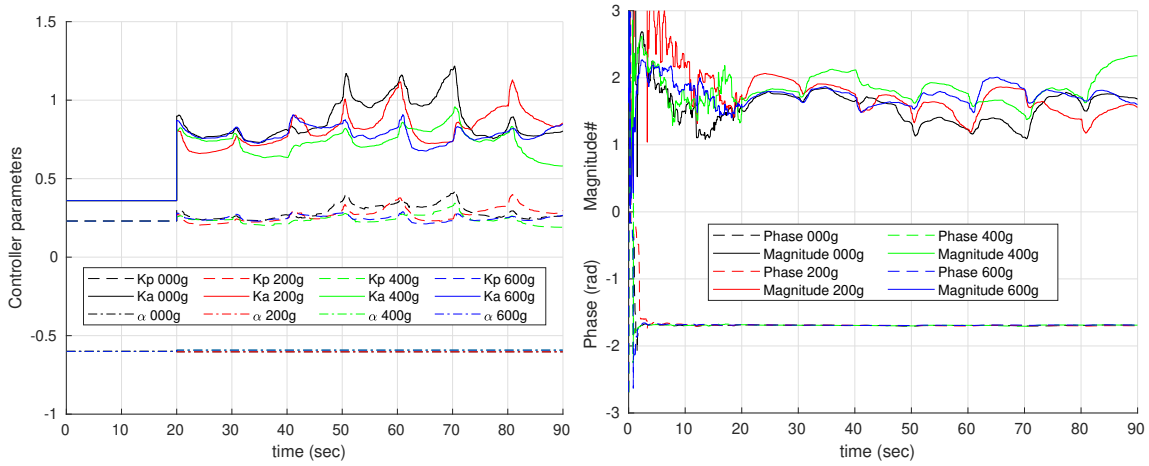

Figure 6.17: Controller parameters obtained using the iso-m method based on the estimated system (left) and magnitude at crossover frequency based on the plant estimates (right).

Since the iso-m tuning is based on the phase and magnitude values shown on the right side of Fig. 6.17, the resulting controller parameters shown on the left side show an inverse relationship with that curve. It can be seen that the high controller gains coincide with low plant magnitudes, which means that the controller counteracts the system gain reductions by increasing its own gain. As a result, the time response of the adaptive system is invariant, as shown in Fig. 6.15.

The information found in the phase and magnitude plot in Fig. 6.17 during the experiment is very interesting. These values were obtained from the system identification parameters and Eqs. (3.21). Note that the phase convergence is fast and remains constant throughout the experiment, while the magnitude changes with inclination similar to the plant gain as discussed before.

Although plant phase and magnitude values are not used in FOPI and IOPI experiments, as their controller parameters are constant, their plots are shown in Fig. 6.18 for comparison. Since the system describes the same trajectory, similar plots are expected for all three experiments.

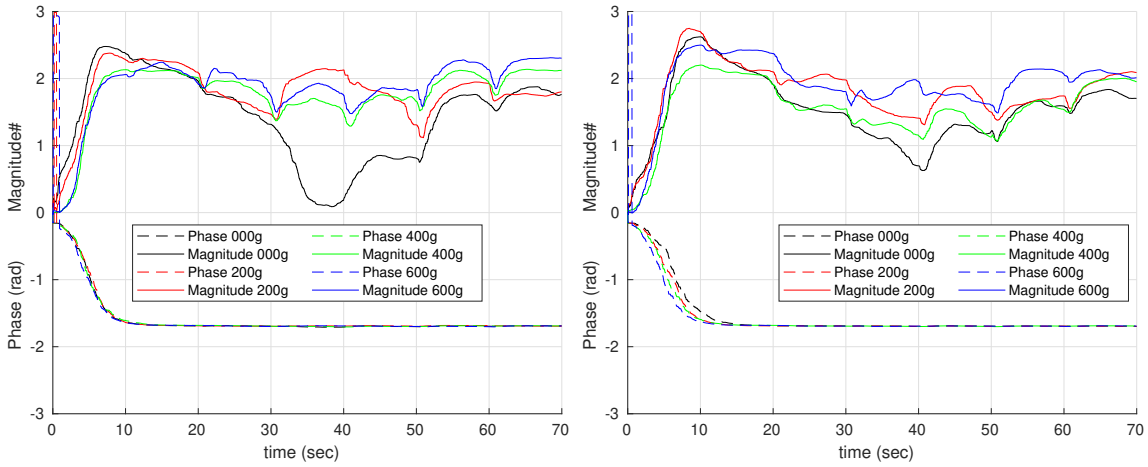

Figure 6.18: Phase and magnitude of the plant estimates using RLS online identification for the FOPI controller (left) and IOPI controller (right) experiments.

See how the phase is quickly set and maintained throughout the experiment while magnitude changes with the inclination, relating high inclinations to low magnitudes. Again, the gain variation with payload is smaller for lower inclinations. These plots are similar in all the experiments, which can be considered as a validation of the results found through the experiments performed.

To further compare the differences in performance for the three tuning methods proposed, the numerical results of the three controllers are now provided.

Table 6.3 shows detailed performance data gathered from Figs. 6.12, 6.13 and 6.15 in the average case of 20 deg step located at 10 s (30 s for the adaptive controller). The worst values are shown within all payload configurations.

Method	Min. (%) Overshoot	Max. (%) Overshoot	(ΔO %) Variation	Max. (s) Rise time	Max. (s) Settling time
IOPI	5.65	8.50	2.85	1.85	> 10
FOPI	1.90	3.05	1.15	2.88	5.98
adaptive	0.95	1.70	0.75	3.05	4.08

Table 6.3: Worst performance data, including overshoot variation (ΔO) for the soft neck.

In addition, table 6.4 shows detailed performance data gathered from Figs. 6.12, 6.13 and 6.15 in the worst case of 30 deg step located at 30 s (50 s for the adaptive controller). The worst values are shown within all payload configurations.

Note that both iso-m and adaptive iso-m methods show similar results, but the adaptive iso-m is able to cope with time varying plants because of the adaptation

Method	Min. (%) Overshoot	Max. (%) Overshoot	(ΔO %) Variation	Max. (s) Rise time	Max. (s) Settling time
IOPI	5.93	10.00	4.07	1.78$*$	∞
FOPI	1.87	2.77	0.90	8.85	9.60
adaptive	0.70	1.27	0.57	3.33	5.83

Table 6.4: Worst performance data, including overshoot variation (ΔO) for the soft neck.

feature, keeping the robustness results always at a very low value. The result of the IOPI controller is not that good in terms of robustness with a variability between 5 and 10 times the adaptive method. As discussed above, the goal of the comparison is not the performance, but its variation.

Regarding stability, both iso-m and adaptive iso-m are able to stabilize the system even if the plant parameters change, while the stability of integer controller (IOPI) is altered by variations in the plant gain, reaching critical values at low gains and showing very long settling times at best, mainly due to oscillations produced by the lower phase margins.

Note that the intention is not to compare the performance of the FOPI and IOPI controllers, but to see their variability based on different payloads and inclinations. Other performances can be used for integer controllers with different overshoots, but these issues are out of scope here, and have been covered extensively in other works such as [31], [39] [42] and [5] to name a few.

The steady state error is zero for all control strategies as expected from an integral controller, with an additional integrator included in the plant.

In summary, a robust behavior is granted from the application of both fractional controllers, obtaining excellent results with the iso-m and adaptive iso-m methods in terms of robustness compared to other non-robust controllers, which validates the new approaches proposed.

A video showing the system performance with the adaptive iso-m controller is available at `https://vimeo.com/438681435`, proving the benefits of this tuning method. More videos showing diverse robust and integer controllers are also available at `https://vimeo.com/user103290293`.

Chapter 7

Conclusions and future works

7.1 Contributions

This thesis proposes two new approaches to tackle the problems caused by uncertainty.

The first proposal is based on the use of robust fractional controllers, and as shown during its description and in the experimental part, it is capable of delivering a robust response despite system mass changes and non-linearities. The presented method is a general solution of the robustness specification in Eq. (1.7), and is applicable to any system and controller. The method focuses on controllers with one fractional operator ($FOPD$, $FOPI$), but the same approach can be used in other classes of controllers, with more operators, or different equations. Unfortunately, these developments will have to be the subject of further works due to time constraints, and will lead to future scientific writing.

Unlike other tuning methods found in the literature, this approach has a graphical nature that allows the designer to visualize the effects of parameter variations in a very simple and intuitive way. This is a very important contribution. Easy and fast controller tuning is possible simply using graphs or tables, without the need to solve a numerical nonlinear equation and allowing the solution of the control problem in a very intuitive and straightforward way.

This is important in applications that require changes in controller parameters during operation to optimize response towards a given target. In these situations, the method offers a fast and reliable solution, as the graphs can be used to directly determine the values of the controller parameters that meet the new control requirements. The proposed method allows not only to intuitively define the controller parameters that satisfy the design constraints, but also to observe at a glance how the parameters modify the loop dynamics.

The computational complexity of non-linear equation solvers used by current tuning methods makes the process difficult, depending on multiple factors such as number

of iterations, accuracy and initial conditions. For example, solving all Eqs. (1.8), (1.9) and (1.7) numerically, besides the high computational complexity, makes the process highly dependent on initial conditions and local minima.

In contrast, thanks to its straightforward solution, the problem of initial conditions and local minima is totally avoided using the iso-m method, providing both good performance and a reduced computing effort. The computational complexity of a lookup table is similar to a memory access, and although exact results are not achieved, any accuracy can be obtained by interpolation or by increasing the granularity of the table.

In fact, the application of the iso-m method in a programmable logic controller (PLC) could be easily addressed, resulting in a good opportunity for industrial widespread of robust controllers, allowing to improve the quality of the current hardware systems.

Another issue found in the current fractional tuning methods is that non-linear equation solvers can only be used in off-line control schemes, due to the high computational effort. That makes their use in adaptive control strategies impossible; in contrast, the iso-m method can be applied in adaptive control strategies, which leads to the second contribution of this thesis.

The second proposal is an unprecedented indirect fractional adaptive scheme that allows robustness to be extended to a wider set of systems, including time varying and nonlinear systems.

Control requirements for nonlinear time varying systems can be difficult to meet. Plant parameters may change due to non-linearity or time variability, forcing the controller to work out of the specifications. As a consequence, the resulting control performance will change accordingly.

The proposed adaptive fractional control uses real time plant parameters obtained through the RLS identification algorithm combined with the fast controller tuning method proposed in the first part to join adaptability and robustness in a single control scheme.

Thanks to the robustness of the system, performance will not change for the operating point, and thanks to the adaptive scheme, plant changes will update the controller tuning to obtain the same original operating point specifications.

Both iso-m and adaptive iso-m methods have proven to be a working solution to the major problem of uncertainty in very different platforms. The experimental chapters show how the resulting system is able to cope with variations in plant parameters while maintaining short and long term performance settings.

7.2 Results

The results obtained in all the proposed systems are excellent, as evidenced in their corresponding chapters. The systems used for validation were:

- The Honda Accord autonomous car available for researchers in the Lawrence Berkeley National Laboratory (US)
- The elbow of the TEO humanoid robot developed by the Robotics Lab team of Carlos III University of Madrid
- The bio-inspired neck made of soft material proposed in [7]

In the autonomous car case, the iso-m controller shows a robust performance, rejecting possible disturbances on the high level response due to different dynamics, powetrains or road slopes. A hierarchical ACC control structure has been used, where the fractional order controller is in charge of the gap distance regulation through a reference acceleration tracked by a lower control layer. The results outperformed an equivalent integer order PD controller used for comparison.

Likewise, the iso-m tuning method has been proposed for the control of the elbow joint of the TEO humanoid robot. The results obtained are very competitive compared to other well-known fractional order tuning methods found in the literature. The system performs according to specifications and shows high robustness to mass changes at the tip (robot hand), showing similar performances compared to other tuning methods of much higher complexity.

For the bio-inspired neck, despite the non-linear and time varying properties of the soft material, the response of the inclination feedback control was totally correct, in accordance with specifications and showing high robustness to mass changes. Even for very high payloads compared to the weight of the neck (895.5% heavier), the system robustness is granted through the proposed iso-m controller. This system was a control challenge, due to the described plant properties, highlighting the benefits of the proposed methods in nonlinear time varying applications compared to other control methods.

Both algorithms have been applied on different platforms, some of them showing unusual actuator dynamics. Its effectiveness has been demonstrated in both simulation environments and real scenarios.

The simulation results show that despite introducing disturbances in the plant gains, the performance of the proposed controller is not only maintained, but also outperforms in results to other equivalent controllers. The iso-damping potential has been therein confirmed to ensure robustness to gain changes in the controlled plant.

The excellent results obtained in the real platforms has showed how easily it could be applied to any type of dynamics, which is convenient to encourage the adoption

of fractional robust controllers in the field of automation. The robustness obtained in the performance of the three test platforms considered, confirm the suitability of the proposed methods for the robust control of LTV and NLTI systems.

To conclude, the robust iso-m controller tuning method can be applied to any real system. The only information needed for its application is the plant's frequency response for the desired specification. This can be obtained from a plant model, from system identification, or even within real-time adaptive control schemes.

The requirements are very low, both from the computing point of view and the mathematical complexity, therefore its application can be easily deployed in many industrial, embedded and low cost environments. There is no limit for its use in any control scheme.

One possible issue for its application can be the fractional operator implementation. Although it is not in the scope of this thesis, the application of a robust fractional controller always carries the implementation of the operators needed in the controller equations. This field of fractional calculus is under development, and still needs to find better ways to define the fractional operators.

Nevertheless, there are already many possible solutions to this problem, as the integer approximations using high order transfer functions, the IIR or FIR modeling of the operators, and a good number of libraries and toolboxes allowing a straightforward use of the fractional order operators.

7.3 Future works

Although the experimental section has validated the method, there is still many pending works in the proposed platforms that need attention. This works will be addressed in the future.

In the case of TEO, future research steps will focus on the application of the method to other joints in the robot. Given the promising results obtained, an overall enhancement is expected from an improved joint behavior. Also, an enhanced motion of the limbs is possible as a result of the improved joint motion.

The application of this approach on car-following in shorter time gaps will be analyzed in future works, adding vehicle-to-vehicle communication links.

For the soft neck, a high quality camera stabilization is being developed for its application in humanoid robots. Given the soft neck quick response properties, a camera balance application can be performed during the humanoid gait, improving the image capture quality while the robot is walking.

Although there is still a lot to do in these platforms, the implementation in other systems will also follow. Soft robotics is an emergent field, with many problems to solve. These new methods have shown a remarkable advantage in the control of this type of systems, therefore, many new soft robots are suitable for their application.

For example, the I-SUPPORT robot, developed at the BioRobotics Institute of Scuola Superiore Sant'Anna, is currently involved in a collaboration paper for the robust control of the robot. Initial results from the iso-m controller are very promising, and thorough experimentation will follow to publish the results in a high impact paper.

Future developments of the robust iso-m method will focus on extending its capabilities to more complex controllers. More specifically, the fractional order proportional integral derivative (FOPID) will be addressed first, in order to achieve a more general application of the method. As these controllers have a total of five tuning parameters, the robustness constraints could be specified in a wider range of frequencies, allowing robustness in systems with large gain changes.

Future work on the adaptive iso-m method will focus on exploring new possibilities in terms of plant parameter estimation. Improving estimate convergence without using persistence excitation is a very interesting line to explore. It would be also exciting to improve the accuracy using more advanced identification techniques. In addition, since the adaptive method is based on the robust iso-m approach, any progress made in the first will be also applicable in the second.

Bibliography

[1] J. Muñoz, C. A. Monje, L. F. Nagua, and C. Balaguer, "A graphical tuning method for fractional order controllers based on iso-slope phase curves," *ISA Transactions*, may 2020.

[2] J. Muñoz, D. Copaci, C. A. Monje, D. Blanco, and C. Balaguer, "Iso-m based adaptive fractional order control with application to a soft robotic neck," *IEEE Access*, 2020.

[3] C. Flores, J. Muñoz, C. A. Monje, V. Milanés, and X.-Y. Lu, "Iso-damping fractional-order control for robust automated car-following," *Journal of Advanced Research*, vol. 25, pp. 181 – 189, sep 2020. Recent Advances in the Fractional-Order Circuits and Systems: Theory, Design and Applications.

[4] J. Munoz, C. A. Monje, F. Martín, and C. Balaguer, "A robust control method for the elbow of the humanoid robot teo based on a fractional order controller," in *2018 IEEE/RSJ International Conference on Intelligent Robots and Systems (IROS)*, pp. 6378–6383, IEEE, IEEE, oct 2018.

[5] J. Muñoz, C. A. Monje, S. M. d. l. Casa, and C. Balaguer, "Joint position control based on fractional-order pd and pi controllers for the arm of the humanoid robot teo," *International Journal of Humanoid Robotics*, vol. 16, p. 1950042, dec 2019.

[6] L. Nagua, J. Muñoz, C. A. Monje, and C. Balaguer, "A first approach to a proposal of a soft robotic link acting as a neck," in *Actas de las XXXIX Jornadas de Automática, Badajoz, 5-7 de Septiembre de 2018*, pp. 522–529, Área de Ingeniería de Sistemas y Automática, Universidad de Extremadura, Sep 2018.

[7] L. Nagua, C. Monje, J. Muñoz Yañez-Barnuevo, and C. Balaguer, "Design and performance validation of a cable-driven soft robotic neck," in *Actas de las Jornadas Nacionales de Robótica*, Universidad de Valladolid, 06 2018.

[8] L. Mena, C. A. Monje, L. Nagua, J. Muñoz, and C. Balaguer, "Sensorización de un sistema de eslabón blando actuando como cuello robótico," in *Actas de*

las Jornadas Nacionales de Robótica, pp. 98–102, Universidad de Alicante, 06 2019.

[9] L. Mena, C. A. Monje, L. Nagua, J. Muñoz, and C. Balaguer, "Test bench for evaluation of a soft robotic link," *Frontiers in Robotics and AI*, vol. 7, p. 27, mar 2020.

[10] F. Quevedo, J. Muñoz, J. A. Castano, C. A. Monje, and C. Balaguer, "Model identification of a soft robotic neck," in *International Conference on Intelligent Robots and Systems (IROS)*, 2020.

[11] H. S. Black, "Stabilized feedback amplifiers," *The Bell System Technical Journal*, vol. 13, pp. 1–18, Jan 1934.

[12] C. A. Monje, Y. Chen, B. M. Vinagre, D. Xue, and V. Feliu-Batlle, *Fractional-order systems and controls: fundamentals and applications*. Springer Science & Business Media, 2010.

[13] I. Podlubny, "Chapter 10 - survey of applications of the fractional calculus," in *Fractional Differential Equations* (I. Podlubny, ed.), vol. 198 of *Mathematics in Science and Engineering*, pp. 261 – 307, Elsevier, 1999.

[14] Y. Zhou, J. Wang, and L. Zhang, *Basic Theory of Fractional Differential Equations*. WORLD SCIENTIFIC, 2nd ed., 2016.

[15] I. Petras, *Stability of Fractional-Order Systems*, pp. 55–101. Berlin, Heidelberg: Springer Berlin Heidelberg, 2011.

[16] R. Cipin, C. Ondrusek, and R. Huzlík, "Fractional-order model of DC motor," in *Mechatronics 2013* (T. Březina and R. Jabloński, eds.), (Cham), pp. 363–370, Springer International Publishing, 2014.

[17] W. Zheng, Y. Luo, Y. Chen, and Y. Pi, "Fractional-order modeling of permanent magnet synchronous motor speed servo system," *Journal of vibration and control*, vol. 22, pp. 2255–2280, may 2016.

[18] H. W. Bode, *Network analysis and feedback amplifier design*. Bell Telephone Laboratory series, New York, NY: Van Nostrand, 1945.

[19] A. Oustaloup, "The crone control (la commande crone)," *Hermès, Paris*, 1991.

[20] B. Hekimoğlu, "Optimal tuning of fractional order PID controller for DC motor speed control via chaotic atom search optimization algorithm," *IEEE Access*, vol. 7, pp. 38100–38114, 2019.

[21] C. I. Muresan *et al.*, "Simplified optimization routine for tuning robust fractional order controllers," *American Journal of Computational Mathematics*, vol. 3, no. 3, pp. 7–12, 2013.

[22] C. I. Muresan, E. H. Dulf, and R. Both, "Vector-based tuning and experimental validation of fractional-order PI/PD controllers," *Nonlinear Dynamics*, vol. 84, pp. 179–188, Apr 2016.

[23] R. De Keyser, C. I. Muresan, and C. M. Ionescu, "A novel auto-tuning method for fractional order pi/pd controllers," *ISA Transactions*, vol. 62, pp. 268 – 275, may 2016. SI: Control of Renewable Energy Systems.

[24] M. M'Saad, R. Ortega, and I. Landau, "Adaptive controllers for discrete-time systems with arbitrary zeros: An overview," *Automatica*, vol. 21, pp. 413 – 423, jul 1985.

[25] I. D. Landau, "Evolution of adaptive control," *Journal of Dynamic Systems, Measurement, and Control*, vol. 115, pp. 381–391, 06 1993.

[26] I. D. Landau, R. Lozano, M. M'Saad, and A. Karimi, *Direct Adaptive Control*, pp. 359–407. London: Springer London, 2011.

[27] I. D. Landau, R. Lozano, M. M'Saad, and A. Karimi, *Parameter Adaptation Algorithms—Deterministic Environment*, pp. 55–120. London: Springer London, 2011.

[28] R. S. Barbosa, J. A. T. Machado, and I. M. Ferreira, "Tuning of PID controllers based on Bode's ideal transfer function," *Nonlinear Dynamics*, vol. 38, pp. 305–321, Dec 2004.

[29] Y. Chen and K. L. Moore, "Relay feedback tuning of robust PID controllers with iso-damping property," *IEEE Transactions on Systems, Man, and Cybernetics, Part B (Cybernetics)*, vol. 35, pp. 23–31, Feb. 2005.

[30] O. Barambones, J. Gonzalez de Durana, and M. De la Sen, "Robust speed control for a variable speed wind turbine," *International journal of innovative computing, information and control: IJICIC*, vol. 8, pp. 7627–7640, 01 2010.

[31] C. A. Monje, B. M. Vinagre, V. Feliu, and Y. Chen, "Tuning and auto-tuning of fractional order controllers for industry applications," *Control Engineering Practice*, vol. 16, pp. 798–812, jul 2008.

[32] H. Nyquist, "Regeneration theory," *Bell System Technical Journal*, vol. 11, no. 1, pp. 126–147, 1932.

[33] N. S. Nise, *Control Systems Engineering*. Wiley, 7 ed., 2019.

[34] V. Feliu, B. M. Vinagre, and C. A. Monje, "Fractional-order control of a flexible manipulator," in *Advances in Fractional Calculus*, vol. 1, pp. 449–462, Springer Netherlands, 2005.

[35] I. Petras, "Fractional order feedback control of a DC motor," *Journal of Electrical Engineering*, vol. 60, no. 3, pp. 117–128, 2009.

[36] T. Qingshun, W. Chunfu, Y. Yuanhui, L. Guodong, and Z. Fengyu, "Design and implementation of fractional order controller for service robots," *International Journal of Control and Automation*, vol. 8, pp. 209–220, may 2015.

[37] N. S. Nise, *Frequency response techniques*, ch. 10, pp. 525–612. Wiley, 2019.

[38] C. A. Monje, B. M. Vinagre, G. E. Santamaría, and I. Tejado, "Auto-tuning of fractional order $PI^{\lambda}D^{\mu}$ controllers using a PLC," in *2009 IEEE Conference on Emerging Technologies Factory Automation*, pp. 1–7, IEEE, Sep. 2009.

[39] F. Padula and A. Visioli, "Tuning rules for optimal PID and fractional-order PID controllers," *Journal of Process Control*, vol. 21, no. 1, pp. 69 – 81, 2011.

[40] A. Rastogi and P. Tiwari, "Optimal tuning of fractional order pid controller for dc motor speed control using particle swarm optimization," *International journal of soft computing and engineering*, vol. 3, no. 2, pp. 150–157, 2013.

[41] F. Merrikh-bayat and M. Afshar, "Extending the root-locus method to fractional-order systems," *Journal of Applied Mathematics*, vol. 2008, p. 12, 2008.

[42] D. Valerio and J. S. da Costa, *An Introduction to Fractional Control*. Control, Robotics and Sensors, Institution of Engineering and Technology, jan 2012.

[43] J. Kennedy and R. Eberhart, "Particle swarm optimization," in *In Proceedings of IEEE International Conference on Neural Networks*, vol. 4, pp. 1942–1948 vol.4, Nov 1995.

[44] D. Karaboga and B. Basturk, "A powerful and efficient algorithm for numerical function optimization: Artificial Bee Colony (ABC) algorithm," *Journal of global optimization*, vol. 39, pp. 459–471, apr 2007.

[45] X. S. Yang and S. Deb, "Engineering optimisation by cuckoo search," *arXiv preprint arXiv:1005.2908*, vol. 1, no. 4, p. 330, 2010.

[46] R. Storn and K. Price, "Differential evolution–a simple and efficient heuristic for global optimization over continuous spaces," *Journal of global optimization*, vol. 11, no. 4, pp. 341–359, 1997.

[47] S. Al-Ratrout, A. Saleem, and H. Soliman, "Optimization methods in fractional order control of electric drives: A comparative study," in *2015 10th International Symposium on Mechatronics and its Applications (ISMA)*, pp. 1–6, Dec 2015.

[48] R. E. Kalman, "Design of a Self-Optimizing Control System," *Journal of Basic Engineering*, vol. 80, pp. 468–478, 02 1958.

[49] K. Åström and T. Hägglund, *Advanced PID Control*. ISA - The Instrumentation, Systems and Automation Society, 2006.

[50] Z. Wang, X. Huang, and H. Shen, "Control of an uncertain fractional order economic system via adaptive sliding mode," *Neurocomputing*, vol. 83, pp. 83 – 88, 2012.

[51] R. K. Saxena and G. Pagnini, "Exact solutions of triple-order time-fractional differential equations for anomalous relaxation and diffusion I: The accelerating case," *Physica A: Statistical Mechanics and its Applications*, vol. 390, no. 4, pp. 602 – 613, 2011.

[52] L. Dorcak, "Numerical models for the simulation of the fractional-order control systems," *arXiv Mathematics e-prints*, p. math/0204108, Apr 2002.

[53] J. Sabatier, A. G. Iturricha, A. Oustaloup, and F. Levron, "Third generation crone control of continuous linear time periodic systems," *IFAC Proceedings Volumes*, vol. 31, pp. 299–304, jul 1998.

[54] J. T. Machado and A. Azenha, "Position/force fractional control of mechanical manipulators," in *AMC'98 - Coimbra. 1998 5th International Workshop on Advanced Motion Control. Proceedings (Cat. No.98TH8354)*, pp. 216–221, IEEE, IEEE, 1998.

[55] I. Podlubny, "Fractional-order systems and $PI^{\lambda}D^{\mu}$-controllers," *IEEE Transactions on Automatic Control*, vol. 44, pp. 208–214, Jan 1999.

[56] D. Xue and Y. Chen, "A comparative introduction of four fractional order controllers," in *Proceedings of the 4th World Congress on Intelligent Control and Automation (Cat. No.02EX527)*, vol. 4, pp. 3228–3235 vol.4, June 2002.

[57] C. Flores and V. Milanés, "Fractional-order-based ACC/CACC algorithm for improving string stability," *Transportation Research Part C: Emerging Technologies*, vol. 95, pp. 381–393, oct 2018.

[58] Q. Chen, T. Chen, H. Yu, J. Song, and D. Liu, "Lateral control for autonomous parking system with fractional order controller.," *JSW*, vol. 6, no. 6, pp. 1075–1081, 2011.

[59] P. Wang, Q. Wang, M. Wan, and N. Chen, "A fractional derivative-based lateral preview driver model for autonomous automobile path tracking," *Mathematical Problems in Engineering*, vol. 2018, p. 7320413, Sept. 2018.

[60] I. Tejado, V. Milanés, J. Villagrá, J. Godoy, H. HosseinNia, and B. M. Vinagre, "Low speed control of an autonomous vehicle by using a fractional pi controller," *IFAC Proceedings Volumes*, vol. 44, no. 1, pp. 15025 – 15030, 2011. 18th IFAC World Congress.

[61] S. H. Hosseinnia, I. Tejado, V. Milanés, J. Villagrá, and B. M. Vinagre, "Experimental application of hybrid fractional-order adaptive cruise control at low speed," *IEEE transactions on control systems technology*, vol. 22, no. 6, pp. 2329–2336, 2014.

[62] A. Rajasekhar, P. Kunathi, A. Abraham, and M. Pant, "Fractional order speed control of DC motor using Levy Mutated Artificial Bee Colony Algorithm," in *2011 World Congress on Information and Communication Technologies*, pp. 7–13, Dec 2011.

[63] K. Khandani and A. A. Jalali, "Robust fractional order control of a DC motor based on particle swarm optimization," in *MEMS, NANO and Smart Systems*, vol. 403 of *Advanced Materials Research*, pp. 5030–5037, Trans Tech Publications, 2 2012.

[64] M. F. Silva and J. A. T. Machado, "Fractional order PD^{α} joint control of legged robots," *Journal of Vibration and Control*, vol. 12, pp. 1483–1501, dec 2006.

[65] B. Deutschmann, C. Ott, C. A. Monje, and C. Balaguer, "Robust motion control of a soft robotic system using fractional order control," in *Advances in Service and Industrial Robotics* (C. Ferraresi and G. Quaglia, eds.), (Cham), pp. 147–155, Springer International Publishing, jul 2018.

[66] A. Kailil, N. Mrani, M. Mliha Touati, S. Choukri, and N. Elalami, "Low earth-orbit satellite attitude stabilization with fractional regulators," *International journal of systems science*, vol. 35, no. 10, pp. 559–568, 2004.

[67] V. H. Haji and C. A. Monje, "Fractional order Fuzzy-PID control of a combined cycle power plant using Particle Swarm Optimization algorithm with an improved dynamic parameters selection," *Applied Soft Computing*, vol. 58, pp. 256–264, 2017.

[68] K. Ranjbaran and M. Tabatabaei, "Fractional order [pi], [pd] and [pi][pd] controller design using Bode's integrals," *International Journal of Dynamics and Control*, vol. 6, pp. 200–212, Mar 2018.

[69] M. Itik, E. Sahin, and M. S. Ayas, "Fractional order control of conducting polymer artificial muscles," *Expert Systems with Applications*, vol. 42, no. 21, pp. 8212 – 8220, 2015.

[70] R. Miranda-Colorado, L. T. Aguilar, and J. E. Herrero-Brito, "Reduction of power consumption on quadrotor vehicles via trajectory design and a controller-gains tuning stage," *Aerospace Science and Technology*, vol. 78, pp. 280 – 296, 2018.

[71] F. Martín, C. A. Monje, L. Moreno, and C. Balaguer, "DE-based tuning of $PI^{\lambda}D^{\mu}$ controllers," *ISA Transactions*, vol. 59, pp. 398 – 407, 2015.

[72] V. Badri and M. S. Tavazoei, "On tuning fractional order [proportional–derivative] controllers for a class of fractional order systems," *Automatica*, vol. 49, no. 7, pp. 2297 – 2301, 2013.

[73] Y. Luo and Y. Chen, *Fractional Order PD Controller Tuning for Position Systems*, ch. 6, pp. 97–111. John Wiley & Sons, Ltd, oct 2012.

[74] A. M. Legendre, *Nouvelles méthodes pour la détermination des orbites des comètes*. F. Didot, 1805.

[75] K. J. Åström and P. Eykhoff, "System identification—a survey," *Automatica*, vol. 7, pp. 123 – 162, mar 1971.

[76] J. Aseltine, A. Mancini, and C. Sarture, "A survey of adaptive control systems," *IRE Transactions on Automatic Control*, vol. 6, pp. 102–108, December 1958.

[77] M. Razmi and C. Macnab, "Near-optimal neural-network robot control with adaptive gravity compensation," *Neurocomputing : an international journal*, vol. 389, pp. 83–92, may 2020.

[78] S. Martinez, J. M. Garcia-Haro, J. G. Victores, A. Jardon, and C. Balaguer, "Experimental robot model adjustments based on force–torque sensor information," *Sensors*, vol. 18, p. 836, mar 2018.

[79] N. Gupta, J. Smith, B. Shrewsbury, and B. Børnich, "2d push recovery and balancing of the ever3 - a humanoid robot with wheel-base, using model predictive control and gain scheduling," in *2019 IEEE-RAS 19th International Conference on Humanoid Robots (Humanoids)*, pp. 365–372, Oct 2019.

[80] A. S. Morse, "Control using logic-based switching," in *Trends in Control* (A. Isidori, ed.), (London), pp. 69–113, Springer London, 1995.

[81] A. Karimi and I. D. Landau, "Robust adaptive control of a flexible transmission system using multiple models," *IEEE Transactions on Control Systems Technology*, vol. 8, pp. 321–331, March 2000.

[82] P. A. Ralston and T. L. Ward, "Mathematical models used for adaptive control of machine tools," *Mathematical and Computer Modelling*, vol. 11, pp. 1151 – 1155, 1988.

[83] R. Swiniarski, "Neural network application to adaptive time-optimal control of nonlinear system," in *Proceedings of the IEEE International Workshop on Intelligent Motion Control*, vol. 1, pp. 233–238, IEEE, Aug 1990.

[84] L. Chen and K. S. Narendra, "Nonlinear adaptive control using neural networks and multiple models," *Automatica*, vol. 37, pp. 1245 – 1255, aug 2001. Neural Network Feedback Control.

[85] L. Yu, S. Fei, L. Sun, and J. Huang, "An adaptive neural network switching control approach of robotic manipulators for trajectory tracking," *International Journal of Computer Mathematics*, vol. 91, pp. 983–995, sep 2014.

[86] X.-H. Chang, J. Xiong, and J. H. Park, "Fuzzy robust dynamic output feedback control of nonlinear systems with linear fractional parametric uncertainties," *Applied Mathematics and Computation*, vol. 291, pp. 213 – 225, dec 2016.

[87] L. Ma, N. Xu, X. Huo, and X. Zhao, "Adaptive finite-time output-feedback control design for switched pure-feedback nonlinear systems with average dwell time," *Nonlinear Analysis: Hybrid Systems*, vol. 37, p. 100908, aug 2020.

[88] H. P. Whitaker, J. Yamron, and A. Kezer, *Design of model-reference adaptive control systems for aircraft*. Massachusetts Institute of Technology, Instrumentation Laboratory, 1958.

[89] K. Astrom, "Direct methods for nonminimum phase systems," *1980 19th IEEE Conference on Decision and Control including the Symposium on Adaptive Processes*, vol. 19, pp. 611 – 615, 1980.

[90] R. Lozano Leal and I. D. Landau, "Quasi-Direct Adaptive Control for Non-minimum Phase Systems," *Journal of Dynamic Systems, Measurement, and Control*, vol. 104, pp. 311–316, dec 1982.

[91] D. Clarke and P. Gawthrop, "Self-tuning control," in *Proceedings of the Institution of Electrical Engineers*, vol. 126, pp. 633–640, IET, 1979.

[92] Z. Ding, N. Paperno, K. Prakash, and A. Behal, "An adaptive control-based approach for 1-click gripping of novel objects using a robotic manipulator," *IEEE Transactions on Control Systems Technology*, vol. 27, pp. 1805–1812, July 2019.

[93] K. Deng, S. Cong, D. Kong, and H. Shen, "Discrete-time direct model reference adaptive control application in a high-precision inertially stabilized platform," *IEEE Transactions on Industrial Electronics*, vol. 66, pp. 358–367, Jan 2019.

[94] K. J. Åström and B. Wittenmark, "On self tuning regulators," *Automatica*, vol. 9, pp. 185 – 199, mar 1973.

[95] I. Landau and H. Silveira, "A stability theorem with applications to adaptive control," *IEEE Transactions on Automatic Control*, vol. 24, pp. 305–312, April 1979.

[96] I. D. Landau, R. Lozano, M. M'Saad, and A. Karimi, *Indirect Adaptive Control*, pp. 409–456. London: Springer London, 2011.

[97] F. Damak, M. B. Nasr, and M. Chtourou, "Indirect adaptive neural control using a hybrid learning algorithm," *ICIC express letters. Part B, Applications: an international journal of research and surveys*, vol. 9, no. 11, pp. 1125–1132, 2018.

[98] M. Santillo and E. D. Sumer, "Non-intrusive indirect adaptive control of an uncertain gasoline engine three-way catalyst," in *2018 Annual American Control Conference (ACC)*, pp. 1–6, June 2018.

[99] J. Zhang, X. Xu, L. Yang, and X. Yang, "Lpv model-based multivariable indirect adaptive control of damaged asymmetric aircraft," *Journal of Aerospace Engineering*, vol. 32, no. 6, p. 04019095, 2019.

[100] I. D. Landau, R. Lozano, M. M'Saad, and A. Karimi, *Introduction to Adaptive Control*, pp. 1–34. London: Springer London, 2011.

[101] K. J. Åström, *History of Adaptive Control*, pp. 526–533. London: Springer London, 2015.

[102] K. J. Åström and B. Wittenmark, "A survey of adaptive control applications," in *Proceedings of 1995 34th IEEE Conference on Decision and Control*, vol. 1, pp. 649–654 vol.1, Dec 1995. 34th IEEE Conference on Decision and Control, 1995.

[103] B. Zhang, X. Zhao, X. Li, and D. Zhang, "Robust indirect adaptive control for a class of nonlinear systems and its application to shape memory alloy actuators," *IEEE Access*, vol. 6, pp. 35809–35823, 2018.

[104] B. Zhang and X.-G. Zhao, "Robust indirect adaptive sliding model control for wiener nonlinear systems," *International Journal of Systems Science*, vol. 51, no. 7, pp. 1307–1323, 2020.

[105] B. Vinagre, I. Petráš, I. Podlubny, and Y. Chen, "Using fractional order adjustment rules and fractional order reference models in model-reference adaptive control," *Nonlinear Dynamics*, vol. 29, no. 1-4, pp. 269–279, 2002.

[106] S. Ladaci, "Adaptive fractional PIλ controller," in *Proceedings of TMCE 2006* (I. Horváth and J. Duhovnik, eds.), Organizing Committee of TMCE 2006, Apr. 2006.

[107] S. Ladaci, J. J. Loiseau, and A. Charef, "Adaptive internal model control with fractional order parameter," *International Journal of Adaptive Control and Signal Processing*, vol. 24, pp. 944–960, apr 2010.

[108] S. Martínez, C. A. Monje, A. Jardón, P. Pierro, C. Balaguer, and D. Munoz, "Teo: Full-size humanoid robot design powered by a fuel cell system," *Cybernetics and Systems*, vol. 43, pp. 163–180, mar 2012.

[109] L. Ljung and T. Söderström, *Theory and practice of recursive identification*, pp. 136–250. MIT press, 1983.

[110] K. J. Åström, "Matching criteria for control and identification," in *European control conference*, vol. 3, pp. 248–251, 1993.

[111] L. Xiao and F. Gao, "A comprehensive review of the development of adaptive cruise control systems," *Vehicle system dynamics*, vol. 48, pp. 1167–1192, oct 2010.

[112] S. Park, H. Rakha, K. Ahn, and K. Moran, "Fuel economy impacts of manual, conventional cruise control, and predictive eco-cruise control driving," *International Journal of Transportation Science and Technology*, vol. 2, pp. 227–242, sep 2013.

[113] V. Milanés and S. E. Shladover, "Modeling cooperative and autonomous adaptive cruise control dynamic responses using experimental data," *Transportation Research Part C: Emerging Technologies*, vol. 48, pp. 285–300, nov 2014.

[114] P. Ioannou, Z. Xu, S. Eckert, D. Clemons, and T. Sieja, "Intelligent cruise control: theory and experiment," in *Proceedings of 32nd IEEE Conference on Decision and Control*, pp. 1885–1890, IEEE, IEEE, 1993.

[115] P. A. Ioannou and C.-C. Chien, "Autonomous intelligent cruise control," *IEEE Transactions on Vehicular Technology*, vol. 42, no. 4, pp. 657–672, 1993.

[116] D. Yanakiev and I. Kanellakopoulos, "Speed tracking and vehicle follower control design for heavy-duty vehicles," *Vehicle System Dynamics*, vol. 25, pp. 251–276, apr 1996.

[117] Y. Sun, X. Wang, L. Li, J. Shi, and Q. An, "Modelling and control for economy-oriented car-following problem of hybrid electric vehicle," *IET Intelligent Transport Systems*, vol. 13, pp. 825–833, may 2019.

[118] F. Gao, Y. Zheng, S. E. Li, and D. Kum, "Robust control of heterogeneous vehicular platoon with uncertain dynamics and communication delay," *IET Intelligent Transport Systems*, vol. 10, pp. 503–513, sep 2016.

[119] P. Wang, Q. Wang, M. Wan, and N. Chen, "A fractional derivative-based lateral preview driver model for autonomous automobile path tracking," *Mathematical Problems in Engineering*, vol. 2018, pp. 1–9, sep 2018.

[120] C. Flores, V. Milanes, and F. Nashashibi, "A time gap-based spacing policy for full-range car-following," in *2017 IEEE 20th International Conference on Intelligent Transportation Systems (ITSC)*, pp. 1–6, IEEE, Oct 2017.

[121] R. Rajamani, *Vehicle dynamics and control*. Springer Science & Business Media, 2011.

[122] O. Sename, P. Gáspár, and J. Bokor, *Robust Control and Linear Parameter Varying Approaches: Application to Vehicle Dynamics*. Springer Berlin Heidelberg, 02 2013.

[123] C. A. Monje, Y. Chen, B. M. Vinagre, D. Xue, and V. Feliu-Batlle, *Fractional-order Proportional Derivative Controller Tuning for Motion Systems*, pp. 107–120. London: Springer London, 01 2010.

[124] J. Sabatier, O. P. Agrawal, and J. A. T. Machado, eds., *Advances in Fractional Calculus: Theoretical Developments and Applications in Physics and Engineering*. Dordrecht: Springer Netherlands, 2007.

[125] M. J. Powell, "A fortran subroutine for solving systems of nonlinear algebraic equations," tech. rep., Atomic Energy Research Establishment, Harwell, England (United Kingdom), 1968.

[126] P. Rabinowitz, *Numerical methods for nonlinear algebraic equations*. Gordon & Breach Science Pub, 1970.

[127] E. C. Levy, "Complex-curve fitting," *Automatic Control, IRE Transactions on*, vol. AC-4, pp. 37–43, 05 1959.

[128] C. Schumacher, E. Knoop, and M. Bächer, "Simulation-ready characterization of soft robotic materials," *IEEE Robotics and Automation Letters*, vol. 5, pp. 3775–3782, July 2020.

[129] A. J. Partridge and A. T. Conn, "Passive, reflex response units for reactive soft robotic systems," *IEEE Robotics and Automation Letters*, vol. 5, pp. 4014–4020, July 2020.

[130] B. K. Johnson, V. Sundaram, M. Naris, E. Acome, K. Ly, N. Correll, C. Keplinger, J. S. Humbert, and M. E. Rentschler, "Identification and control of a nonlinear soft actuator and sensor system," *IEEE Robotics and Automation Letters*, vol. 5, pp. 3783–3790, July 2020.

[131] U. Jeong and K. Cho, "Control of a bowden-cable actuation system with embedded boasensor for soft wearable robots," *IEEE Transactions on Industrial Electronics*, vol. 67, pp. 7669–7680, Sep. 2020.

[132] P. Lloyd, A. K. Hoshiar, T. da Veiga, A. Attanasio, N. Marahrens, J. H. Chandler, and P. Valdastri, "A learnt approach for the design of magnetically actuated shape forming soft tentacle robots," *IEEE Robotics and Automation Letters*, vol. 5, pp. 3937–3944, July 2020.

[133] C. Laschi, M. Cianchetti, B. Mazzolai, L. Margheri, M. Follador, and P. Dario, "Soft robot arm inspired by the octopus," *Advanced Robotics*, vol. 26, no. 7, pp. 709–727, 2012.

[134] D. Trivedi, C. D. Rahn, W. M. Kier, and I. D. Walker, "Soft robotics: Biological inspiration, state of the art, and future research," *Applied Bionics and Biomechanics*, vol. 5, pp. 99–117, 2008.

[135] D. Z. De Beyl and P. Salvia, "Neck movement speed in cervical dystonia," *Movement Disorders*, vol. 24, no. 15, pp. 2267–2271, 2009.